

University of Windsor

Scholarship at UWindor

Electronic Theses and Dissertations

Theses, Dissertations, and Major Papers

1995

Computational investigation of heat transfer from an oscillating cylinder.

Dinakara. Karanth
University of Windsor

Follow this and additional works at: <https://scholar.uwindsor.ca/etd>

Recommended Citation

Karanth, Dinakara., "Computational investigation of heat transfer from an oscillating cylinder." (1995).
Electronic Theses and Dissertations. 1514.
<https://scholar.uwindsor.ca/etd/1514>

This online database contains the full-text of PhD dissertations and Masters' theses of University of Windsor students from 1954 forward. These documents are made available for personal study and research purposes only, in accordance with the Canadian Copyright Act and the Creative Commons license—CC BY-NC-ND (Attribution, Non-Commercial, No Derivative Works). Under this license, works must always be attributed to the copyright holder (original author), cannot be used for any commercial purposes, and may not be altered. Any other use would require the permission of the copyright holder. Students may inquire about withdrawing their dissertation and/or thesis from this database. For additional inquiries, please contact the repository administrator via email (scholarship@uwindsor.ca) or by telephone at 519-253-3000ext. 3208.



National Library
of Canada

Bibliothèque nationale
du Canada

Acquisitions and
Bibliographic Services Branch

Direction des acquisitions et
des services bibliographiques

395 Wellington Street
Ottawa, Ontario
K1A 0N4

395, rue Wellington
Ottawa (Ontario)
K1A 0N4

Author: [illegible]

Editor: [illegible]

NOTICE

AVIS

The quality of this microform is heavily dependent upon the quality of the original thesis submitted for microfilming. Every effort has been made to ensure the highest quality of reproduction possible.

La qualité de cette microforme dépend grandement de la qualité de la thèse soumise au microfilmage. Nous avons tout fait pour assurer une qualité supérieure de reproduction.

If pages are missing, contact the university which granted the degree.

S'il manque des pages, veuillez communiquer avec l'université qui a conféré le grade.

Some pages may have indistinct print especially if the original pages were typed with a poor typewriter ribbon or if the university sent us an inferior photocopy.

La qualité d'impression de certaines pages peut laisser à désirer, surtout si les pages originales ont été dactylographiées à l'aide d'un ruban usé ou si l'université nous a fait parvenir une photocopie de qualité inférieure.

Reproduction in full or in part of this microform is governed by the Canadian Copyright Act, R.S.C. 1970, c. C-30, and subsequent amendments.

La reproduction, même partielle, de cette microforme est soumise à la Loi canadienne sur le droit d'auteur, SRC 1970, c. C-30, et ses amendements subséquents.

COMPUTATIONAL INVESTIGATION OF HEAT TRANSFER
FROM AN
OSCILLATING CYLINDER

by

DINAKARA KARANTH

A Dissertation

Submitted to the Faculty of Graduate Studies and Research
through the Department of Mechanical and Materials Engineering in
Partial Fulfillment of the Requirements for the
Degree of Doctor of Philosophy at the
University of Windsor

Windsor, Ontario, Canada

1995



National Library
of Canada

Acquisitions and
Bibliographic Services Branch

395 Wellington Street
Ottawa, Ontario
K1A 0N4

Bibliothèque nationale
du Canada

Direction des acquisitions et
des services bibliographiques

395, rue Wellington
Ottawa (Ontario)
K1A 0N4

Author's Acknowledgement

Author's Acknowledgement

The author has granted an irrevocable non-exclusive licence allowing the National Library of Canada to reproduce, loan, distribute or sell copies of his/her thesis by any means and in any form or format, making this thesis available to interested persons.

L'auteur a accordé une licence irrévocable et non exclusive permettant à la Bibliothèque nationale du Canada de reproduire, prêter, distribuer ou vendre des copies de sa thèse de quelque manière et sous quelque forme que ce soit pour mettre des exemplaires de cette thèse à la disposition des personnes intéressées.

The author retains ownership of the copyright in his/her thesis. Neither the thesis nor substantial extracts from it may be printed or otherwise reproduced without his/her permission.

L'auteur conserve la propriété du droit d'auteur qui protège sa thèse. Ni la thèse ni des extraits substantiels de celle-ci ne doivent être imprimés ou autrement reproduits sans son autorisation.

ISBN 0-612-10941-0

Canada

Name MECHANICAL ENGINEERING

Dissertation Abstracts International is arranged by broad, general subject categories. Please select the one subject which most nearly describes the content of your dissertation. Enter the corresponding four-digit code in the spaces provided.

MECHANICAL ENGINEERING

SUBJECT TERM

0548

SUBJECT CODE

Subject Categories

THE HUMANITIES AND SOCIAL SCIENCES

COMMUNICATIONS AND THE ARTS

Architecture 0729
Art History 0377
Cinema 0900
Dance 0378
Fine Arts 0357
Information Science 0723
Journalism 0391
Library Science 0399
Mass Communications 0708
Music 0413
Speech Communication 0459
Theater 0465

EDUCATION

General 0515
Administration 0514
Adult and Continuing 0516
Agricultural 0517
Art 0273
Bilingual and Multicultural 0282
Business 0688
Community College 0275
Curriculum and Instruction 0727
Early Childhood 0518
Elementary 0524
Finance 0277
Guidance and Counseling 0519
Health 0680
Higher 0745
History of 0520
Home Economics 0278
Industrial 0521
Language and Literature 0279
Mathematics 0280
Music 0522
Philosophy of 0998
Physical 0523

Psychology 0525
Reading 0535
Religious 0527
Sciences 0714
Secondary 0533
Social Sciences 0534
Sociology of 0340
Special 0529
Teacher Training 0530
Technology 0710
Tests and Measurements 0288
Vocational 0747

LANGUAGE, LITERATURE AND LINGUISTICS

Language 0679
General 0289
Ancient 0290
Linguistics 0291
Modern
Literature 0401
General 0294
Classical 0295
Comparative 0297
Medieval 0298
Modern 0316
African 0591
American 0305
Asian 0352
Canadian (English) 0355
Canadian (French) 0593
English 0311
Germanic 0312
Latin American 0315
Middle Eastern 0313
Romance 0314
Slavic and East European

PHILOSOPHY, RELIGION AND THEOLOGY

Philosophy 0422
Religion
General 0318
Biblical Studies 0321
Clergy 0319
History of 0320
Philosophy of 0322
Theology 0469

SOCIAL SCIENCES

American Studies 0323
Anthropology
Archaeology 0324
Cultural 0326
Physical 0327
Business Administration
General 0310
Accounting 0272
Banking 0770
Management 0454
Marketing 0338
Canadian Studies 0385
Economics
General 0501
Agricultural 0503
Commerce-Business 0505
Finance 0508
History 0509
Labor 0510
Theory 0511
Folklore 0358
Geography 0366
Gerontology 0351
History
General 0578

Ancient 0579
Medieval 0581
Modern 0582
Black 0328
African 0331
Asia, Australia and Oceania 0332
Canadian 0334
European 0335
Latin American 0336
Middle Eastern 0333
United States 0337
History of Science 0585
Law 0398
Political Science
General 0615
International Law and Relations 0616
Public Administration 0617
Recreation 0814
Social Work 0452
Sociology
General 0626
Criminology and Penology 0627
Demography 0938
Ethnic and Racial Studies 0631
Individual and Family Studies 0628
Industrial and Labor Relations 0629
Public and Social Welfare 0630
Social Structure and Development 0700
Theory and Methods 0344
Transportation 0709
Urban and Regional Planning 0999
Women's Studies 0453

THE SCIENCES AND ENGINEERING

BIOLOGICAL SCIENCES

Agriculture 0473
General 0285
Agronomy
Animal Culture and Nutrition 0475
Animal Pathology 0476
Food Science and Technology 0359
Forestry and Wildlife 0478
Plant Culture 0479
Plant Pathology 0480
Plant Physiology 0817
Range Management 0777
Wood Technology 0746
Biology
General 0306
Anatomy 0287
Biostatistics 0308
Botany 0309
Cell 0379
Ecology 0329
Entomology 0353
Genetics 0369
Limnology 0793
Microbiology 0410
Molecular 0307
Neuroscience 0317
Oceanography 0416
Physiology 0433
Radiation 0821
Veterinary Science 0778
Zoology 0472
Biophysics
General 0786
Medical 0760
EARTH SCIENCES
Biogeochemistry 0425
Geochemistry 0996

Geodesy 0370
Geology 0372
Geophysics 0373
Hydrology 0388
Mineralogy 0411
Paleobotany 0345
Paleoecology 0426
Paleontology 0418
Paleozoology 0985
Palynology 0427
Physical Geography 0368
Physical Oceanography 0415

HEALTH AND ENVIRONMENTAL SCIENCES

Environmental Sciences 0768
Health Sciences
General 0566
Audiology 0300
Chemotherapy 0992
Dentistry 0567
Education 0350
Hospital Management 0769
Human Development 0758
Immunology 0982
Medicine and Surgery 0564
Mental Health 0347
Nursing 0569
Nutrition 0570
Obstetrics and Gynecology 0380
Occupational Health and Therapy 0354
Ophthalmology 0381
Pathology 0571
Pharmacology 0419
Pharmacy 0572
Physical Therapy 0382
Public Health 0573
Radiology 0574
Recreation 0575

Speech Pathology 0460
Toxicology 0383
Home Economics 0386

PHYSICAL SCIENCES

Pure Sciences
Chemistry
General 0485
Agricultural 0749
Analytical 0486
Biochemistry 0487
Inorganic 0488
Nuclear 0738
Organic 0490
Pharmaceutical 0491
Physical 0494
Polymer 0495
Radiation 0754
Mathematics 0405
Physics
General 0605
Acoustics 0986
Astronomy and Astrophysics 0606
Atmospheric Science 0608
Atomic 0748
Electronics and Electricity 0607
Elementary Particles and High Energy 0798
Fluid and Plasma 0759
Molecular 0609
Nuclear 0610
Optics 0752
Radiation 0756
Solid State 0611
Statistics 0463
Applied Sciences
Applied Mechanics 0346
Computer Science 0984

Engineering
General 0537
Aerospace 0538
Agricultural 0539
Automotive 0540
Biomedical 0541
Chemical 0542
Civil 0543
Electronics and Electrical 0544
Heat and Thermodynamics 0348
Hydraulic 0545
Industrial 0546
Marine 0547
Materials Science 0794
Mechanical 0548
Metallurgy 0743
Mining 0551
Nuclear 0552
Packaging 0549
Petroleum 0765
Sanitary and Municipal 0554
System Science 0790
Geotechnology 0428
Operations Research 0796
Plastics Technology 0795
Textile Technology 0994

PSYCHOLOGY

General 0621
Behavioral 0384
Clinical 0622
Developmental 0620
Experimental 0623
Industrial 0624
Personality 0625
Physiological 0989
Psychobiology 0349
Psychometrics 0632
Social 0451



© Dinakara Karanth 1995

To
My Wife Chetana
and
My Parents

ABSTRACT

The problem of convective heat transfer from an oscillating cylinder is investigated numerically. An isothermal cylinder was forced to oscillate in the in-line and transverse directions at the mid-point lock-in frequencies with different position amplitudes of oscillation. The governing equations in a non-inertial frame of reference are simplified to obtain the vorticity, stream function and energy equations. After applying the log-polar coordinate transformation, the non-dimensional vorticity and energy equations, with appropriate boundary conditions, were solved using an alternating direction implicit method. The Poisson equation for stream function was solved iteratively using the successive over relaxation technique.

The time dependent average Nusselt number and the local Nusselt number distribution on the cylinder surface were computed at a Reynolds number of 200 with the cylinder oscillating in the in-line direction, transverse direction and combined in-line and transverse directions with position amplitudes ranging from 0.1 diameter to 0.8 diameter. The dominant frequency in the average Nusselt number variation was found to be twice the natural shedding frequency. The location of the maximum local Nusselt number depends on the direction and the velocity amplitude of oscillation. With both forced and mixed convection, the local Nusselt number distribution approximately repeats after one cycle of oscillation. In

comparison with the heat transfer from a stationary cylinder, an increased mean Nusselt number and amplitude of the average Nusselt number variation were predicted with the in-line, transverse and combined oscillation. A maximum increase of 18.46% in the mean Nusselt number was predicted when the position amplitude of oscillation was 0.2 diameter in the in-line direction and 0.8 diameter in the transverse direction. Two cases of oscillating hot-wire responses were also computationally predicted in terms of average Nusselt number. The time history of the average Nusselt number agrees qualitatively with the oscillating hot-wire output voltage response.

ACKNOWLEDGEMENTS

I wish to express my sincere gratitude to supervisors Dr. K. Sridhar and Dr. G.W. Rankin for their excellent support, encouragement and guidance. I am also indebted to Dr. R. Barron for his help during this study. Thanks are also extended to the other members of the dissertation committee for their suggestions.

Vijayakanthan was of great help and was always there when I needed him. I am thankful to Satya, Narinder and Eappen for their useful suggestions. I would like to acknowledge the understanding and cooperation of Jack Williams and Peter Kanefsky of Ford Motor Company. Thanks are also due to Dr. Lakshmi Sridhar, whose interest and enthusiasm helped me to finish my dissertation. I also appreciate the love, support and encouragement provided by my family during this study.

I wish to thank the University of Windsor and Ontario Ministry of Education and Training for providing me with graduate scholarships and travel grants. The facilities and assistance provided by the University of Windsor Computer Centre are also acknowledged. The work was financially supported through Natural Science and Engineering Research Council of Canada Grant Numbers A-2190 and A-1403.

TABLE OF CONTENTS

ABSTRACT	Page v
ACKNOWLEDGEMENTS	vii
TABLE OF CONTENTS	viii
LIST OF TABLES	x
LIST OF FIGURES	xi
NOMENCLATURE	xx
Chapter I INTRODUCTION	1
1.1 Motivation and Statement of the Problem	1
1.2 Scope and Objectives	4
Chapter II LITERATURE SURVEY	7
2.1 Stationary Cylinder in a Cross Flow	7
2.1.1 Without Heat Transfer	8
2.1.2 With Heat Transfer	11
2.2 Oscillating Cylinder in a Cross Flow	15
2.2.1 Without Heat Transfer	15
2.2.2 With Heat Transfer	20
Chapter III FORMULATION	24
3.1 Non-inertial Coordinate Transformation	24
3.2 Governing Equations	26
3.3 Vorticity - Stream Function Formulation	29
3.4 Initial and Boundary Conditions	33
3.4.1 Boundary Condition on the Cylinder Surface	34
3.4.2 Far-field Boundary Conditions	35
Chapter IV NUMERICAL PROCEDURE	38
4.1 Numerical Methods	39
4.2 Boundary Conditions	42
4.3 Solution Procedure	43

Chapter V	RESULTS AND DISCUSSION	46
5.1	Dependency Tests	47
5.1.1	Grid Dependency	47
5.1.2	Location of the Far-field Boundary	48
5.1.3	Magnitude of Numerical Triggering	48
5.2	Validation	49
5.3	Stationary Cylinder in a Cross Flow	51
5.4	Oscillating Cylinder in a Cross Flow	52
5.4.1	In-line Oscillation	53
5.4.2	Transverse Oscillation	56
5.4.3	Combined Oscillation	59
5.5	Oscillating Hot-Wire Anemometer Studies	62
Chapter VI	CONCLUSIONS AND RECOMMENDATIONS	161
6.1	Conclusions	161
6.2	Recommendations	163
	REFERENCES	164
Appendix A	DRAG AND LIFT INFORMATION	174
	VITA AUCTORIS	177

LIST OF TABLES

Table	Title	Page
5.1	Mean Nusselt number for different dependency tests ($Re = 200$)	66
5.2	Location and magnitude of maximum $Nu(\theta)$ in a cycle of oscillation (in-line oscillation, $Gr/Re^2 = 0$)	67
5.3	Location and magnitude of maximum $Nu(\theta)$ in a cycle of oscillation (in-line oscillation, $Gr/Re^2 = 1$)	68
5.4	Location and magnitude of maximum $Nu(\theta)$ in a cycle of oscillation (transverse oscillation, $Gr/Re^2 = 0$)	69
5.5	Location and magnitude of maximum $Nu(\theta)$ in a cycle of oscillation (transverse oscillation, $Gr/Re^2 = 1$)	70
5.6	Location and magnitude of maximum $Nu(\theta)$ in a cycle of oscillation (combined oscillation, $a_x = 0.2D$, $Gr/Re^2 = 0$)	71
5.7	Location and magnitude of maximum $Nu(\theta)$ in a cycle of oscillation (combined oscillation, $a_x = 0.2D$, $Gr/Re^2 = 1$)	72
A.1	Mean drag coefficient and amplitude of the drag coefficient at various conditions of cylinder oscillation	175
A.2	Mean lift coefficient and amplitude of the lift coefficient at various conditions of cylinder oscillation	176

LIST OF FIGURES

Figure	Title	Page
3.1	Coordinate systems	37
4.1	Computational domain	45
5.1	Time history of the average Nusselt number (stationary cylinder, $Re = 200$, dependency test with grid size)	73
5.2	Time history of the average Nusselt number (stationary cylinder, $Re = 200$, dependency test with far-field boundary location)	74
5.3	Time history of the average Nusselt number (stationary cylinder, $Re = 200$, dependency test with the magnitude of numerical triggering)	75
5.4	Mean Nusselt number at different Reynolds numbers	76
5.5	Strouhal number at different Reynolds numbers	77
5.6	Mean drag coefficient at different Reynolds numbers	78
5.7	Time history of the average Nusselt number (stationary cylinder, $Re = 200$)	79
5.8	Power spectra of the average Nusselt number (stationary cylinder, $Re = 200$)	80
5.9	Local Nusselt number distribution in a full vortex shedding cycle (stationary cylinder, $Re = 200$, $Gr/Re^2 = 0$)	81
5.10	Local Nusselt number distribution in a full vortex shedding cycle (stationary cylinder, $Re = 200$, $Gr/Re^2 = 1$)	82
5.11	Streamline contour map for the case of forced convection ($Re = 200$, minimum and maximum contour level: -2 and 2, contour interval: 0.1)	83
5.12	Vorticity contour map for the case of forced convection ($Re = 200$, minimum and maximum contour level: -10.25 and 10.25,	83

	contour interval: 0.5)	
5.13	Isothermal contours for the case of forced convection (Re = 200, minimum and maximum contour level: 0.05 and 1, contour interval: 0.05)	84
5.14	Streamline contour map for the case of mixed convection (Re = 200, minimum and maximum contour level: -2 and 2, contour interval: 0.1)	85
5.15	Vorticity contour map for the case of mixed convection (Re = 200, minimum and maximum contour level: -10.25 and 10.25, contour interval: 0.5)	85
5.16	Isothermal contours for the case of mixed convection (Re = 200, minimum and maximum contour level: 0.05 and 1, contour interval: 0.05)	86
5.17	Schematic diagram of the cylinder oscillation	87
5.18	Details of forced oscillation of the cylinder (in-line oscillation, $F_x = 2F_n$) (a) position of the cylinder (b) magnitude of the relative free stream velocity	88
5.19	Time history of the average Nusselt number (in-line oscillation, $F_x = 2F_n$, $Gr/Re^2 = 0$)	89
5.20	Time history of the average Nusselt number (in-line oscillation, $F_x = 2F_n$, $Gr/Re^2 = 1$)	90
5.21	Average Nusselt number in a cycle of oscillation (in-line oscillation, $F_x = 2F_n$, $Gr/Re^2 = 0$)	91
5.22	Average Nusselt number in a cycle of oscillation (in-line oscillation, $F_x = 2F_n$, $Gr/Re^2 = 1$)	92
5.23	Power spectra of the average Nusselt number (in-line oscillation, $F_x = 2F_n$, $Gr/Re^2 = 0$)	93
5.24	Power spectra of the average Nusselt number (in-line oscillation, $F_x = 2F_n$, $Gr/Re^2 = 1$)	94
5.25	Amplitude of Nu_{avg} at different position amplitudes of oscillation (in-line oscillation, $F_x = 2F_n$)	95

5.26	Mean Nusselt number at different position amplitudes of oscillation (in-line oscillation, $F_x = 2F_n$)	96
5.27	Local Nusselt number distribution in a full cycle of oscillation (in-line oscillation, $F_x = 2F_n$, $a_x = 0.1D$, $Gr/Re^2 = 0$)	97
5.28	Local Nusselt number distribution in a full cycle of oscillation (in-line oscillation, $F_x = 2F_n$, $a_x = 0.2D$, $Gr/Re^2 = 0$)	98
5.29	Local Nusselt number distribution in a full cycle of oscillation (in-line oscillation, $F_x = 2F_n$, $a_x = 0.4D$, $Gr/Re^2 = 0$)	99
5.30	Local Nusselt number distribution in a full cycle of oscillation (in-line oscillation, $F_x = 2F_n$, $a_x = 0.1D$, $Gr/Re^2 = 1$)	100
5.31	Local Nusselt number distribution in a full cycle of oscillation (in-line oscillation, $F_x = 2F_n$, $a_x = 0.2D$, $Gr/Re^2 = 1$)	101
5.32	Local Nusselt number distribution in a full cycle of oscillation (in-line oscillation, $F_x = 2F_n$, $a_x = 0.4D$, $Gr/Re^2 = 1$)	102
5.33	Isothermal contours for the case of forced convection (in-line oscillation, $\tau^* = 0$, $a_x = 0.2D$, minimum and maximum contour level: 0.05 and 1, contour interval: 0.05)	103
5.34	Isothermal contours for the case of forced convection (in-line oscillation, $\tau^* = 0.25$, $a_x = 0.2D$, minimum and maximum contour level: 0.05 and 1, contour interval: 0.05)	103
5.35	Isothermal contours for the case of forced convection (in-line oscillation, $\tau^* = 0.50$, $a_x = 0.2D$, minimum and maximum contour level: 0.05 and 1, contour interval: 0.05)	104
5.36	Isothermal contours for the case of forced convection (in-line oscillation, $\tau^* = 0.75$, $a_x = 0.2D$, minimum and maximum contour level: 0.05 and 1, contour interval: 0.05)	104
5.37	Isothermal contours for the case of forced convection (in-line oscillation, $\tau^* = 1$, $a_x = 0.2D$, minimum and maximum contour level: 0.05 and 1, contour interval: 0.05)	105
5.38	Isothermal contours for the case of mixed convection (in-line oscillation, $\tau^* = 0$, $a_x = 0.2D$, minimum and maximum contour level: 0.05 and 1, contour interval: 0.05)	106

5.39	Isothermal contours for the case of mixed convection (in-line oscillation, $\tau^* = 0.25$, $a_x = 0.2D$, minimum and maximum contour level: 0.05 and 1, contour interval: 0.05)	106
5.40	Isothermal contours for the case of mixed convection (in-line oscillation, $\tau^* = 0.50$, $a_x = 0.2D$, minimum and maximum contour level: 0.05 and 1, contour interval: 0.05)	107
5.41	Isothermal contours for the case of mixed convection (in-line oscillation, $\tau^* = 0.75$, $a_x = 0.2D$, minimum and maximum contour level: 0.05 and 1, contour interval: 0.05)	107
5.42	Isothermal contours for the case of mixed convection (in-line oscillation, $\tau^* = 1$, $a_x = 0.2D$, minimum and maximum contour level: 0.05 and 1, contour interval: 0.05)	108
5.43	Details of forced oscillation of the cylinder (transverse oscillation, $F_y = F_n$) (a) position of the cylinder (b) incident angle of the relative free stream velocity (c) magnitude of the relative free stream velocity	109
5.44	Time history of the average Nusselt number (transverse oscillation, $F_y = F_n$, $Gr/Re^2 = 0$)	110
5.45	Time history of the average Nusselt number (transverse oscillation, $F_y = F_n$, $Gr/Re^2 = 1$)	111
5.46	Average Nusselt number in a cycle of oscillation (transverse oscillation, $F_y = F_n$, $Gr/Re^2 = 0$)	112
5.47	Average Nusselt number in a cycle of oscillation (transverse oscillation, $F_y = F_n$, $Gr/Re^2 = 1$)	113
5.48	Power spectra of the average Nusselt number (transverse oscillation, $F_y = F_n$, $Gr/Re^2 = 0$)	114
5.49	Power spectra of the average Nusselt number (transverse oscillation, $F_y = F_n$, $Gr/Re^2 = 1$)	115
5.50	Amplitude of Nu_{avg} at different position amplitudes of oscillation (transverse oscillation, $F_y = F_n$)	116
5.51	Mean Nusselt number at different position amplitudes of oscillation	117

	(transverse oscillation, $F_y = F_n$)	
5.52	Local Nusselt number distribution in a full cycle of oscillation (transverse oscillation, $F_y = F_n$, $a_y = 0.2D$, $Gr/Re^2 = 0$)	118
5.53	Local Nusselt number distribution in a full cycle of oscillation (transverse oscillation, $F_y = F_n$, $a_y = 0.4D$, $Gr/Re^2 = 0$)	119
5.54	Local Nusselt number distribution in a full cycle of oscillation (transverse oscillation, $F_y = F_n$, $a_y = 0.8D$, $Gr/Re^2 = 0$)	120
5.55	Local Nusselt number distribution in a full cycle of oscillation (transverse oscillation, $F_y = F_n$, $a_y = 0.2D$, $Gr/Re^2 = 1$)	121
5.56	Local Nusselt number distribution in a full cycle of oscillation (transverse oscillation, $F_y = F_n$, $a_y = 0.4D$, $Gr/Re^2 = 1$)	122
5.57	Local Nusselt number distribution in a full cycle of oscillation (transverse oscillation, $F_y = F_n$, $a_y = 0.8D$, $Gr/Re^2 = 1$)	123
5.58	Isothermal contours for the case of forced convection (transverse oscillation, $\tau^* = 0$, $a_y = 0.4D$, minimum and maximum contour level: 0.05 and 1, contour interval: 0.05)	124
5.59	Isothermal contours for the case of forced convection (transverse oscillation, $\tau^* = 0.25$, $a_y = 0.4D$, minimum and maximum contour level: 0.05 and 1, contour interval: 0.05)	124
5.60	Isothermal contours for the case of forced convection (transverse oscillation, $\tau^* = 0.50$, $a_y = 0.4D$, minimum and maximum contour level: 0.05 and 1, contour interval: 0.05)	125
5.61	Isothermal contours for the case of forced convection (transverse oscillation, $\tau^* = 0.75$, $a_y = 0.4D$, minimum and maximum contour level: 0.05 and 1, contour interval: 0.05)	125
5.62	Isothermal contours for the case of forced convection (transverse oscillation, $\tau^* = 1$, $a_y = 0.4D$, minimum and maximum contour level: 0.05 and 1, contour interval: 0.05)	126
5.63	Isothermal contours for the case of mixed convection (transverse oscillation, $\tau^* = 0$, $a_y = 0.4D$, minimum and maximum contour level: 0.05 and 1, contour interval: 0.05)	127

5.64	Isothermal contours for the case of mixed convection (transverse oscillation, $\tau^* = 0.25$, $a_y = 0.4D$, minimum and maximum contour level: 0.05 and 1, contour interval: 0.05)	127
5.65	Isothermal contours for the case of mixed convection (transverse oscillation, $\tau^* = 0.50$, $a_y = 0.4D$, minimum and maximum contour level: 0.05 and 1, contour interval: 0.05)	128
5.66	Isothermal contours for the case of mixed convection (transverse oscillation, $\tau^* = 0.75$, $a_y = 0.4D$, minimum and maximum contour level: 0.05 and 1, contour interval: 0.05)	128
5.67	Isothermal contours for the case of mixed convection (transverse oscillation, $\tau^* = 1$, $a_y = 0.4D$, minimum and maximum contour level: 0.05 and 1, contour interval: 0.05)	129
5.68	Details of forced oscillation of the cylinder (combined oscillation, $F_x = 2F_n$, $F_y = F_n$, $a_x = 0.2D$) (a) position of the cylinder (b) incident angle of the relative free stream velocity (c) magnitude of the relative free stream velocity	130
5.69	Time history of the average Nusselt number (combined oscillation, $F_x = 2F_n$, $F_y = F_n$, $a_x = 0.2D$, $Gr/Re^2 = 0$)	131
5.70	Time history of the average Nusselt number (combined oscillation, $F_x = 2F_n$, $F_y = F_n$, $a_x = 0.2D$, $Gr/Re^2 = 1$)	132
5.71	Average Nusselt number in a cycle of oscillation (combined oscillation, $F_x = 2F_n$, $F_y = F_n$, $a_x = 0.2D$, $Gr/Re^2 = 0$)	133
5.72	Average Nusselt number in a cycle of oscillation (combined oscillation, $F_x = 2F_n$, $F_y = F_n$, $a_x = 0.2D$, $Gr/Re^2 = 1$)	134
5.73	Power spectra of the average Nusselt number (combined oscillation, $F_x = 2F_n$, $F_y = F_n$, $a_x = 0.2D$, $Gr/Re^2 = 0$)	135
5.74	Power spectra of the average Nusselt number (combined oscillation, $F_x = 2F_n$, $F_y = F_n$, $a_x = 0.2D$, $Gr/Re^2 = 1$)	136
5.75	Amplitude of Nu_{avg} at different position amplitudes of oscillation (combined oscillation, $F_x = 2F_n$, $F_y = F_n$, $a_x = 0.2D$)	137
5.76	Mean Nusselt number at different position amplitudes of oscillation (combined oscillation, $F_x = 2F_n$, $F_y = F_n$, $a_x = 0.2D$)	138

5.77	Local Nusselt number distribution in a full cycle of oscillation (combined oscillation, $F_x = 2F_n$, $F_y = F_n$, $a_x = a_y = 0.2D$, $Gr/Re^2 = 0$)	139
5.78	Local Nusselt number distribution in a full cycle of oscillation (combined oscillation, $F_x = 2F_n$, $F_y = F_n$, $a_x = 0.2D$, $a_y = 0.4D$, $Gr/Re^2 = 0$)	140
5.79	Local Nusselt number distribution in a full cycle of oscillation (combined oscillation, $F_x = 2F_n$, $F_y = F_n$, $a_x = 0.2D$, $a_y = 0.8D$, $Gr/Re^2 = 0$)	141
5.80	Local Nusselt number distribution in a full cycle of oscillation (combined oscillation, $F_x = 2F_n$, $F_y = F_n$, $a_x = a_y = 0.2D$, $Gr/Re^2 = 1$)	142
5.81	Local Nusselt number distribution in a full cycle of oscillation (combined oscillation, $F_x = 2F_n$, $F_y = F_n$, $a_x = 0.2D$, $a_y = 0.4D$, $Gr/Re^2 = 1$)	143
5.82	Local Nusselt number distribution in a full cycle of oscillation (combined oscillation, $F_x = 2F_n$, $F_y = F_n$, $a_x = 0.2D$, $a_y = 0.8D$, $Gr/Re^2 = 1$)	144
5.83	Isothermal contours for the case of forced convection (combined oscillation, $\tau^* = 0$, $a_x = 0.2D$, $a_y = 0.4D$, minimum and maximum contour level: 0.05 and 1, contour interval: 0.05)	145
5.84	Isothermal contours for the case of forced convection (combined oscillation, $\tau^* = 0.25$, $a_x = 0.2D$, $a_y = 0.4D$, minimum and maximum contour level: 0.05 and 1, contour interval: 0.05)	145
5.85	Isothermal contours for the case of forced convection (combined oscillation, $\tau^* = 0.50$, $a_x = 0.2D$, $a_y = 0.4D$, minimum and maximum contour level: 0.05 and 1, contour interval: 0.05)	146
5.86	Isothermal contours for the case of forced convection (combined oscillation, $\tau^* = 0.75$, $a_x = 0.2D$, $a_y = 0.4D$, minimum and maximum contour level: 0.05 and 1, contour interval: 0.05)	146
5.87	Isothermal contours for the case of forced convection (combined oscillation, $\tau^* = 1$, $a_x = 0.2D$, $a_y = 0.4D$, minimum and maximum contour level: 0.05 and 1, contour interval: 0.05)	147

5.88	Isothermal contours for the case of mixed convection (combined oscillation, $\tau^* = 0$, $a_x = 0.2D$, $a_y = 0.4D$, minimum and maximum contour level: 0.05 and 1, contour interval: 0.05)	148
5.89	Isothermal contours for the case of mixed convection (combined oscillation, $\tau^* = 0.25$, $a_x = 0.2D$, $a_y = 0.4D$, minimum and maximum contour level: 0.05 and 1, contour interval: 0.05)	148
5.90	Isothermal contours for the case of mixed convection (combined oscillation, $\tau^* = 0.50$, $a_x = 0.2D$, $a_y = 0.4D$, minimum and maximum contour level: 0.05 and 1, contour interval: 0.05)	149
5.91	Isothermal contours for the case of mixed convection (combined oscillation, $\tau^* = 0.75$, $a_x = 0.2D$, $a_y = 0.4D$, minimum and maximum contour level: 0.05 and 1, contour interval: 0.05)	149
5.92	Isothermal contours for the case of mixed convection (combined oscillation, $\tau^* = 1$, $a_x = 0.2D$, $a_y = 0.4D$, minimum and maximum contour level: 0.05 and 1, contour interval: 0.05)	150
5.93	Oscillating hot-wire response ($Re = 0.25$, $Gr = 3.988 \times 10^{-6}$, $A_x = 0.712$, $F_x = 4.48 \times 10^{-3}$) (a) magnitude of the relative free stream velocity (b) experimental hot-wire response (H3) (c) computed Nu_{avg} in a cycle of oscillation	151
5.94	Local Nusselt number distribution in a full cycle of oscillation (oscillating hot-wire, $Re = 0.25$, $Gr = 3.988 \times 10^{-6}$, $A_x = 0.712$, $F_x = 4.48 \times 10^{-3}$)	152
5.95	Isothermal contours surrounding the oscillating hot-wire ($\tau^* = 0$, $A_x = 0.712$, minimum and maximum contour level: 0.4 and 1, contour interval: 0.025)	153
5.96	Isothermal contours surrounding the oscillating hot-wire ($\tau^* = 0.25$, $A_x = 0.712$, minimum and maximum contour level: 0.4 and 1, contour interval: 0.025)	153
5.97	Isothermal contours surrounding the oscillating hot-wire ($\tau^* = 0.50$, $A_x = 0.712$, minimum and maximum contour level: 0.4 and 1, contour interval: 0.025)	154
5.98	Isothermal contours surrounding the oscillating hot-wire ($\tau^* = 0.75$, $A_x = 0.712$, minimum and maximum contour level: 0.4 and 1, contour interval: 0.025)	154

5.99	Isothermal contours surrounding the oscillating hot-wire ($\tau^* = 1$, $A_x = 0.712$, minimum and maximum contour level: 0.4 and 1, contour interval: 0.025)	155
5.100	Oscillating hot-wire response ($Re = 0.06$, $Gr = 3.988 \times 10^{-6}$, $A_x = 2.986$, $F_x = 1.87 \times 10^{-3}$) (a) magnitude of the relative free stream velocity (b) experimental hot-wire response (H3) (c) computed Nu_{avg} in a cycle of oscillation	156
5.101	Local Nusselt number distribution in a full cycle of oscillation (oscillating hot-wire, $Re = 0.06$, $Gr = 3.988 \times 10^{-6}$, $A_x = 2.986$, $F_x = 1.87 \times 10^{-3}$)	157
5.102	Isothermal contours surrounding the oscillating hot-wire ($\tau^* = 0$, $A_x = 2.986$, minimum and maximum contour level: 0.4 and 1, contour interval: 0.025)	158
5.103	Isothermal contours surrounding the oscillating hot-wire ($\tau^* = 0.25$, $A_x = 2.986$, minimum and maximum contour level: 0.4 and 1, contour interval: 0.025)	158
5.104	Isothermal contours surrounding the oscillating hot-wire ($\tau^* = 0.50$, $A_x = 2.986$, minimum and maximum contour level: 0.4 and 1, contour interval: 0.025)	159
5.105	Isothermal contours surrounding the oscillating hot-wire ($\tau^* = 0.75$, $A_x = 2.986$, minimum and maximum contour level: 0.4 and 1, contour interval: 0.025)	159
5.106	Isothermal contours surrounding the oscillating hot-wire ($\tau^* = 1$, $A_x = 2.986$, minimum and maximum contour level: 0.4 and 1, contour interval: 0.025)	160

NOMENCLATURE

a	transformation parameter
a'_{cx}, a'_{cy}	acceleration of the forced cylinder oscillation in the in-line and transverse directions, respectively
a_x, a_y	position amplitude of forced cylinder oscillation in the in-line and transverse directions, respectively ($A'_x t_x / 2\pi$, $A'_y t_y / 2\pi$)
A'_x, A'_y	velocity amplitude of forced cylinder oscillation in the in-line and transverse directions, respectively
A_x, A_y	nondimensional velocity amplitude of forced cylinder oscillation in the in-line and transverse directions, respectively (A'_x / U_∞ , A'_y / U_∞)
$\text{Amp}(\text{Nu}_{\text{avg}})$	amplitude of the average Nusselt number
C_d	drag coefficient ($d / \rho U_\infty^2 R$)
C_{d_m}	mean drag coefficient
$C_{d_{\text{amp}}}$	amplitude of the drag coefficient
C_l	lift coefficient ($l / \rho U_\infty^2 R$)
C_{l_m}	mean lift coefficient
$C_{l_{\text{max}}}$	amplitude of the lift coefficient
d	drag force
D	diameter of the cylinder
E	hot-wire response in millivolts
f_x, f_y	force in the x and y directions, respectively

F_n	nondimensional natural shedding frequency (Strouhal number, $D/t_n U_\infty$)
F_x, F_y	nondimensional forced frequency parameter in the in-line and transverse directions, respectively ($D/t_x U_\infty, D/t_y U_\infty$)
Gr	Grashoff Number ($g\beta(T_s - T_\infty)D^3/\nu^2$)
I	lift force
$Nu(\theta)$	local Nusselt number
Nu_{avg}	average Nusselt number
Nu_m	mean Nusselt number
p	pressure
p_∞	free stream pressure
P	nondimensional pressure, $(p - p_\infty)/\rho U_\infty^2$
Pr	Prandtl number (ν/α)
PSD	power spectral density
(r, θ)	radial and tangential coordinates in a frame of reference attached to the cylinder
R	radius of the cylinder
Re	Reynolds number based on cylinder diameter ($U_\infty D/\nu$)
t	time
T	temperature
t_x, t_y	period of oscillation in the in-line and transverse directions, respectively
T_s	cylinder surface temperature

T_{∞}	ambient temperature
t_d	time delay
T_n	natural shedding period
u', v'	absolute velocity in the x' and y' directions, respectively
u, v	velocity relative to a non-inertial frame of reference in the x and y directions, respectively
U, V	nondimensional velocity in the ξ and η directions, respectively (Eq. 3.21)
U_{∞}	free stream velocity
U'	nondimensional free stream velocity relative to the frame of reference attached to the cylinder
v_r, v_{θ}	relative velocity in the r and θ directions, respectively
V_r, V_{θ}	nondimensional relative velocity in the r and θ directions, respectively ($v_r/U_{\infty}, v_{\theta}/U_{\infty}$)
(x, y)	Cartesian coordinates in the frame of reference attached to the cylinder
(x', y')	Cartesian coordinates in the inertial frame of reference
x_c, y_c	position of the cylinder centre in the in-line and transverse directions, respectively

Greek Symbols

α	thermal diffusivity
----------	---------------------

ϵ	incident angle of the nondimensional free stream velocity relative to the frame of reference attached to the cylinder
λ	relaxation parameter
ν	kinematic viscosity of the fluid
(ξ, η)	nondimensional log-polar coordinates ($r/R = e^{a\xi}$, $\theta = a\eta$)
ρ	density of the fluid
τ	nondimensional time (tU_∞/R)
τ_{cycle}	nondimensional time in a natural vortex shedding cycle or an oscillation cycle of the cylinder
τ_d	nondimensional time delay ($t_d U_\infty/R$)
τ_n	nondimensional natural vortex shedding period
τ^*	ratio $\tau_{\text{cycle}}/\tau_n$
ϕ	phase difference between the transverse and in-line oscillations
Φ	nondimensional temperature
ψ	stream function relative to the frame attached to the cylinder
Ψ	nondimensional stream function relative to the frame attached to the cylinder (ψ/rU_∞)
ω	vorticity
Ω	nondimensional vorticity ($\omega R/U_\infty$)

Chapter I

INTRODUCTION

1.1 Motivation and Statement of the Problem

Fluid flow past a bluff body is of great importance in various engineering applications. The main feature of the flow is its separation from the body surface and formation of a large wake downstream. The existence of the wake alters the flow and pressure distributions around the body and results in a deficit of pressure on the downstream side. This causes a pressure induced drag.

Over a wide range of Reynolds number, a vortex street is formed in the wake of a cylindrical bluff body. At low Reynolds numbers, a steady symmetrical pair of vortices is formed on the downstream side of the cylinder. At a Reynolds number above about 40, periodic shedding of the vortices from the cylinder surface results in an alternating vortex street. Experimental observations and numerical predictions have shown that the vortices in the wake interact with the cylinder and induce oscillating lift and drag forces and torque on the cylinder. The oscillation frequencies of the lift and drag forces and torque are directly related to the vortex shedding frequency which may be expressed nondimensionally as a Strouhal number. The drag force and torque oscillates at twice the vortex shedding frequency and the lift force oscillates at a frequency equal to the vortex shedding frequency. These oscillating forces are known to cause vibrations in a variety of

cylindrical structures. The incident flow can excite resonant oscillations if the cylinder is flexible. The oscillating lift and drag forces may cause the flexible cylinder in a cross flow to vibrate in the in-line and transverse directions. The study of a cylinder oscillating in a cross flow is considered essential to understand the dynamics of many offshore structures.

The convective heat transfer from a stationary cylinder is a fundamental engineering problem with applications ranging from isolated heat exchanger tubes to hot-wire anemometers. The unsteady behaviour of the flow close to the surface strongly affects the heat transfer from the cylinder. In many industrial applications, it is necessary to avoid over-design of heat transfer elements subjected to flow induced vibration. In order to obtain an adequate design of the heating elements, it is necessary to investigate the effects of oscillation of the cylinder in the in-line and transverse directions. Another application of the study of convective heat transfer from an oscillating cylinder is to oscillating hot-wire anemometers (F1, H3). Oscillating hot-wires can solve the problem of directional ambiguity associated with conventional anemometers. In order to explain the behaviour of the oscillating hot-wire anemometers, it is essential to study the problem of convective heat transfer from an oscillating cylinder in a cross flow.

In the case of flow past a stationary cylinder, vortices are shed at a constant nondimensional natural shedding frequency (Strouhal number), for a flow at a particular Reynolds number. Within a range of forced frequencies, vortex shedding is controlled by the oscillation of the cylinder and a considerable increase in the

time mean lift and drag force is observed. This is referred to as the "lock-in" or "wake capture" or "synchronization" phenomenon (K3). During transverse oscillation, lock-in occurs when the forced frequency approaches the natural shedding frequency causing a considerable increase in the drag force with the vortices being shed at the same frequency as that of the cylinder oscillation. The lock-in phenomenon occurs with an in-line oscillation, when the frequency of the cylinder oscillation approaches twice the natural shedding frequency. The vibration of the cylinder, in the lock-in range of frequencies, causes vortex shedding to occur at half the cylinder frequency and produces a significant increase in the lift force. Both the in-line and transverse oscillations of the cylinder alter the phase, sequence and pattern of vortices in the wake and increase the vortex strength within the respective lock-in frequency range. In the case of flow induced oscillation, the position amplitude of the cylinder oscillation in the in-line direction is less than in the transverse direction (V2). Lock-in occurs both with forced oscillation of the cylinder and flow induced oscillation of the cylinder. The influence of the lock-in phenomenon on the heat transfer is not discussed in the literature.

In the past two decades, numerous experimental results have been reported regarding the convective heat transfer from an oscillating cylinder in a still fluid. All of the experimental studies regarding the heat transfer from an oscillating cylinder reported in the literature (A2, A3, D1, D2, F1, K2, L2 and S3) are at frequencies lower than the lock-in range of frequencies. In a cross flow, it has been experimentally observed that the oscillation in the direction transverse to that of the

mean flow, increases the heat transfer rate from the cylinder. In the case of an oscillation in the direction in-line to that of the mean flow, highly contradictory experimental observations have been reported.

The problem of the present investigation is the flow past an isothermal cylinder which is subjected to forced oscillations in directions in-line and transverse to that of the mean flow. The intricate details of the heat transfer from the oscillating cylinder are difficult to analyze experimentally or theoretically. In this study, the approach adopted to solve the problem is purely computational. A thoroughly validated numerical simulation code can be highly reliable, economical and gives accurate results in less time than an experimental study. To the candidate's knowledge, no numerical simulation of heat transfer convected from a sinusoidally oscillating cylinder has been reported in the past. Many experimental and numerical studies of cylinder oscillation without heat transfer can be found in the literature. No numerical prediction or experimental results have been reported for the case of combined oscillation.

1.2 Scope and Objectives

Flow past an oscillating cylinder is the subject of interest in designing ocean pipelines (risers) and offshore platform supports. The study of forced and mixed (forced and free) convective heat transfer from an oscillating cylinder in a cross flow is of interest in the areas of oscillating hot-wire anemometers and flow induced vibration of isolated heat exchanger tubes. The purpose of the present

investigation is to study the cross flow past an oscillating cylinder and to analyze the heat transfer from it. The present numerical study may help to fill the information gap and to explain some of the contradictory experimental results.

The main objective of this study is to investigate the effects of in-line and transverse oscillations of the cylinder at the mid-point lock-in frequency on the time history of the average Nusselt number over the cylinder surface. It is also important to determine the influence of cylinder oscillation on the local Nusselt number distribution on the surface of the cylinder. The effects of mixed convection on the heat transfer rate are also discussed. The influence of the alternating vortex street on the isotherm contours and the time history of the Nusselt number are also examined.

The secondary objective is to qualitatively compare the experimental output responses of an oscillating hot-wire anemometer with the computational predictions. The behaviour of the oscillating hot-wire anemometer at two different velocity amplitudes of oscillation is also discussed.

In this study, the non-dimensionalized vorticity transport and energy equations in a non-inertial reference frame (attached to the cylinder) are solved on a rectangular grid based on log-polar coordinates (ξ, η) . Finite difference calculations were made at different Reynolds numbers, Grashof numbers, as well as nondimensional frequencies and amplitudes of oscillation. As the maximum Reynolds number considered in this study is 1000, the laminar flow assumption is considered to be valid. Air is taken to be the fluid medium.

The following format will be adopted for presenting the different stages of the present computational investigation. In the beginning, a review of the past research work on the subject of interest will be provided. Subsequently, the formulation of the governing equations and a brief description of the numerical procedure employed to solve them are presented. The numerical results obtained are discussed afterwards. This will be followed by conclusions and recommendations which are based on an interpretation of the numerically obtained results.

Chapter II

LITERATURE REVIEW

The problem of flow past a stationary cylinder has been studied experimentally and theoretically for the past hundred years. Extensive experimental results for unsteady periodic flow around cylinders are available in the literature. Cylinders shed alternating vortices with a constant Strouhal number of approximately 0.21 in the range of Reynolds number from about 200 to 10^5 . The Strouhal number is lower for a Reynolds number less than 200 and higher for a Reynolds number more than 10^5 . One of the widely used references in this field is the experimental study of Roshko (R2). The main emphasis of this review is on the numerical investigation of the flow field around a cylindrical body and the heat transfer from a cylinder in a cross flow. Some of the related experimental research work is also discussed. This survey is divided into two categories: stationary cylinder in a cross flow and oscillating cylinder in a cross flow. In both categories, research work done with and without heat transfer from the cylinder is presented.

2.1. Stationary Cylinder in a Cross Flow

As there are numerous experimental and numerical studies concerning the flow past a stationary cylinder, only a few important numerical and experimental research papers are discussed in this survey.

2.1.1 Without Heat Transfer

One of the first numerical simulations of flow around a circular cylinder was conducted by Thom (T8) at Reynolds numbers 10 and 20. Later, Takami and Keller (T3) solved the steady state vorticity transport equations for the problem of flow past a circular cylinder at low Reynolds numbers. In their study, the flow was assumed to be uniform at an infinite distance upstream and the range of Reynolds number extended from 1 to 60. They also gave correlations for the drag coefficient and base pressure in terms of Reynolds number. Hamielec and Raal (H2) obtained numerical solutions using the two-dimensional vorticity transport equations. They compared the drag coefficients, pressure distributions and vortex dimensions with available experimental data. Excellent agreement with the experimental results was obtained up to a Reynolds number of 50.

The problem of unsteady viscous flow past a circular cylinder was numerically solved by Payne (P1) by integrating the vorticity transport equation. In his studies, the general features of the flow such as the formation of the eddies attached to the rear of the cylinder were obtained. The author also concluded that the drag on the cylinder reduces with time to a value near that for the steady flow. Jain and Rao (J3) performed computational studies of unsteady flow past a cylinder using an explicit scheme. They showed the dependence of the flow pattern, vorticity distribution, pressure distribution and drag on the Reynolds number and the time. They were not able to show any vortex street formation for a Reynolds number of 100. Similarly, Son and Hanratty (S5) used an alternating

direction implicit scheme to solve the unsteady vorticity transport equations and did not show any vortex street formation up to a Reynolds number of 500. The reason for this is that they did not use any form of numerical triggering to initiate the alternate vortex shedding. In this study, the forces on the cylinder due to viscous drag and due to pressure drag were found to be smaller than the values obtained in laboratory experiments in which the wake was unsteady.

A comprehensive numerical study of unsteady flow past a cylinder was conducted by Jordan and Fromm (J5) in which a numerical triggering procedure was used to initiate the Karman vortex street. The numerical triggering procedure consisted of rotating the cylinder counterclockwise and then clockwise for a short period of time. The timing and the amplitude of rotation were adjusted in order to initiate the vortex street as quickly as possible without causing any long duration effects. Jordan and Fromm's study also reveals the oscillatory nature of the drag, lift and torque that are experienced by the cylinder.

Swanson and Spaulding (S8) were the first to develop a fully three-dimensional finite difference model simulating the steady and unsteady flow around a cylinder at a Reynolds number of 100. The three-dimensional case was run with a uniform vertical shear flow using a primitive variable formulation. In 1980, Loc (L4) analyzed the growth of the primary and secondary vortices with time for Reynolds numbers up to 1000. He used the fourth order compact scheme to solve the Poisson equation of the stream function and the second order alternating direction implicit scheme to resolve the vorticity transport equation. Later, Loc and

Bouard (L5) numerically studied the early stage of the unsteady viscous flow around a cylinder at $Re = 3000$ and $Re = 9500$. Evolution of the flow structure with time was studied in detail. A symmetrical boundary condition was used and no vortex shedding was generated. Borthwick (B6) compared the alternating direction implicit (ADI) and directional difference explicit (DDE) numerical schemes for computing the flow around a cylinder. He concluded that the DDE scheme produces artificial viscosity, damps the wake and suppresses the vortex shedding. The ADI scheme was found to be more reliable.

The dynamic characteristics of the pressure and velocity fields of the unsteady incompressible laminar wake behind a cylinder were investigated by Braza et al. (B7) using a two-dimensional primitive variable formulation. They used a finite volume formulation and concluded that phase relations exist between the pressure and velocity in the wake. Rumsey (R4) computationally studied the details of the flow field around a circular cylinder at $Re = 1200$ using the complete form of the compressible Navier-Stokes equations. In comparison with the experimental results, this numerical scheme predicted a more rapid onset of flow reversal over the cylinder. A direct numerical simulation of unsteady flow past a cylinder was carried out by Braza and Minh (B8) in the Reynolds number range of 2000 to 10000 using the 2-D Navier-Stokes equations. In their study, the time dependent evolution of drag and lift oscillations were computed and analyzed over large time intervals using a CRAY supercomputer.

In order to understand the shedding patterns of the near-wake vortices

behind a cylinder, Sa and Chang (S1) used fourth order Hermitian relations for the convection terms and solved the vorticity transport equations. They also developed a new integral series method for far-field stream function condition on a two-dimensional computational domain.

Wang and Dalton (W1) gave the numerical solutions for impulsively started and decelerated viscous flow past a cylinder. A two-step, predictor-corrector finite difference scheme was used to solve the vorticity transport equation. A sharp increase in the drag coefficient was predicted for the case of a suddenly stopped flow past a cylinder. In 1993, Green and Gerrard (G1) measured the vorticity in the near-wake of a cylinder at low Reynolds numbers using the particle streak method. Their vorticity measurements agree well with the two-dimensional numerical results. However, the lift coefficients were overpredicted by the numerical simulation.

2.1.2 With Heat Transfer

Many experimental correlations exist relating the Reynolds number, Prandtl number and the mean Nusselt number for the case of forced and mixed convective heat transfer from a stationary cylinder. One of the first general correlations for the forced convective heat transfer from a stationary cylinder in a cross flow given by Kramers (K4) is

$$Nu_m = 0.42(Pr)^{0.20} + 0.57 (Pr)^{0.33} (Re)^{0.5}. \quad (2.1)$$

This correlation is valid up to a Reynolds number of 10^4 . Later, Cole and Roshko

(C4) conducted experiments to measure the mean Nusselt number in the low Reynolds number range ($Re < 1$) and compared with their analytical solutions. This work also deals with the effect of aspect ratio of the cylinder on the heat transfer rate from the cylinder.

Hegge Zijnen (H4) assembled the experimental data from various origins and presented modified correlation formulae for the heat transfer by natural and by forced convection from horizontal cylinders. A generalized correlation for the forced convective heat transfer from the cylinder for air and diatomic gases was given as

$$Nu_m = 0.38Pr^{0.2} + (0.56Re^{0.5} + 0.001Re)Pr^{0.33}. \quad (2.2)$$

This correlation is considered to be better than Kramers' correlation for Reynolds numbers above 10^3 . Hegge Zijnen also suggested that a correlation for mixed convection can be obtained by taking the vectorial sum (square root of the sum of the squares) of the Nusselt numbers obtained separately from the free convection and forced convection. Even though the correlation may agree with some of the experimental results, it is not accepted by the scientific community because the vectorial summing of the scalar quantities is invalid.

Heat transfer by combined free and forced convection from a heated cylinder in a transverse air stream was studied experimentally over a wide range of Grashof and Reynolds numbers by Sharma and Sukhatme (S4). The criteria for transition from free convection to mixed convection and from mixed convection to forced convection were also obtained by them. Oosthuizen and Madan (O3, O4)

conducted experiments to determine the effects of flow direction on the mixed convective heat transfer from cylinders to air. They also gave different criteria for purely forced convection to exist in terms of the ratio Gr/Re^2 for different flow directions with respect to the direction of the free convection. In the case of a cross flow situation, pure forced convection exists if $Gr/Re^2 < 0.53$.

Recently, Armaly et. al. (A4) summarized the analytical and experimental results of several representative studies for the mixed convection in air flow across horizontal cylinders. They presented simple correlation equations that can be employed in heat transfer calculations. This work can be considered as a good source of reference for calculating the heat transfer from cylinders in different flow configurations such as assisted flow, opposed flow and cross flow. An assisted flow situation exists when the direction of the flow and the free convection are the same and the opposed flow situation exists when the direction of the flow is opposite to the direction of free convection. In the cross flow situation, the direction of the flow is perpendicular to the direction of free convection.

In the past two decades, several numerical investigations of the unsteady heat transfer from a stationary circular cylinder have been made. Most of these were carried out for Reynolds numbers less than 500. Jain and Goel (J1) carried out a numerical investigation of unsteady laminar forced convection from a cylinder at Reynolds numbers of 100 and 200. Finite difference calculations were made to obtain the temperature field and local Nusselt number around the cylinder at different times. The computed results were found to be in good agreement with the

experimental results. Later, Jain and Lohar (J2) conducted a numerical study of unsteady mixed convective heat transfer from a horizontal cylinder in an assisted flow situation. They discussed the effects of free convection on the vortex shedding frequency and the separation points. The time dependent local Nusselt number distribution was presented at different Reynolds numbers and Grashof numbers.

In a computational study of forced and mixed convection from a cylinder, Ha Minh et al. (H1) discussed the effects of direction of the flow on the Strouhal number, total drag and mean Nusselt number. Badr (B1, B2) numerically studied the mixed convection from a cylinder in cross flow , assisted flow and opposing flow situations at low Reynolds numbers ($Re < 60$) and Grashof numbers ($Gr < 7200$). The procedure that was employed to solve the asymmetrical flow field was a series-truncation method and a Crank-Nicolson finite difference scheme for advancing in time. In these studies, the influence of free convection on the vorticity and pressure distributions on the cylinder was discussed. Moon et al. (M3) calculated the pressure distributions for combined convection around a cylinder in an assisted flow configuration. They employed a vorticity-stream function formulation and for the recovery of pressure distribution, the Poisson equation for pressure was solved.

Recently, Chun and Boehm (C2) carried out a finite volume calculation of forced convective heat transfer at various Reynolds numbers as high as 3480 without initiating an alternating vortex street. In their work, a comparison of the solution techniques using the central difference and power law forms was

presented for the cases of uniform wall temperature and uniform heat flux condition on the cylinder surface. The same authors (C3) investigated the effects of nonuniform thermal boundary conditions on the surface on the forced convection heat transfer from the cylinder. With the same mean surface temperature, nonuniform surface temperature cases showed considerable differences in total heat transfer between one another.

2.2 Oscillating Cylinder in a Cross Flow

In the case of an oscillating cylinder in a cross flow, all of the available experimental and numerical studies are discussed in the following sections.

2.2.1 Without Heat Transfer

There are several reports of experimental investigations of cylinders oscillating in a direction in-line or transverse to that of the mean flow direction. Koopmann (K3) was one of the first to examine the effects of transverse oscillation of the cylinder on the structure of the wake. This author also established conditions for which the vortex wake frequency is controlled by the driving frequency of the cylinder. Later, Tanaka and Takahara (T6) conducted experiments to measure the time dependent lift force on a transversely oscillating cylinder in a cross flow. It was concluded that the lift force increased with the amplitude of the cylinder oscillation. Bublitz (B9) studied the problem of transversely oscillating cylinder in the Reynolds number range of 10^5 to 6.7×10^5 and concluded that the oscillations

of the cylinder cause a laminar to turbulent transition at lower Reynolds numbers than that for the cylinder at rest. The stability of a cylinder oscillating in the in-line and transverse directions to that of the mean flow has been studied by Tanida et al. (T7) by measuring the lift and drag forces in the Reynolds number range of 40 to 10^4 . Their study concludes that the transverse oscillation of the cylinder may become unstable when the cylinder motion and the vortex shedding are synchronized.

Griffin and Ramberg (G3, G4, G5) carried out several experimental studies to obtain the characteristics of the lock-in phenomenon with cylinder oscillation in the in-line direction and transverse direction to the incident uniform flow. In the case of in-line oscillation of the cylinder in the lock-in region, two distinct vortex wake patterns were observed. The first is a symmetric vortex shedding near the cylinder in which two vortices are shed during each cycle of the vibration and form an alternating pattern of vortex pairs downstream. The second pattern is an alternating street which results from the shedding of a single vortex during each cycle of cylinder motion. The street geometry in the latter case shares many basic characteristics with the wake of a transversely oscillating cylinder in a cross flow.

The frequencies of vortex shedding from cylinders forced to oscillate transversely in low-turbulence uniform and shear flows were investigated by Stansby (S7). These experiments reveal that the range of cylinder frequency for locking-on was dependent on the amplitude of the oscillation and Reynolds number. Vandiver (V1), as well as Vandiver and Jong (V2) conducted experiments

to investigate the vibration response of long flexible cylinders subjected to vortex shedding in a steady, uniform current. In this study, displacement of the cylinder in the in-line and transverse directions were recorded. It was clearly evident that the displacement amplitude in the transverse direction was about twice the displacement amplitude in the in-line direction. Under lock-in conditions, drag coefficients in excess of 3.0 were measured with Reynolds numbers up to 2.2×10^4 .

An experimental investigation was performed by Takahashi et al.(T2) to study the in-line forces on oscillating cylinders. They presented a correlation for the energy dissipation for an oscillating body in a fluid flow in terms of energy dissipation for a stationary body in a fluid flow and that for an oscillating body in a fluid at rest. Extremely detailed experimental studies of the flow structure resulting from an oscillating cylinder were conducted by Ongoren and Rockwell (O1, O2). In their work, different modes of vortex shedding from an oscillating cylinder and the competition between the modes of vortex shedding are discussed. Moe and Wu (M2) carried out experimental studies of both forced and self excited vibration of a cylinder in a cross flow. Under the same conditions of oscillation, their study showed that both the forced and self excited vibration yield approximately the same variation of lift force with time.

A selective review of vortex induced oscillation of cylinders was given by Sarpkaya (S2). This review discusses various details of the vortex shedding mechanism and different characteristics of the lock-in phenomenon. In another comprehensive review, Bearman (B3) discusses various mathematical models

developed to predict vortex induced oscillations of cylindrical bodies. Recently, Griffin and Hall (G2) presented another review of both experimental and computational work done in the area of vortex shedding from oscillating cylinders in the in-line and transverse directions.

Several finite difference, finite volume and finite element simulations have been carried out using the concept of a non-inertial frame of reference. Most of the simulations were carried out using the primitive variables. Flow past an oscillating cylinder either in the in-line or transverse direction has been experimentally and numerically studied by several researchers for many years. Hurlbut et al. (H6) were the first to numerically study the problem of flow past a cylinder with in-line oscillation. They used the non-inertial coordinate transformation for the governing equations. In their simulations, the "lock-in" phenomenon was successfully predicted with the cylinder oscillating in the in-line direction to that of the mean flow. The same researchers (H7) extended their work for transverse oscillations of the cylinder in a uniform flow. Their model uses the Marker and Cell (MAC) method to solve the incompressible continuity and Navier-Stokes equations in terms of pressure and velocity. Later, Chilukuri (C1) studied the problem of a transversely oscillating cylinder using the non-inertial coordinate transformation and Simplified Marker and Cell (SMAC) method to solve the governing equations in primitive variable form. At large vibration amplitudes, amplification of the mean drag and reduction of mean lift were numerically predicted with transverse oscillation.

Tamura et al. (T4, T5) used a generalized coordinate transformation to study the forced and vortex induced vibration of a cylinder in the Reynolds number range of 3×10^3 to 6×10^5 . The MAC method was used to solve the governing equations in the primitive variable form in conjunction with a third order upwinding scheme for the convective terms. The drag in the critical regime ($Re > 10^5$) was predicted to be considerably smaller than in the subcritical regime ($Re \leq 10^5$). Lecointe and Piquet (L1) carried out a numerical study of flow structure in the wake of an oscillating cylinder in the in-line and transverse directions using a stream function and vorticity formulation. A similar formulation and numerical approach is used in the present investigation. In their study, both asymmetric and symmetric vortex shedding was predicted in the case of in-line oscillation under different values of oscillation frequency. A numerical solution for the vortex induced vibration of a cylinder in a cross flow was given by Berger and Rokni (B5). The coupled Navier-Stokes and rigid body motion equations were solved to obtain the time evolution of the displacement of the cylinder in the in-line and transverse directions, as well as the drag and lift forces. Triantafyllou and Karniadakis (T9) calculated the fluid forces on a cylinder oscillating transversely to a uniform flow during an amplitude-modulated ("beating") motion and compared with the numerical results obtained with the harmonic oscillation of the cylinder. The simulation was carried out using the spectral element method. The numerical results show that the beating motion of the cylinder results in a reduction of the mean drag and an increase in the fluctuating drag, compared to the values

obtained from the harmonically oscillating cylinders.

A finite element solution for 2-D flow over a transversely oscillating cylinder was obtained by Anagnostopoulos (A1) using the vorticity-stream function formulation. In this study, the mesh system was translated with the cylinder at each time step and the field was interpolated to the new nodal points. A similar method of translating the mesh system was used by Mittal and Tezduyar (M1) in order to solve the problems of both forced and vortex induced oscillation of the cylinder in a cross flow. The computations were based on the stabilized space-time finite element formulation. A direct finite element simulation was carried out by Li et al. (L3) to study the response of an oscillating cylinder in uniform flow and in the wake of an upstream cylinder. For a cylinder oscillating in the wake of an upstream cylinder, the flow structure was strongly influenced by the distance between the two cylinders.

Rao et al. (R1) performed a numerical simulation of flow around a transversely and longitudinally oscillating cylinder in a cross flow at Reynolds numbers of 4×10^3 and 4×10^4 . A moving grid system based on a time dependent coordinate transformation was employed to solve the governing equations. Detailed frequency analyses of the drag and lift forces were presented in their study.

2.2.2 With Heat Transfer

Many experimental investigations have shown that oscillation of the cylinder in a still fluid medium results in an increased heat transfer rate. In the case of

an oscillating cylinder in a cross flow, fewer experimental studies have been reported in the literature. Hegge Zijnen (H5) observed a decrease in the heat transfer rate at a Reynolds number of 5 with the cylinder undergoing oscillation in the direction in-line to that of the mean flow. Hegge Zijnen presented an equation of a general form relating the Nu_m , free stream velocity and the velocity amplitudes in the in-line and transverse directions. This relation is modified to fit Kramers' correlation and is presented as follows

$$Nu_m = 0.42 + 0.57 (1 - 1/16A_x^2 + 1/8A_y^2) Re^{1/2}. \quad (2.3)$$

This equation was validated for the case of in-line oscillation of the cylinder for $Re < 5$ and $A_x < 0.5$.

Anantanarayanan and Ramachandran (A2) investigated the influence of vibration on heat transfer from electrically heated Nichrome wire to an air stream flowing parallel to the wire. Both frequency and amplitude of vibration increased the heat transfer coefficient by as much as 130 percent. Later, Sreenivasan and Ramachandran (S6) experimentally studied the effects of the oscillation of a cylinder in the direction transverse to that of the air stream. No appreciable change in the heat transfer coefficient was observed with a maximum vibrational velocity amplitude of 0.2 in the Reynolds number range of 2500 to 15000.

The effect of oscillation of a cylinder in the in-line direction on the instantaneous local heat transfer coefficient was investigated by Mori and Tokuda (M4) with the use of an optical method. At smaller velocity amplitudes of oscillation, it was concluded that the distribution of the Nusselt number in the

circumferential direction is almost similar to that in the upstream part of a stationary cylinder in a cross flow. Other investigators such as Kezios and Prasanna (K1) reported a 20% increase in the average heat transfer coefficient with a transversely oscillating cylinder. At a Reynolds number of 3500, Saxena and Laird (S3) observed that some local heat transfer coefficients were up to 60% larger with a vertical cylinder undergoing forced oscillations in the direction transverse to the mean water flow. Due to the larger flow disturbances that result from the wake capture, the largest increases in local heat transfer coefficient occurred on the downstream side of the cylinder. Leung et al. (L2) observed an enhanced heat transfer rate for Reynolds numbers less than about 15000 with in-line oscillation.

In order to overcome the directional ambiguity associated with the hot-wire anemometers, Fernandez (F1) and Heckadon and Wong (H3) investigated the response of oscillating hot-wire anemometers. In these studies, the wire was oscillated in a frequency range of 50-90 Hz and at different velocity amplitudes of oscillation. The instantaneous hot-wire voltage responses were recorded at very low Reynolds numbers ($Re < 1.0$). These results are compared with the computational results in the present investigation.

At Reynolds numbers 1400, 2100 and 3500, Takahashi and Endoh (T1) experimentally investigated the effects of in-line oscillation of the cylinder on the heat transfer rate at various vibrational Reynolds numbers. In this study, it was concluded that the heat transfer rate increased during the in-line oscillation above

certain velocity amplitude. In the literature, no conclusive experimental results have been reported regarding the effects that an oscillating cylinder has on the forced or mixed convective heat transfer.

To the candidate's knowledge, no numerical simulation has been reported to study the effects of oscillation of the cylinder on the forced or the mixed convective heat transfer. It was also found that no numerical investigation has been reported for the case of flow past a cylinder with combined oscillation, i.e., the cylinder oscillating in the in-line and transverse directions simultaneously.

Chapter III

FORMULATION

The physical system consists of a long horizontal cylinder oscillating in a cross flow of air. The unsteady flow past an oscillating cylinder can be treated as a two-dimensional problem provided the length to diameter ratio of the cylinder is very large. To formulate the problem it is assumed that: (a) the fluid motion and temperature distribution are two-dimensional (2-D), (b) the fluid is Newtonian and incompressible, (c) frictional heating is negligible, (d) fluid properties are constant except for the density variation with temperature, (e) the laminar flow is uniform at an infinite distance upstream, and (f) the surface temperature of the cylinder is uniform and higher than the ambient temperature.

3.1 Non-inertial Coordinate Transformation

In general, the boundaries of the cylinder travelling through a finite difference grid system do not coincide with the computational cell boundaries at each time step. An alignment of the solid boundary and the computational cells is necessary to allow for the proper specification of no-slip wall boundary conditions. One method to circumvent this problem is to translate the grid system at each time step and interpolate the dependent variables in the old grid locations to new translated grid locations. This method is computationally very expensive. An easier

way of accomplishing the same objective is to use a non-inertial coordinate transformation.

In this method, the grid system is attached to the oscillating cylinder. The effect of this attached grid system is the addition of a relative acceleration term in the Navier-Stokes equations. This can be demonstrated by considering a simple form of the x-momentum equation as follows:

$$\rho \frac{Du'}{Dt} = f_x \quad (3.1)$$

where u' is the absolute velocity of the fluid in the x-direction. The above equation is a statement of Newton's second law and is valid only when Du'/Dt is the absolute acceleration with respect to an inertial frame of reference. Therefore, in a non-inertial coordinate system, the velocity term must include the velocity of the coordinate system relative to an inertial reference frame. Equation (3.1) becomes

$$\rho \frac{D(u+u_c)}{Dt} = f_x \quad (3.2)$$

where u is the velocity of the fluid relative to the non-inertial reference frame and u_c is the absolute velocity of the non-inertial reference frame. If the velocity of the reference frame is only time dependent, Equation (3.2) becomes

$$\rho \left(\frac{Du}{Dt} + \frac{du_c}{dt} \right) = f_x \quad (3.3)$$

Thus the result of attaching the computational grid system to the oscillating

cylinder is the addition of a simple acceleration term which is constant over the field at each time step. Using the concept of the non-inertial transformation, the governing equations for the present problem are presented in the following section.

3.2 Governing Equations

The isothermal cylinder is forced to oscillate sinusoidally with velocities, $A'_x \sin(2\pi(t - t_d)/t_x)$ and $A'_y \sin(2\pi(t - t_d)/t_y - \phi)$ in the in-line and transverse directions respectively, relative to the upstream uniform velocity, U_∞ , as indicated in figure 3.1. A'_x and A'_y are the velocity amplitudes of the oscillating cylinder in x' and y' directions respectively. The phase difference, ϕ , between the in-line and transverse oscillations is set equal to zero in this study. The time delay, t_d , is the time allowed for the development of a stable alternating vortex street in the wake of a stationary cylinder.

The governing equations for a two-dimensional flow problem are the continuity equation, two momentum component equations and the energy equation. In order to incorporate buoyancy forces due to the temperature difference between the cylinder surface and the fluid in the free stream, the Boussinesq approximation is used in the momentum equations. With the Boussinesq approximation, the density of the fluid is taken as being temperature dependent only in the buoyancy force term. Thus, within the Boussinesq approximation, the four governing

equations (one continuity, two momentum and one energy) in Cartesian coordinates are given below.

Continuity Equation

$$\frac{\partial u}{\partial x} + \frac{\partial v}{\partial y} = 0 \quad (3.4)$$

Momentum Equations

In the x - direction

$$\frac{Du}{Dt} + a'_{cx} = -\frac{1}{\rho} \frac{\partial p}{\partial x} + \nu \nabla^2 u \quad (3.5)$$

In the y - direction

$$\frac{Dv}{Dt} + a'_{cy} = -\frac{1}{\rho} \frac{\partial p}{\partial y} + \nu \nabla^2 v + g\beta(T-T_\infty) \quad (3.6)$$

Energy Equation

$$\frac{DT}{Dt} = \alpha \nabla^2 T \quad (3.7)$$

where

$$\frac{D}{Dt} = \frac{\partial}{\partial t} + u \frac{\partial}{\partial x} + v \frac{\partial}{\partial y}$$

$$\nabla^2 = \frac{\partial^2}{\partial x^2} + \frac{\partial^2}{\partial y^2}$$

It is convenient to transform the above governing equations into polar coordinates (r,θ,t) as given below.

Continuity Equation

$$\frac{\partial(r v_r)}{\partial r} + \frac{\partial v_\theta}{\partial \theta} = 0 \quad (3.8)$$

Momentum Equations

In the r - direction

$$\begin{aligned} \frac{Dv_r}{Dt} - \frac{v_\theta^2}{r} + [a'_{cx}\cos\theta + a'_{cy}\sin\theta] &= -\frac{1}{\rho} \frac{\partial p}{\partial r} \\ + v \left(\nabla^2 v_r - \frac{v_r}{r^2} - \frac{2}{r^2} \frac{\partial v_\theta}{\partial \theta} \right) &+ g\beta(T-T_\infty)\sin\theta \end{aligned} \quad (3.9)$$

In the θ - direction

$$\begin{aligned} \frac{Dv_\theta}{Dt} + \frac{v_r v_\theta}{r} + [-a'_{cx}\sin\theta + a'_{cy}\cos\theta] &= -\frac{1}{\rho r} \frac{\partial p}{\partial \theta} \\ + v \left(\nabla^2 v_\theta - \frac{v_\theta}{r^2} + \frac{2}{r^2} \frac{\partial v_r}{\partial \theta} \right) &+ g\beta(T-T_\infty)\cos\theta \end{aligned} \quad (3.10)$$

Energy Equation

$$\frac{DT}{Dt} = \alpha \nabla^2 T \quad (3.11)$$

where

$$\begin{aligned} \frac{D}{Dt} &= \frac{\partial}{\partial t} + v_r \frac{\partial}{\partial r} + \frac{v_\theta}{r} \frac{\partial}{\partial \theta} \\ \nabla^2 &= \frac{\partial^2}{\partial r^2} + \frac{1}{r} \frac{\partial}{\partial r} + \frac{1}{r^2} \frac{\partial^2}{\partial \theta^2} \end{aligned}$$

Although it is possible to obtain numerical solutions for the primitive variables, it is advantageous to solve this problem using the vorticity-stream function formulation. The use of the vorticity-stream function formulation eliminates the pressure variable and hence reduces the number of equations to be solved by one.

3.3 Vorticity - Stream Function Formulation

The relative radial and tangential velocities are related to the stream function as follows

$$v_r = \frac{1}{r} \frac{\partial \psi}{\partial \theta}, \quad v_\theta = -\frac{\partial \psi}{\partial r}. \quad (3.12)$$

The vorticity is defined as

$$\omega = \frac{1}{r} \left(\frac{\partial(v_\theta r)}{\partial r} - \frac{\partial v_r}{\partial \theta} \right) \quad (3.13)$$

By introducing the stream function and vorticity into the continuity and momentum equations, they can be simplified and reduced to two equations: the vorticity transport equation and a Poisson equation for the stream function. By differentiating equation (3.9) with respect to θ and equation (3.10) with respect to r , subtracting one from another and subsequently using the continuity equation (3.8), the vorticity transport equation is obtained as given below.

Vorticity Transport Equation

$$\begin{aligned} \frac{\partial \omega}{\partial t} + \frac{1}{r} \left[\frac{\partial}{\partial r} \left(\omega \frac{\partial \psi}{\partial \theta} \right) - \frac{\partial}{\partial \theta} \left(\omega \frac{\partial \psi}{\partial r} \right) \right] = \nu \nabla^2 \omega \\ + g\beta \left(\frac{\partial T}{\partial r} \cos \theta - \frac{1}{r} \frac{\partial T}{\partial \theta} \sin \theta \right), \end{aligned} \quad (3.14)$$

where

$$\nabla^2 = \frac{\partial^2}{\partial r^2} + \frac{1}{r} \frac{\partial}{\partial r} + \frac{1}{r^2} \frac{\partial^2}{\partial \theta^2}$$

The definition of vorticity yields the Poisson equation for the stream function,

$$\omega = -\nabla^2 \psi. \quad (3.15)$$

With the use of a non-inertial frame of reference the vorticity transport equation retains the same form for both the oscillating and stationary cylinder problem. It is to be noticed that both the pressure term and the additional acceleration terms are eliminated in the vorticity transport equation. The energy equation in the non-inertial frame of reference attached to the cylinder is given as follows:

Energy Equation

$$\frac{\partial T}{\partial t} + \frac{1}{r} \left[\frac{\partial}{\partial r} \left(T \frac{\partial \psi}{\partial \theta} \right) - \frac{\partial}{\partial \theta} \left(T \frac{\partial \psi}{\partial r} \right) \right] = \alpha \nabla^2 T \quad (3.16)$$

High vorticity and temperature gradients exist near the surface of the cylinder. In order to achieve a more accurate numerical solution, it is essential to have a finer grid near the cylinder. This can be accomplished by the use of the log-polar coordinate transformation given by:

$$r/R = e^{a\xi} \quad \text{and} \quad \theta = a\eta \quad (3.17)$$

where ξ and η are the transformed coordinates and "a" is the transformation parameter which is set equal to π for this study. This log-polar coordinate transformation allows us to have a uniform grid in a transformed rectangular domain. The nondimensional variables are defined as:

$$\begin{aligned} \tau &= \frac{t U_{\infty}}{R}, \quad \Psi = \frac{\psi}{RU_{\infty}}, \quad \Omega = \frac{\omega R}{U_{\infty}}, \quad \Phi = \frac{T - T_{\infty}}{T_s - T_{\infty}}, \quad V_r = \frac{v_r}{U_{\infty}}, \quad V_{\theta} = \frac{v_{\theta}}{U_{\infty}}, \\ Re &= \frac{2RU_{\infty}}{\nu}, \quad Gr = \frac{g\beta(T_s - T_{\infty})D^3}{\nu^2}, \quad Pr = \frac{\nu}{\alpha}, \\ A_x &= \frac{A'_x}{U_{\infty}}, \quad A_y = \frac{A'_y}{U_{\infty}}, \quad F_x = \frac{2R}{t_x U_{\infty}}, \quad F_y = \frac{2R}{t_y U_{\infty}} \end{aligned}$$

After applying the log-polar coordinate transformation and nondimensionalizing, the vorticity transport and energy equations are

$$\begin{aligned} g(\xi) \frac{\partial \Omega}{\partial \tau} + \frac{\partial}{\partial \xi} \left(\Omega \frac{\partial \Psi}{\partial \eta} \right) - \frac{\partial}{\partial \eta} \left(\Omega \frac{\partial \Psi}{\partial \xi} \right) &= \frac{2}{Re} \nabla^2 \Omega \\ + \sqrt{g(\xi)} \frac{Gr}{2Re^2} \left(\frac{\partial \Phi}{\partial \xi} \cos(a\eta) - \frac{\partial \Phi}{\partial \eta} \sin(a\eta) \right) & \end{aligned} \quad (3.18)$$

$$g(\xi) \Omega = -\nabla^2 \Psi \quad (3.19)$$

$$g(\xi) \frac{\partial \Phi}{\partial \tau} + \frac{\partial}{\partial \xi} \left(\Phi \frac{\partial \Psi}{\partial \eta} \right) - \frac{\partial}{\partial \eta} \left(\Phi \frac{\partial \Psi}{\partial \xi} \right) = \frac{2}{Re Pr} \nabla^2 \Phi \quad (3.20)$$

where

$$g(\xi) = a^2 e^{2a\xi}$$

and

$$\nabla^2 = \frac{\partial^2}{\partial \xi^2} + \frac{\partial^2}{\partial \eta^2} .$$

It is to be noted that both the vorticity equation (3.18) and the energy equation (3.20) are parabolic in time and the stream function equation (3.19) is elliptic in space. The stream function equation is coupled with both the vorticity and energy equations. The vorticity and the energy equations are coupled through the buoyancy force. Furthermore, the vorticity and the energy equation are nonlinear due to the convective terms.

The nondimensional relative velocity components are given by

$$V_r = \frac{U}{\sqrt{g(\xi)}} , \quad V_\theta = \frac{V}{\sqrt{g(\xi)}} . \quad (3.21)$$

where

$$U = \frac{\partial \Psi}{\partial \eta} , \quad V = - \frac{\partial \Psi}{\partial \xi}$$

The main goal of the present problem is to seek $\Omega(\xi, \eta, \tau)$, $\Phi(\xi, \eta, \tau)$ and $\Psi(\xi, \eta, \tau)$ which satisfy the three partial differential equations (3.18), (3.19) and (3.20), as well as the following initial and boundary conditions.

3.4 Initial and Boundary Conditions

Initially (at $t < 0$), the vorticity, stream function and temperature fields are zero everywhere in the computational domain. The use of a non-inertial frame of reference adds unsteady components to the boundary velocities. To an observer attached to the cylinder, the fluid velocity at the cylinder surface is zero from the no-slip condition. The velocity component in the x-direction at the outer boundary is the sum of the free stream velocity and the negative of the instantaneous cylinder velocity in the x-direction. The velocity component in the y-direction at the outer boundary is the negative of the cylinder velocity in the y-direction. The upstream relative free stream velocities are as follows

$$u = U_{\infty} - A'_x \sin(2\pi(t-t_d)/t_x) \text{ and } v = -A'_y \sin(2\pi(t-t_d)/t_y - \phi). \quad (3.22)$$

In polar coordinates, the radial and tangential far-field velocity boundary conditions are obtained by modifying the potential flow solution of Janna (J4):

$$v_r = \left[\{U_{\infty} - A'_x \sin(2\pi(t-t_d)/t_x)\}^2 + \{A'_y \sin(2\pi(t-t_d)/t_y - \phi)\}^2 \right]^{1/2} (1 - R^2/r^2) \cos(\theta - \varepsilon) \quad (3.23)$$

$$v_{\theta} = -\left[\{U_{\infty} - A'_x \sin(2\pi(t-t_d)/t_x)\}^2 + \{A'_y \sin(2\pi(t-t_d)/t_y - \phi)\}^2 \right]^{1/2} (1 + R^2/r^2) \sin(\theta - \varepsilon),$$

$$\text{where } \varepsilon = \tan^{-1} \left(\frac{-A'_y \sin(2\pi(t-t_d)/t_y - \phi)}{U_{\infty} - A'_x \sin(2\pi(t-t_d)/t_x)} \right).$$

A constant temperature (T_s) boundary condition is assumed on the cylinder surface. These boundary conditions are interpreted in terms of non-dimensional stream function, vorticity and temperature in the following sections.

3.4.1 Boundary Condition on the Cylinder Surface

The boundary conditions for the nondimensional stream function on the cylinder surface is given by

$$\Psi = \frac{\partial \Psi}{\partial \xi} = 0 \quad \text{on} \quad \xi = 0. \quad (3.24)$$

These conditions correspond to the no-slip boundary condition on the cylinder surface.

The vorticity boundary condition at the cylinder surface is given by applying equation (3.19) locally as given below.

$$\Omega_o = -\frac{1}{g(\xi)_o} (\nabla^2 \Psi)_o \quad (3.25)$$

The subscript "o" represents a point on the surface ($\xi = 0$). On the surface of the cylinder

$$g(\xi)_o = a^2$$

and

$$\left(\frac{\partial U}{\partial \eta} \right)_o = 0, \quad \text{hence} \quad \left(\frac{\partial^2 \Psi}{\partial \eta^2} \right)_o = 0.$$

Now, the vorticity at the surface of the cylinder can be written as

$$(\Omega)_o = -\frac{1}{a^2} \left(\frac{\partial^2 \Psi}{\partial \xi^2} \right)_o \quad (3.26)$$

The isothermal boundary condition on the cylinder surface is represented as

$$\Phi = 1 \text{ on } \xi = 0. \quad (3.27)$$

3.4.2 Far-field Boundary Conditions

The time-dependent far-field boundary condition for the stream function is obtained by modifying the potential flow solution of Janna (J4):

$$\Psi = 2\sqrt{\left[1 - A_x \sin(\pi(\tau - \tau_d) F_x)\right]^2 + \left[A_y \sin(\pi(\tau - \tau_d) F_y - \phi)\right]^2} \sinh(a\xi_{\infty}) \sin(a\eta - \epsilon) \quad (3.28)$$

where

$$\epsilon = \tan^{-1} \left[\frac{-A_y \sin(\pi(\tau - \tau_d) F_y - \phi)}{1 - A_x \sin(\pi(\tau - \tau_d) F_x)} \right].$$

The far-field vorticity boundary conditions (L5) are

$$\left[g(\xi) \frac{\partial \Omega}{\partial \tau} + \frac{\partial}{\partial \xi} \left(\Omega \frac{\partial \Psi}{\partial \eta} \right) - \frac{\partial}{\partial \eta} \left(\Omega \frac{\partial \Psi}{\partial \xi} \right) \right]_{\xi_{\infty}} = 0, \quad 0 < \eta < \frac{1}{2}, \quad \frac{3}{2} < \eta < 2, \quad (3.29)$$

and

$$\Omega = 0, \quad \frac{1}{2} \leq \eta \leq \frac{3}{2}.$$

Similarly, the far-field boundary conditions for the temperature are taken to be

$$\left[g(\xi) \frac{\partial \Phi}{\partial \tau} + \frac{\partial}{\partial \xi} \left(\Phi \frac{\partial \Psi}{\partial \eta} \right) - \frac{\partial}{\partial \eta} \left(\Phi \frac{\partial \Psi}{\partial \xi} \right) \right]_{\xi} = 0, \quad 0 < \eta < \frac{1}{2}, \quad \frac{3}{2} < \eta < 2, \quad (3.30)$$

and

$$\Phi = 0, \quad \frac{1}{2} \leq \eta \leq \frac{3}{2}.$$

The time-dependent downstream boundary conditions for the vorticity and the temperature are called the "radiant-Sommerfeld like" conditions where the diffusion of vorticity and temperature are neglected. Upstream of the cylinder, the irrotational boundary condition is always valid.

In the present computational investigation, the governing equations (3.18), (3.19) and (3.20) are to be solved with the boundary conditions given by equations (3.24), (3.26), (3.27), (3.28), (3.29) and (3.30).

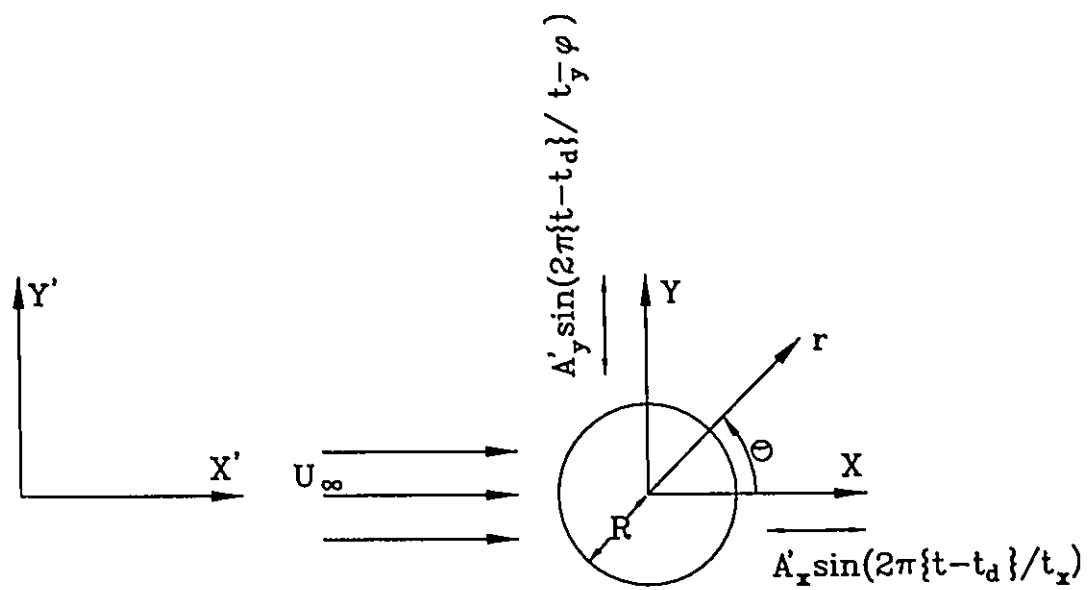


Figure 3.1 Coordinate systems

Chapter IV

NUMERICAL PROCEDURE

The three governing equations to be solved in this study are the vorticity transport equation, the stream function equation and the energy equation. Figure 4.1 shows the computational domain in the (ξ, η) coordinate system. The governing equations can be discretized in space using a central differencing scheme as follows:

Vorticity transport equation

$$\begin{aligned}
 g(\xi_j) \frac{\partial \Omega_{ij}}{\partial \tau} = & - \left(\frac{U_{i,j+1} \Omega_{i,j+1} - U_{i,j-1} \Omega_{i,j-1}}{2\Delta\xi} \right) - \left(\frac{V_{i+1,j} \Omega_{i+1,j} - V_{i-1,j} \Omega_{i-1,j}}{2\Delta\eta} \right) \\
 & + \frac{2}{Re} \left(\frac{\Omega_{i,j+1} - 2\Omega_{ij} + \Omega_{i,j-1}}{\Delta\xi^2} + \frac{\Omega_{i+1,j} - 2\Omega_{ij} + \Omega_{i-1,j}}{\Delta\eta^2} \right) \quad (4.1) \\
 & + \sqrt{g(\xi_j)} \frac{Gr}{2Re^2} \left(\frac{\Phi_{i,j+1} - \Phi_{i,j-1}}{2\Delta\xi} \cos(a\eta_j) - \frac{\Phi_{i+1,j} - \Phi_{i-1,j}}{2\Delta\eta} \sin(a\eta_j) \right)
 \end{aligned}$$

Stream function equation

$$-g(\xi_j) \Omega_{ij} = \left(\frac{\Psi_{i,j+1} - 2\Psi_{ij} + \Psi_{i,j-1}}{\Delta\xi^2} + \frac{\Psi_{i+1,j} - 2\Psi_{ij} + \Psi_{i-1,j}}{\Delta\eta^2} \right) \quad (4.2)$$

Energy equation

$$g(\xi_j) \frac{\partial \Phi_{i,j}}{\partial \tau} = - \left(\frac{U_{i,j+1} \Phi_{i,j+1} - U_{i,j-1} \Phi_{i,j-1}}{2\Delta\xi} \right) - \left(\frac{V_{i+1,j} \Phi_{i+1,j} - V_{i-1,j} \Phi_{i-1,j}}{2\Delta\eta} \right) \quad (4.3)$$

$$+ \frac{2}{Re \, Pr} \left(\frac{\Phi_{i,j+1} - 2\Phi_{i,j} + \Phi_{i,j-1}}{\Delta\xi^2} + \frac{\Phi_{i+1,j} - 2\Phi_{i,j} + \Phi_{i-1,j}}{\Delta\eta^2} \right)$$

The subscripts i,j represent the (i,j) mesh point in the (η, ξ) coordinates. In order to solve these finite difference equations in time and space, an appropriate numerical method must be selected.

4.1 Numerical Methods

The vorticity transport and the energy equations are solved numerically using the alternating direction implicit (ADI) scheme. Borthwick (B6) showed that the ADI scheme is more reliable and more accurate than the upwind directional difference explicit scheme. The time derivative is approximated using a forward difference scheme. The vorticity transport equation in an ADI two step finite difference form is given as follows:

$$\begin{aligned}
& \frac{2g(\xi_j)}{\Delta\tau} \Omega_{i,j}^{n+1/2} + \left(\frac{(V^n \Omega^{n+1/2})_{i+1,j} - (V^n \Omega^{n+1/2})_{i-1,j}}{2\Delta\eta} \right) - \frac{2}{Re} \left(\frac{(\Omega_{i+1,j} - 2\Omega_{i,j} + \Omega_{i-1,j})^{n+1/2}}{\Delta\eta^2} \right) \\
& = \frac{2g(\xi_j)}{\Delta\tau} \Omega_{i,j}^n - \left(\frac{(U^n \Omega^n)_{i,j+1} - (U^n \Omega^n)_{i,j-1}}{2\Delta\xi} \right) + \frac{2}{Re} \left(\frac{(\Omega_{i,j+1} - 2\Omega_{i,j} + \Omega_{i,j-1})^n}{\Delta\xi^2} \right) \\
& + \sqrt{g(\xi_j)} \frac{Gr}{2Re^2} \left(\frac{(\Phi^{n+1})_{i,j+1} - (\Phi^{n+1})_{i,j-1}}{2\Delta\xi} \cos(a\eta_j) - \frac{(\Phi^{n+1})_{i+1,j} - (\Phi^{n+1})_{i-1,j}}{2\Delta\eta} \sin(a\eta_j) \right) \quad (4.4)
\end{aligned}$$

$$\begin{aligned}
& \frac{2g(\xi_j)}{\Delta\tau} \Omega_{i,j}^{n+1} + \left(\frac{(U^n \Omega^{n+1})_{i,j+1} - (U^n \Omega^{n+1})_{i,j-1}}{2\Delta\xi} \right) - \frac{2}{Re} \left(\frac{(\Omega_{i,j+1} - 2\Omega_{i,j} + \Omega_{i,j-1})^{n+1}}{\Delta\xi^2} \right) \\
& = \frac{2g(\xi_j)}{\Delta\tau} \Omega_{i,j}^{n+1/2} - \left(\frac{(V^n \Omega^{n+1/2})_{i+1,j} - (V^n \Omega^{n+1/2})_{i-1,j}}{2\Delta\eta} \right) + \frac{2}{Re} \left(\frac{(\Omega_{i+1,j} - 2\Omega_{i,j} + \Omega_{i-1,j})^{n+1/2}}{\Delta\eta^2} \right) \\
& + \sqrt{g(\xi_j)} \frac{Gr}{2Re^2} \left(\frac{(\Phi^{n+1})_{i,j+1} - (\Phi^{n+1})_{i,j-1}}{2\Delta\xi} \cos(a\eta_j) - \frac{(\Phi^{n+1})_{i+1,j} - (\Phi^{n+1})_{i-1,j}}{2\Delta\eta} \sin(a\eta_j) \right) \quad (4.5)
\end{aligned}$$

The superscript "n" represents the nth time step. Similarly, the energy equation can be written in the finite difference form by replacing the dependent variable with Φ and the Reynolds number with the product of Reynolds number and Prandtl number. The ADI two step finite difference form of the energy equation is as follows:

$$\begin{aligned}
& \frac{2g(\xi_j)}{\Delta\tau} \Phi_{i,j}^{n+1/2} + \left(\frac{(V^n \Phi^{n+1/2})_{i+1,j} - (V^n \Phi^{n+1/2})_{i-1,j}}{2\Delta\eta} \right) - \frac{2}{RePr} \left(\frac{(\Phi_{i+1,j} - 2\Phi_{i,j} + \Phi_{i-1,j})^{n+1/2}}{\Delta\eta^2} \right) \\
& = \frac{2g(\xi_j)}{\Delta\tau} \Phi_{i,j}^n - \left(\frac{(U^n \Phi^n)_{i,j+1} - (U^n \Phi^n)_{i,j-1}}{2\Delta\xi} \right) + \frac{2}{RePr} \left(\frac{(\Phi_{i,j+1} - 2\Phi_{i,j} + \Phi_{i,j-1})^n}{\Delta\xi^2} \right) \quad (4.6)
\end{aligned}$$

$$\begin{aligned}
& \frac{2g(\xi_j)}{\Delta\tau} \Phi_{i,j}^{n+1} + \left(\frac{(U^n \Phi^{n+1})_{i,j+1} - (U^n \Phi^{n+1})_{i,j-1}}{2\Delta\xi} \right) - \frac{2}{RePr} \left(\frac{(\Phi_{i,j+1} - 2\Phi_{i,j} + \Phi_{i,j-1})^{n+1}}{\Delta\xi^2} \right) \\
& = \frac{2g(\xi_j)}{\Delta\tau} \Phi_{i,j}^{n+1/2} - \left(\frac{(V^n \Phi^{n+1/2})_{i+1,j} - (V^n \Phi^{n+1/2})_{i-1,j}}{2\Delta\eta} \right) + \frac{2}{RePr} \left(\frac{(\Phi_{i+1,j} - 2\Phi_{i,j} + \Phi_{i-1,j})^{n+1/2}}{\Delta\eta^2} \right) \quad (4.7)
\end{aligned}$$

At every time step, the stream function equation is solved by the iteration technique of successive line over-relaxation (SLOR). The appropriate finite difference form of the stream function equation is given by

$$\begin{aligned}
& \frac{\Psi_{i-1,j}^*}{\Delta\eta^2} - 2\Psi_{i,j}^* \left(\frac{1}{\Delta\eta^2} + \frac{1}{\Delta\xi^2} \right) + \frac{\Psi_{i+1,j}^*}{\Delta\eta^2} = - \left(\frac{\Psi_{i,j+1}^m + \Psi_{i,j-1}^{m+1}}{\Delta\xi^2} \right) - g(\xi_j) \Omega_{i,j}^{n+1} \quad (4.8) \\
& \Psi_{i,j}^{m+1} = \Psi_{i,j}^m + \lambda \left(\Psi_{i,j}^* - \Psi_{i,j}^m \right)
\end{aligned}$$

where λ is the relaxation parameter and the superscripts *, m and (m+1) represent the iteration levels. An optimum relaxation parameter, given by Son and Hanratty [S5], is used to enhance the convergence rate and given as follows:

$$\lambda = \frac{2}{1 + \pi \sqrt{\frac{1}{2} \left[\frac{1}{I^2} + \frac{1}{J^2} \right]}} \quad (4.9)$$

where I and J represent the number of grid points in the η and ξ directions, respectively.

The velocities in the convective terms are calculated using the fourth order accurate Hermitian relations and are given by

$$U_{i-1,j} + 4U_{ij} + U_{i+1,j} = \frac{3}{\Delta\eta}(\Psi_{i+1,j} - \Psi_{i-1,j}) \quad (4.10)$$

$$V_{i,j-1} + 4V_{ij} + V_{i,j+1} = \frac{-3}{\Delta\xi}(\Psi_{i,j+1} - \Psi_{i,j-1}) \quad (4.11)$$

The Hermitian relations have been used successfully by Loc and Bouard (L5) up to a Reynolds number of 9500. In order to solve the governing equations in finite difference form, appropriate boundary conditions must be imposed on the computational domain.

4.2 Boundary Conditions

On the boundaries $\eta = 0$ and $\eta = 2$, a cyclic boundary condition is imposed on the dependent variables. This implies that both the values and the spatial derivatives in the η direction for the vorticity, stream function and temperature are the same

on these two boundaries. The vorticity boundary condition on the cylinder ($\xi = 0$) can be approximated numerically in different ways. In this study, a second order accurate cubic polynomial approximation is used and is given by

$$\Omega_{t,0} = -\frac{1}{a^2} \left(\frac{8\Psi_{t,1} - \Psi_{t,2}}{2\Delta\xi^2} \right) \quad (4.12)$$

The vorticity on the cylinder must be calculated at every time step. The stream function on the cylinder ($\xi = 0$) is taken to be zero. The nondimensional temperature on the cylinder is taken as unity. At every time step, the far-field ($\xi = \xi_\infty$) conditions for the vorticity, stream function and the temperature are calculated using equations (3.28) , (3.29) and (3.30) respectively. The procedure for solving the governing equations with these boundary conditions is explained in the following section.

4.3 Solution Procedure

The solution procedure consisted of the following steps.

1. At $t = 0$, the stream function values were calculated assuming zero vorticity in the entire computational domain (i.e., obtained the solution of the homogenous form of equation (3.19) using the SLOR scheme).
2. A zero time step value of the wall vorticity was calculated using equation (4.12).
3. The velocities U and V were computed using the Hermitian relations given

in equations (4.10), (4.11).

4. At $t = \Delta t/2$, the temperature field was calculated using equation (4.6) and a periodic tridiagonal solver.
5. At $t = \Delta t$, the temperature field was calculated using equation (4.7) and a tridiagonal solver.
6. At $t = \Delta t/2$, the vorticity field was calculated using equation (4.4) and a periodic tridiagonal solver.
7. At $t = \Delta t$, the vorticity field was calculated using equation (4.5) and a tridiagonal solver.
8. At $t = \Delta t$, the new stream function values were obtained iteratively using equation (4.8).
9. At $t = \Delta t$, the new values for wall vorticity were calculated using equation (4.12).
10. Steps 3 to 9 were repeated for the desired time periods of oscillation of the cylinder.

In the initial stage of simulation, the cylinder was rotated counterclockwise and then clockwise for a small duration of time with a constant angular velocity. This numerical triggering procedure was required to initiate the alternating vortex street and is similar to the procedure used by Jordan and Fromm (J5). A non-dimensional time of 50 (τ_d) was allowed for the development of an alternating vortex street. The numerical solution obtained is first order accurate in time and second order accurate in space.

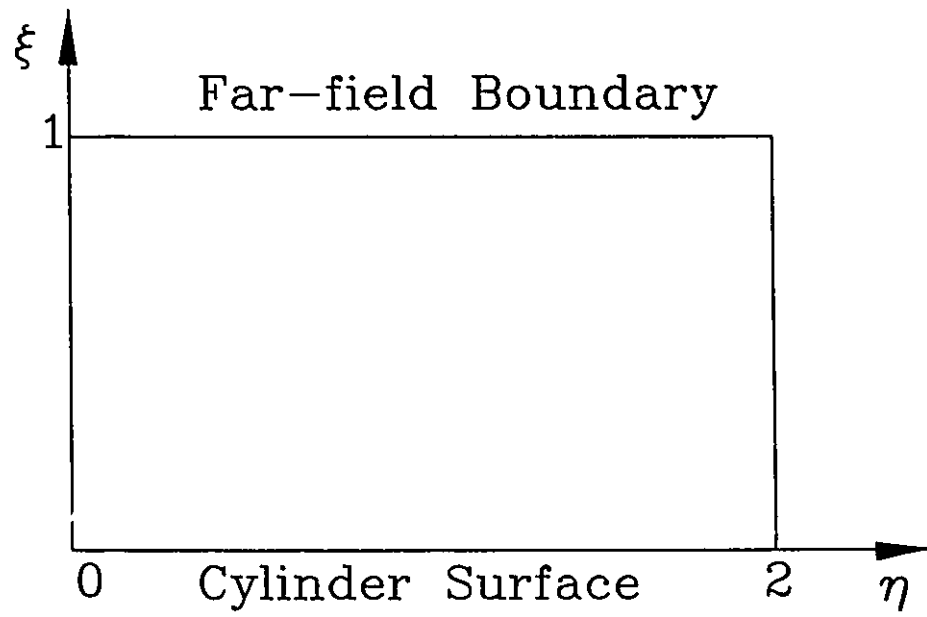


Figure 4.1 Computational Domain

Chapter V

RESULTS AND DISCUSSION

Numerical results for the problem of heat transfer from an oscillating cylinder in a cross flow are presented in the following sections. The first part of the chapter is concerned with the influence of the grid size, location of the far-field boundary and the magnitude of the numerical triggering on the numerical solution. A subsequent section deals with the validation of the present formulation with other available results. Following that section, the results obtained for the present problem of heat transfer from both stationary and oscillating cylinder in a cross flow are presented. In the last section, numerical results for the case of an oscillating hot-wire anemometer are compared with the available experimental results.

The heat transfer between the cylinder and the surrounding stream of fluid is calculated in the form of a nondimensional number, the Nusselt number. The local Nusselt number is calculated using the following equation.

$$Nu(\theta) = \frac{-2 \left(\frac{\partial \Phi}{\partial \xi} \right)_{\xi=0}}{a} \quad (5.1)$$

The average Nusselt number represents the net heat transfer from the cylinder surface to the fluid at any instant of time and is expressed as follows.

$$Nu_{avg} = \frac{1}{2\pi} \int_0^{2\pi} Nu(\theta) d\theta \quad (5.2)$$

In order to compare with the experimental results, it is essential to calculate the mean Nusselt number over a period of time. In this study, mean Nusselt number was calculated in any cycle of cylinder oscillation using the following expression.

$$Nu_m = \frac{1}{\tau_{cycle}} \int_0^{\tau_{cycle}} Nu_{avg}(\tau) d\tau \quad (5.3)$$

5.1 Dependency Tests

In order to reduce the influence of the grid size, location of the far-field boundary and the magnitude of numerical triggering on the time history of Nu_{avg} , and the mean Nusselt number, several dependency tests were conducted. These tests were carried out at a Reynolds number of 200 as most of the simulations in this study were at that Reynolds number.

5.1.1 Grid Dependency

Numerical simulations were conducted with grid sizes 101x81, 121x101 and 141x121 while keeping the far-field boundary location at $\xi = 1.0$. Figure 5.1 shows the time dependent Nu_{avg} with different grid sizes. The mean Nusselt numbers are listed in Table 5.1 for different grid sizes. The 121x101 and the 141x121 grids produce approximately the same time histories of Nu_{avg} and equal values of Nu_m . Hence, the grid size 121x101 was selected.

5.1.2 Location of the Far-field Boundary

The far-field boundary location was varied between $\xi = 0.8$ and $\xi = 1.2$. The number of grids were proportionately increased in the ξ direction ($\Delta\xi = \text{constant}$). The influence of the location of the far-field boundary on the average Nusselt number is shown in figure 5.2. The mean Nusselt numbers are listed in table 5.1 at different far-field boundary locations. It can be observed that the time history of Nu_{avg} with $\xi = 1$ and 1.2 have approximately the same mean value (Nu_m) and amplitude of variation. The phase difference between the Nu_{avg} variations may be attributed to the difference in the onset of vortex shedding with different far-field boundary locations. The far-field boundary location was chosen to be 1.0 .

5.1.3 Magnitude of Numerical Triggering

The circumferential velocity of the cylinder in the log-polar coordinates (V) is taken to be the numerical triggering parameter. The numerical simulations were carried out with V values of 3 , 5 and 10 as the magnitude of the numerical triggering. Figure 5.3 shows the influence of these parameters on the time dependent Nu_{avg} . The Nu_m values are listed in table 5.1 for different magnitudes of V . It can be concluded that the magnitude of numerical triggering influences the results only in the early stages of numerical simulation. After reaching the stage of alternate vortex shedding ($\tau \approx 50$), numerical triggering does not have any

significant influence on the time history of Nu_{avg} or on the Nu_m . The magnitude of the numerical triggering was chosen to be 3.

5.2 Validation

In order to validate the numerical model, simulations were run at Reynolds numbers of 5, 60, 100, 200, 500 and 1000. The Prandtl number was assumed to be equal to 0.707. The predicted mean Nusselt numbers, Strouhal numbers and drag coefficients are compared with the experimental values given by Kramers (K4) , Roshko (R3) and Tanida et al. (T7) in the following paragraphs.

Figure 5.4 shows the Nu_m variation with Reynolds number. The computed values of Nu_m agree well with the experimental results of Kramers (K4). At $Re = 200$, the error between the computed and experimental results is about -1.45%. The variation of the Strouhal number with the Reynolds number is shown in figure 5.5. The Strouhal numbers are obtained by taking the FFT of the lift variation and choosing the frequency with the largest amplitude. The computed values of Strouhal number are in good agreement with the experimental values (R3) up to a Reynolds number of 200. At Reynolds numbers of 500 and 1000, the Strouhal numbers are significantly overpredicted by the present computations. Figure 5.6 shows the variation of C_d with the Reynolds number. The predicted values of drag coefficients are in good agreement with the experimental values of Tanida et al. (T7) up to a Reynolds number of 500. At a Reynolds number of 1000, a large

discrepancy exists between the computed C_d and the measured value of C_d . Similar discrepancies were observed by other computational investigations both in the drag coefficient and the Strouhal number at higher Reynolds numbers. These discrepancies may be due to insufficient grid resolution and the three-dimensional nature of vortex shedding with finite length cylinders at high Reynolds numbers. Hence, the present numerical model can be considered valid up to a Reynolds number of 200.

In the following sections, the results are given in the form of local Nusselt number distribution on the cylinder, average Nusselt number, amplitude of the Nu_{avg} , mean Nusselt number and power spectrum of the average Nusselt number at various conditions of cylinder oscillation. The time histories of the Nu_{avg} are shown for $F_x = 2F_n$, i.e., the forcing frequency in the in-line direction which is equal to twice the Strouhal frequency and $F_y = F_n$, i.e., the forcing frequency in the transverse direction which is equal to the Strouhal frequency. In the case of combined oscillation, the time histories of the Nu_{avg} are shown for $F_x = 2F_n$ and $F_y = F_n$. The power spectrum of the Nu_{avg} is obtained by taking the FFT of the Nu_{avg} variation minus the mean Nusselt number. Forced and mixed convective heat transfer are represented by $Gr/Re^2 = 0$ and 1 respectively. Unless specified, all the isothermal contour maps presented in the following sections are with a contour interval of 0.05 and with the minimum and maximum levels of contour as 0.05 and 1.0 respectively.

5.3 Stationary Cylinder in a Cross Flow

The nondimensional natural shedding frequency (F_n) was determined from the present investigation to be equal to 0.2 which agrees exactly with the computed value by Lecointe and Piquet (L1). The corresponding nondimensional natural vortex shedding period (τ_n) is 10. Figures 5.7 and 5.8 show the time dependent average Nusselt number (Nu_{avg}) and the power spectra of the Nu_{avg} respectively for $Gr/Re^2 = 0$ and 1. With forced convection ($Gr/Re^2 = 0$), the Nu_{avg} was found to oscillate at twice the natural shedding frequency ($2F_n$) about a mean value of 7.47. This may be explained by the shedding of two vortices (one from the upper and the other from the lower half of the cylinder) in a complete vortex shedding cycle. In the case of mixed convection ($Gr/Re^2 = 1$), the Nu_{avg} was found to be oscillating at the natural shedding frequency (F_n) about a mean value of 7.61. This behaviour may be attributed to the strong presence of free convection near the cylinder surface. The amplitude of oscillation of the Nu_{avg} with forced convection was smaller than the case of mixed convection.

Figures 5.9 and 5.10 show the local Nusselt number distributions on the cylinder at different τ in a complete vortex shedding cycle at $Gr/Re^2 = 0$ and 1 respectively. It can be observed that the local Nusselt number distribution varies only on the downstream side of the cylinder where the vortices are shed alternately. In both the cases of forced convection and mixed convection, the

maximum heat transfer rate occurs at the upstream stagnation point. In the case of forced convection, minimum heat transfer occurs between the separation points and downstream stagnation point ($\theta \approx 51^\circ$ and 309°). With mixed convection, the location of minimum heat transfer always lies on the top half of the cylinder ($\theta \approx 51^\circ$).

Figures 5.11 , 5.12 and 5.13 show the contour maps of streamline, vorticity and isotherms respectively at the same instant of time ($\tau = 130.0$) for the case of forced convection. The streamline contour map clearly depicts the alternating vortex street in the wake and a vortex being shed from the top half of the cylinder. The vorticity generated on the cylinder surface is being convected and then diffused in the wake. As both vorticity and thermal energy is being transported by the flow in the wake, the contour maps of vorticity and isotherms have some similar features. A high concentration of vorticity and temperature contours exist near the cylinder surface. Similarly, figures 5.14 , 5.15 and 5.16 show the contour maps of streamline, vorticity and isotherms respectively at the same instant of time ($\tau = 130.0$) for the case of mixed convection.

5.4 Oscillating Cylinder in a Cross Flow

In the following sections, the numerical results obtained at a Reynolds number of 200 with the cylinder oscillating in the in-line direction ($a_x = 0.1D, 0.2D$

and $0.4D$), transverse direction ($a_y = 0.2D, 0.4D$ and $0.8D$) and combined in-line and transverse directions ($a_x = 0.2D, a_y = 0.2D, 0.4D$ and $0.8D$) are discussed. Figure 5.17 shows a schematic diagram of the sign conventions used with the displacement of the cylinder in the in-line and transverse directions.

5.4.1 In-line Oscillation

The cylinder was forced to oscillate in the in-line direction with a frequency parameter $F_x = 2F_n$ and with position amplitudes (a_x) of $0.1D, 0.2D$ and $0.4D$. The equivalent velocity amplitudes are $0.25, 0.5$ and 1.0 respectively. The selected frequency parameter corresponds to the mid-point lock-in frequency. The time variation of the position of the cylinder (x_c/D) and relative free stream velocity ($U^* = 1 - A_x \sin(\pi F_x \tau)$) are shown in figure 5.18 for reference.

Figures 5.19 and 5.20 show the time histories of Nu_{avg} at $Gr/Re^2 = 0$ and 1 respectively. The corresponding Nu_{avg} variations in a cycle of oscillation are shown in figures 5.21 and 5.22. The average Nusselt number reaches a maximum and a minimum value in a full cycle of forced oscillation. The maximum values of Nu_{avg} in all oscillation cycles are attained when the cylinder is moving in the opposite direction to that of the free stream flow (U_∞) and is slightly after the zero position of the cylinder ($\tau^* \approx 0.8$). The minimum value of Nu_{avg} occurs slightly after the point of minimum relative velocity ($\tau^* = 0.25$) for low values of amplitudes of oscillation

and moves later in the cycle as the amplitude of oscillation increases. The reason for the minimum value of Nu_{avg} to occur later than the point of minimum relative velocity is that the fluid surrounding the cylinder in the downstream location is warmer than the upstream location. The power spectra of the Nu_{avg} at $Gr/Re^2 = 0$ and 1 are shown in figures 5.23 and 5.24 respectively. Both with forced and mixed convection, the average Nusselt number oscillates at the forcing frequency of oscillation. With $a_x = 0.4D$, the higher harmonic of the forcing frequency also exists. At $Gr/Re^2 = 1$, a "sub" harmonic exists for $a_x = 0.1D$ which is equal to half of the forcing frequency of oscillation.

Figures 5.25 and 5.26 show variation of the amplitude of Nu_{avg} and the mean Nusselt number (Nu_m) with the position amplitudes of oscillation. Both the amplitude of Nu_{avg} and the Nu_m increase with the increasing a_x . With forced convection and $a_x = 0.4D$, an increase of 16.44% in Nu_m over the case of stationary cylinder is predicted. In the case of mixed convection, an increase of 14.65% in Nu_m is computed with $a_x = 0.4D$.

With $Gr/Re^2 = 0$, figures 5.27, 5.28 and 5.29 show the local Nusselt number distribution on the cylinder at different times in a full cycle of oscillation ($0 \leq \tau \leq 1$) at position amplitudes $a_x = 0.1D$, $0.2D$ and $0.4D$ respectively. Similarly, figures 5.30, 5.31 and 5.32 show the local Nusselt number distributions with $Gr/Re^2 = 1.0$. From these diagrams, the location and magnitudes of the maximum heat transfer

rate at different instants of time during one complete cycle of oscillation are taken and listed in tables 5.2 and 5.3 for the case of forced convection and mixed convection respectively. On the upstream side of the cylinder ($90^\circ < \theta < 270^\circ$), the Nusselt number distributions at $\tau^* = 0$ and $\tau^* = 1$ are approximately the same. With $a_x = 0.1D$, the maximum heat transfer rate always occurs near the upstream stagnation point ($\theta = 180^\circ$). However, with $a_x = 0.2D$ and $0.4D$, the location of the maximum local Nusselt number is near the downstream stagnation point when the cylinder is moving in the same direction as that of the flow (i.e., at $\tau^* = 0.25$). With mixed convection, the local Nusselt number distribution is more asymmetric than with forced convection alone.

Figures 5.33 to 5.37 show the contour maps of the isotherms for the case of forced convection at different stages in a full cycle of oscillation ($a_x = 0.2D$). The isothermal contours do not repeat after one cycle as seen from figures 5.33 and 5.37. The reason is that the period of oscillation is half of the natural vortex shedding period. Figures 5.38 to 5.42 show the isothermal contours with mixed convection ($a_x = 0.2D$). Approximately symmetric isothermal contours exist near the cylinder. The cylinder motion in the in-line direction produces symmetrical perturbations which, under certain conditions, dominate over the naturally occurring antisymmetric mode of vortex shedding. This has also been reported by Ongoren and Rockwell (O1, O2). A high concentration of isothermal contours can be observed near the upstream and downstream stagnation points.

5.4.2 Transverse Oscillation

The cylinder was forced to oscillate in the transverse direction with a frequency parameter $F_y = F_n$ and with position amplitudes (a_y) of 0.2D, 0.4D and 0.8D. The equivalent velocity amplitudes were 0.25, 0.5 and 1.0 respectively. The selected frequency parameter corresponds to the mid-point lock-in frequency. The time dependent position of the cylinder in the transverse direction (y_c/D), magnitude and incident angle of the relative free stream velocity ($U' = \sqrt{1 + A_y^2 \sin^2(\pi F_x \tau)}$ and ε) are shown in figure 5.43 for reference. The maximum value of U' occurs at the zero position of the cylinder ($\tau = 0.25$ and 0.75). The maximum value of U' is the magnitude of the vector sum of the free stream velocity and the maximum velocity of the cylinder oscillation.

Figures 5.44 and 5.45 show the time histories of Nu_{avg} at $Gr/Re^2 = 0$ and 1 respectively. The corresponding Nu_{avg} variations in a cycle of oscillation are shown in figures 5.46 and 5.47. In any cycle of oscillation, both maximum values of Nu_{avg} occur slightly after the point of maximum U' ($\tau \approx 0.3$ and 0.8) during the upward and downward motion of the cylinder. The time difference between the maximum Nu_{avg} and the maximum U' may be due to the time at which the vortex shedding occurs from the top and bottom surface of the cylinder which will influence the temperature gradients near the cylinder surface. The minimum values of Nu_{avg} are predicted near the minimum y_c/D and the maximum y_c/D . In the case of forced

convection, approximately the same pattern of oscillation of Nu_{avg} is repeated twice in every cycle of oscillation. With mixed convection, the pattern of oscillation of Nu_{avg} does not repeat and the extreme values of heat transfer rate that occurs in one cycle significantly differ from one another. The power spectra of the Nu_{avg} at $Gr/Re^2 = 0$ and 1 are shown in figures 5.48 and 5.49 respectively. Unlike in the case of in-line oscillation, Nu_{avg} oscillates at twice the frequency of oscillation of the cylinder. It is to be noticed that the magnitude of the relative free stream velocity also oscillates at $2F_y$ (see figure 5.43) which directly influences the time variation of the average Nusselt number. However, in the case of mixed convection, other frequency components such as F_n also exist in the Nu_{avg} variation.

Figures 5.50 and 5.51 show variation of the amplitude of Nu_{avg} and the mean Nusselt number (Nu_m) with the position amplitudes of oscillation in the transverse direction. The amplitude of Nu_{avg} increases after a certain value of the position amplitude of oscillation. The mean Nusselt number Nu_m increases with the increasing a_y . The amount of increase in Nu_m with a_y is comparable with the case of in-line oscillation. However, the amplitude of oscillation of Nu_{avg} is much smaller than with the case of in-line oscillation. With forced convection and $a_y = 0.8D$, an increase of 15.68% in Nu_m over the case of stationary cylinder is predicted. In the case of mixed convection, an increase of 10.23% in Nu_m is computed with $a_y = 0.8D$.

Figures 5.52 , 5.53 and 5.54 show the local Nusselt number distribution on the cylinder at different times in a full cycle of oscillation ($0 \leq \tau \leq 1$) at position amplitude (a_y) values of 0.2D, 0.4D and 0.8D respectively with $Gr/Re^2 = 0$. Similarly, figures 5.55, 5.56 and 5.57 show the local Nusselt number distributions with $Gr/Re^2 = 1.0$. The location and magnitude of maximum $Nu(\theta)$ are given in tables 5.4 and 5.5 at different times in a single cycle of oscillation of the cylinder ($0 \leq \tau \leq 1$) for the case of forced and mixed convection respectively. It can be observed that the location of the maximum heat transfer rate oscillates at the same frequency as that of the cylinder (F_y). The location of the maximum local Nusselt number depends on the direction of the relative velocity of the flow with respect to the cylinder. This implies that the incident angle of the relative free stream velocity which is also oscillating at a nondimensional frequency F_y (Figure 5.43), directly influences the location the maximum local Nusselt number on the cylinder. The maximum heat transfer occurs at a location on the upper surface or the lower surface during the upward or downward motion of the cylinder at maximum velocity respectively. Both with forced and mixed convection, the local Nusselt number distribution approximately repeats after one cycle.

Figures 5.58 to 5.62 show the isothermal contour maps for the case of forced convection at different stages in a single cycle of oscillation with $a_y = 0.4D$. Similarly, figures 5.63 to 5.67 show the isothermal contours with mixed convection. In both the cases of forced and mixed convection, asymmetric isothermal contours

exist at different stages of oscillation and approximately repeat after one cycle. A high concentration of isothermal contours are found to exist near the location of the maximum heat transfer rate which depends on the incident angle of the relative free stream velocity (ϵ).

5.4.3 Combined Oscillation

The cylinder was forced to oscillate simultaneously in the in-line and transverse directions with frequency parameters $F_x = 2F_n$ and $F_y = F_n$ respectively. The position amplitude of oscillation in the in-line direction (a_x) is held constant at $0.2D$. In the transverse direction, the cylinder was forced to oscillate with position amplitudes $0.2D$, $0.4D$ and $0.8D$. The time dependent position of the cylinder in the in-line and transverse directions (x_c/D and y_c/D), magnitude and the incident angle of the relative free stream velocity ($U^* = \sqrt{\{(1 - A_x \sin(\pi F_x \tau))^2 + A_y^2 \sin^2(\pi F_x \tau)\}}$ and ϵ) are shown in figure 5.68 for reference.

Figures 5.69 and 5.70 show the time histories of Nu_{avg} at $Gr/Re^2 = 0$ and 1 respectively. The corresponding Nu_{avg} variations in a cycle of oscillation are shown in figures 5.71 and 5.72. In any cycle of oscillation, both maximum values of Nu_{avg} occur near the zero position of the cylinder in the in-line direction ($x_c/D = 0$) with the cylinder moving in the direction opposite to that of the free stream flow (U_∞). Two minimum values of Nu_{avg} occur between the zero x_c location and the

maximum x_c location with the cylinder moving in the same direction as that of the free stream flow. The reason for the minimum value of Nu_{avg} to occur between the zero x_c location and the maximum x_c location is that the fluid surrounding the cylinder in the downstream location is warmer than the upstream location. In the case of forced convection, approximately the same maximum values of Nu_{avg} occur at the same positions in every cycle of oscillation. With mixed convection, the extreme values Nu_{avg} significantly differ from one another in a cycle of oscillation. The power spectra of Nu_{avg} at $Gr/Re^2 = 0$ and 1 are shown in figures 5.73 and 5.74 respectively. The dominant frequency in the Nu_{avg} variation is the forcing frequency of oscillation in the in-line direction ($2F_n$). With mixed convection and $a_y = 0.8D$, other frequencies such as F_n and $3F_n$ exists in the Nu_{avg} variation.

Figures 5.75 and 5.76 show variation of the amplitude of Nu_{avg} and the mean Nusselt number (Nu_m) with the position amplitudes of oscillation in the transverse direction. With forced convection, the Nu_m increases with a_y and the amplitude of Nu_{avg} decreases after a certain position amplitude of oscillation (a_y). In the case of mixed convection, both the amplitude of Nu_{avg} and the Nu_m increase after a certain position amplitude of oscillation (a_y). The amount of increase in Nu_m with a_y is comparable with the case of transverse oscillation. However, the amplitude of oscillation of Nu_{avg} is much higher than with the case of transverse oscillation. This can be attributed to the effect of in-line oscillation. With $Gr/Re^2 = 0$ and $a_x = 0.2D$, $a_y = 0.8D$ an increase of 18.46% in Nu_m over the case of

stationary cylinder is predicted. At the same position amplitudes of oscillation, an increase of 15.30% in Nu_m is computed with mixed convection ($Gr/Re^2 = 1$).

Figures 5.77 , 5.78 and 5.79 show the local Nusselt number distribution on the cylinder at different times in a full cycle of oscillation ($0 \leq \tau' \leq 1$) at position amplitudes $a_y = 0.2D$, $0.4D$ and $0.8D$ respectively with $Gr/Re^2 = 0$ and $a_x = 0.2D$. Similarly, figures 5.80, 5.81 and 5.82 show the local Nusselt number distributions with $Gr/Re^2 = 1.0$. The location and magnitude of maximum $Nu(\theta)$ are taken from these plots and are given in tables 5.6 and 5.7 at different times in a single cycle of oscillation of the cylinder ($0 \leq \tau' \leq 1$) for the case of forced and mixed convection respectively. Similar to the case of transverse oscillation, the location of the maximum heat transfer rate oscillates at the same frequency as that of the cylinder in the transverse direction (F_y). The location of the maximum local Nusselt number depends on the direction of the relative velocity of the flow with respect to the cylinder. As in the case of transverse oscillation, the incident angle of the relative free stream velocity which is also oscillating at a nondimensional frequency F_y (Figure 5.70), directly influences the location of the maximum local Nusselt number on the cylinder. During the upward or downward motion of the cylinder with maximum velocity ($\tau' = 0.25$ and 0.75), the maximum heat transfer occurs at a location on the upper surface or the lower surface respectively.

The isothermal contour maps at different stages in a single cycle of

oscillation are shown in figures 5.83 to 5.87 for $a_x = 0.2D$, $a_y = 0.4D$ and $Gr/Re^2 = 0$. Similarly, plots are shown for $a_x = 0.2D$, $a_y = 0.4D$ and $Gr/Re^2 = 1$ in figures 5.88 to 5.92. With forced convection, isothermal contours approximately repeat after one complete cycle of oscillation. However, with mixed convection, isothermal contours do not repeat after one cycle. A significant amount of difference in the pattern of the isothermal contours can be observed between forced convection and mixed convection.

5.5 Oscillating Hot-Wire Anemometer Studies

In this section, a numerical simulation of the response of an oscillating hot-wire anemometer is presented. The experimental investigation conducted by Heckadon et al. [H3] is taken as the source of information for this numerical study. The hot-wire was oscillated in the direction parallel to the free stream flow at different velocity amplitudes and frequencies of oscillation. The free stream flow was essentially a jet flow of air from a 19 mm diameter nozzle. The hot-wire was kept in the potential core of the jet. The hot-wire was oscillated sinusoidally using a magnetic shaker. The motion of the wire was normal to its length and in-line with the direction of the jet flow. An accelerometer attached to the shaker was used to determine the velocity of oscillation. The hot-wire used was a 5 micron DISA probe and DISA Constant Temperature Anemometer instrumentation was used to measure the hot-wire response. The free stream velocity, amplitude and frequency

of oscillation were varied in the ranges of 0.06-3.13 m/s, 1.2-1.6 mm and 50-90 Hz respectively.

With a constant temperature anemometer, the hot-wire voltage response (E) depends on the heat transfer from the wire to the surrounding fluid. The average Nusselt number represents the heat transfer from a heated wire. Hence, the Nu_{avg} can be used to compare qualitatively with the hot-wire voltage response. In the numerical study, the Reynolds number (Re), Grashof number (Gr), velocity amplitude (A_x) and frequency (F_x) of oscillation were taken to be the same as that in the experimental study. Two cases of oscillating hot-wire responses were computationally predicted. In the first case, the velocity amplitude of oscillation (A_x) was less than the free stream velocity and equal to 0.712. The Reynolds number, Grashof number and frequency parameter were set equal to 0.25, 3.988×10^{-6} and 4.48×10^{-3} respectively. In the second case, the velocity amplitude of oscillation (A_x) was higher than the free stream velocity and was equal to 2.986. The Reynolds number, Grashof number and frequency parameter were set equal to 0.06, 3.988×10^{-6} and 1.87×10^{-3} respectively. In both the cases, digitized experimental hot-wire response, predicted computational response in terms of Nu_{avg} and the magnitude of the relative free stream velocity ($U' = 1 - A_x \sin(\pi F_x \tau)$) were plotted and qualitatively compared with each other.

Figure 5.93 shows the comparison between the experimental and

computational hot-wire response with velocity amplitude of oscillation (A_u) of 0.712. The Nu_{avg} is oscillating at the same frequency as that of the hot-wire. A maximum value of hot-wire response occurs near the zero position with wire moving in the opposite direction to that of the free stream flow. A minimum value of Nu_{avg} is predicted near the zero position with the cylinder moving in the same direction as that of the free stream flow. The local Nusselt number distribution on the wire at different times in a full cycle of oscillation are shown in figure 5.94. At the point of maximum relative velocity ($\tau^* = 0.75$), local Nusselt number distribution is approximately symmetric about the upstream stagnation point (180°). At other times ($\tau^* = 0, 0.25, 0.5$ and 1), it is clearly evident that the Nusselt number distribution is asymmetric about 180° . This is due to the strong influence of free convection at low Reynolds numbers. The local Nusselt number distribution is approximately the same at times when the velocity of the hot-wire equals zero. The isothermal contours at different times in a complete cycle of oscillation are shown in figures 5.95 to 5.99. All the isothermal contour maps presented in this section are with a contour interval of 0.025 and with the minimum and maximum levels of contour as 0.4 and 1.0 respectively. With the hot-wire moving in the direction opposite to that of the mean flow and at the zero position ($\tau^* = 0.75$ and $U^* = 1.712$), a higher concentration of isothermal contours exist near the wire than at other positions in a cycle of oscillation. At this time and position, the influence of free convection is negligible.

Figure 5.100 shows the comparison between the experimental response and the computational response with the velocity amplitude (A_v) of oscillation of 2.986. The magnitude of the relative free stream velocity (U') is also plotted for easy reference. Qualitatively, the Nu_{avg} variation is the rectified form of the relative free stream velocity. It can be observed that the hot-wire responds to the absolute value of U' . At the times when the relative free stream velocity become zero, minimum values of average Nusselt number and the hot-wire output voltage are attained. At $\tau' = 0.25$ and 0.5 , the magnitudes of the relative free stream velocity are -1.986 and 3.986 respectively. The highest value of average Nusselt number and the hot-wire output occurs at the $\tau' = 0.75$. This position corresponds to the hot-wire moving with maximum velocity in the opposite direction to that of the free stream flow. Figure 5.101 shows the local Nusselt number distribution on the hot-wire at different instants of time in a full cycle of oscillation. The local Nusselt number distribution is approximately the same at times when the velocity of the hot-wire equals zero ($\tau' = 0, 0.5$ and 1). The local Nusselt number distribution is asymmetric about 180° at all the times ($\tau' = 0, 0.25, 0.5, 0.75$ and 1). The isothermal contours at different times in a complete cycle of oscillation are shown in figures 5.102 to 5.106. Influence of free convection is clearly evident in all the contour maps by the slight upward skew of the isothermal contours.

Grid Size	ξ_{∞} (r/R)	V	Computed Nu_m
Grid Dependency			
101x81	1 (23.14)	3	7.461
121x101	1 (23.14)	3	7.467
141x121	1 (23.14)	3	7.466
Location of the Far-field Boundary			
121x81	0.8 (12.35)	3	7.438
121x101	1.0 (23.14)	3	7.467
121x121	1.2 (43.38)	3	7.465
Magnitude of Numerical Triggering			
121x101	1.0 (23.14)	3	7.467
121x101	1.0 (23.14)	5	7.466
121x101	1.0 (23.14)	10	7.466

Table 5.1 Mean Nusselt number for different dependency tests (Re = 200)

	$a_x = 0.1D$		$a_x = 0.2D$		$a_x = 0.4D$	
τ	Max. Nu(θ)	Angle (deg.)	Max. Nu(θ)	Angle (deg.)	Max. Nu(θ)	Angle (deg.)
0.00	14.59	180	15.14	180	15.65	180
0.25	12.38	180	11.49	0	18.12	0
0.50	12.96	180	11.78	177	10.38	0
0.75	15.40	180	16.87	180	19.12	180
1.00	14.59	180	15.14	180	15.65	180

Table 5.2 Location and magnitude of maximum Nu(θ) in a cycle of oscillation
(in-line oscillation, $Gr/Re^2 = 0$)

τ	$a_x = 0.1D$		$a_x = 0.2D$		$a_x = 0.4D$	
	Max. Nu(θ)	Angle (deg.)	Max. Nu(θ)	Angle (deg.)	Max. Nu(θ)	Angle (deg.)
0.00	14.61	180	15.00	180	15.66	180
0.25	12.41	180	13.18	0	17.70	0
0.50	12.98	180	11.56	180	10.39	0
0.75	15.37	180	16.71	180	19.13	180
1.00	14.53	180	15.00	180	15.66	180

Table 5.3 Location and magnitude of maximum Nu(θ) in a cycle of oscillation
(in-line oscillation, $Gr/Re^2 = 1$)

	$a_y = 0.2D$		$a_y = 0.4D$		$a_y = 0.8D$	
τ	Max. Nu(θ)	Angle (deg.)	Max. Nu(θ)	Angle (deg.)	Max. Nu(θ)	Angle (deg.)
0.00	13.84	183	13.88	186	14.00	192
0.25	14.06	165	14.72	153	16.87	132
0.50	13.84	177	13.88	174	13.94	168
0.75	14.07	195	14.72	207	16.80	228
1.00	13.84	183	13.88	186	14.00	192

Table 5.4 Location and magnitude of maximum Nu(θ) in a cycle of oscillation
(transverse oscillation, $Gr/Re^2 = 0$)

	$a_y = 0.2D$		$a_y = 0.4D$		$a_y = 0.8D$	
τ^*	Max. Nu(θ)	Angle (deg.)	Max. Nu(θ)	Angle (deg.)	Max. Nu(θ)	Angle (deg.)
0.00	13.95	183	14.10	186	13.98	192
0.25	13.99	165	14.60	156	16.29	135
0.50	13.72	177	13.66	171	14.57	318
0.75	14.13	195	14.85	207	15.90	222
1.00	13.95	183	14.10	186	13.97	192

Table 5.5 Location and magnitude of maximum Nu(θ) in a cycle of oscillation
(transverse oscillation, $Gr/Re^2 = 1$)

τ	$a_y = 0.2D$		$a_y = 0.4D$		$a_y = 0.8D$	
	Max. Nu(θ)	Angle (deg.)	Max. Nu(θ)	Angle (deg.)	Max. Nu(θ)	Angle (deg.)
0.00	15.10	180	15.06	183	15.10	186
0.25	12.16	159	13.00	147	15.81	126
0.50	15.13	180	15.08	177	15.21	174
0.75	12.15	201	12.93	213	15.87	234
1.00	15.10	180	15.06	183	15.09	186

Table 5.6 Location and magnitude of maximum Nu(θ) in a cycle of oscillation
(combined oscillation, $a_x = 0.2D$, $Gr/Re^2 = 0$)

τ	$a_y = 0.2D$		$a_y = 0.4D$		$a_y = 0.8D$	
	Max. $Nu(\theta)$	Angle (deg.)	Max. $Nu(\theta)$	Angle (deg.)	Max. $Nu(\theta)$	Angle (deg.)
0.00	15.11	183	15.12	186	15.07	189
0.25	13.35	6	12.57	0	15.01	129
0.50	14.94	177	14.88	177	14.91	174
0.75	11.86	195	12.85	210	15.74	231
1.00	15.01	183	15.10	183	15.07	189

Table 5.7 Location and magnitude of maximum $Nu(\theta)$ in a cycle of oscillation
(combined oscillation, $a_x = 0.2D$, $Gr/Re^2 = 1$)

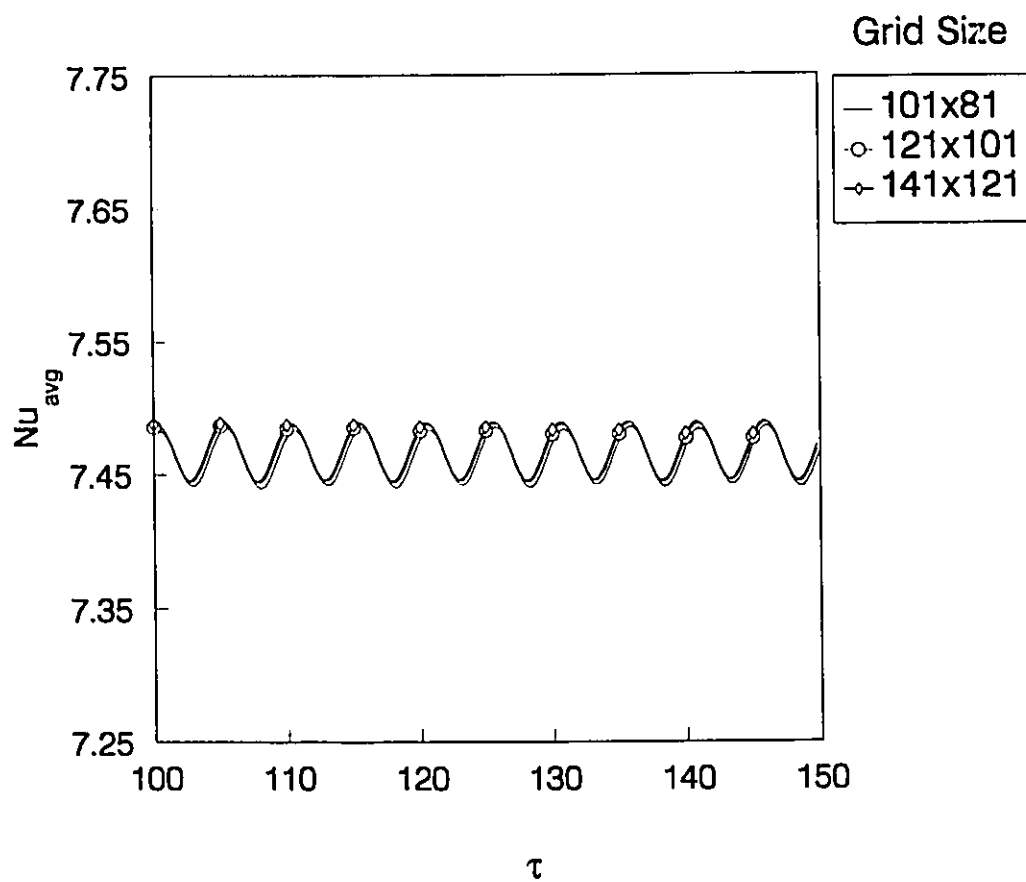


Figure 5.1 Time history of the average Nusselt number (stationary cylinder, $Re = 200$, dependency test with grid size)

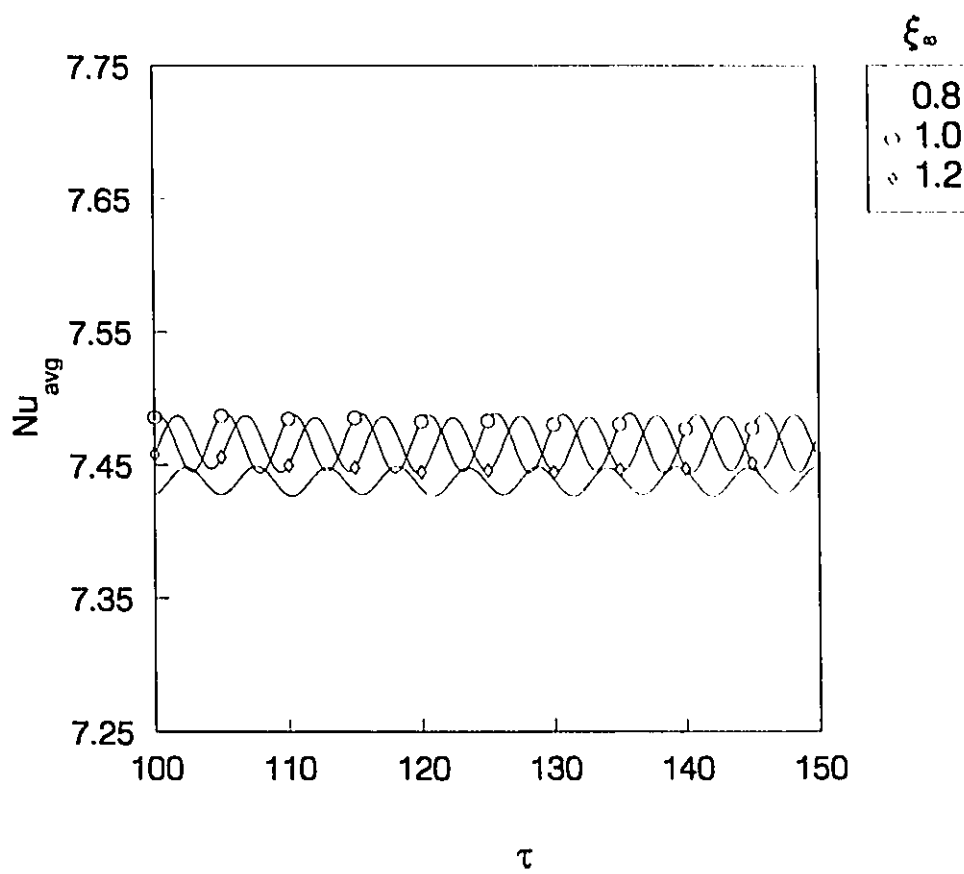


Figure 5.2 Time history of the average Nusselt number
(stationary cylinder, $Re = 200$, dependency test with far-field boundary location)

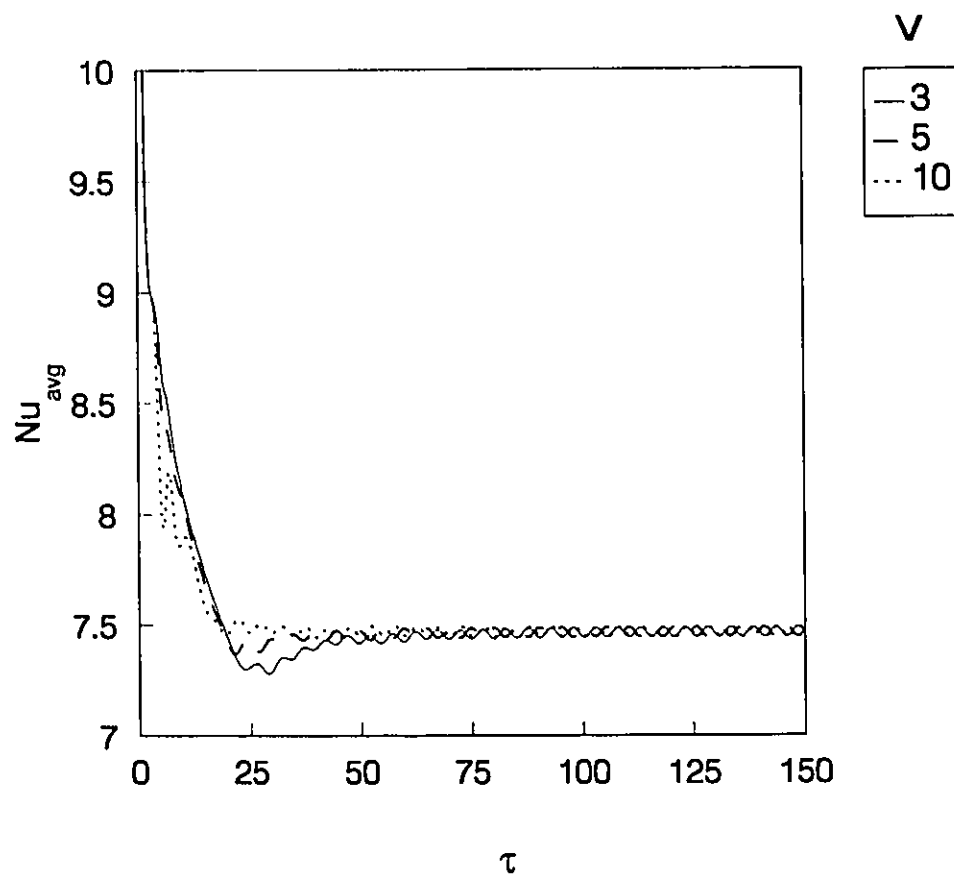


Figure 5.3 Time history of the average Nusselt number
(stationary cylinder, $Re = 200$, dependency test with the magnitude of numerical triggering)

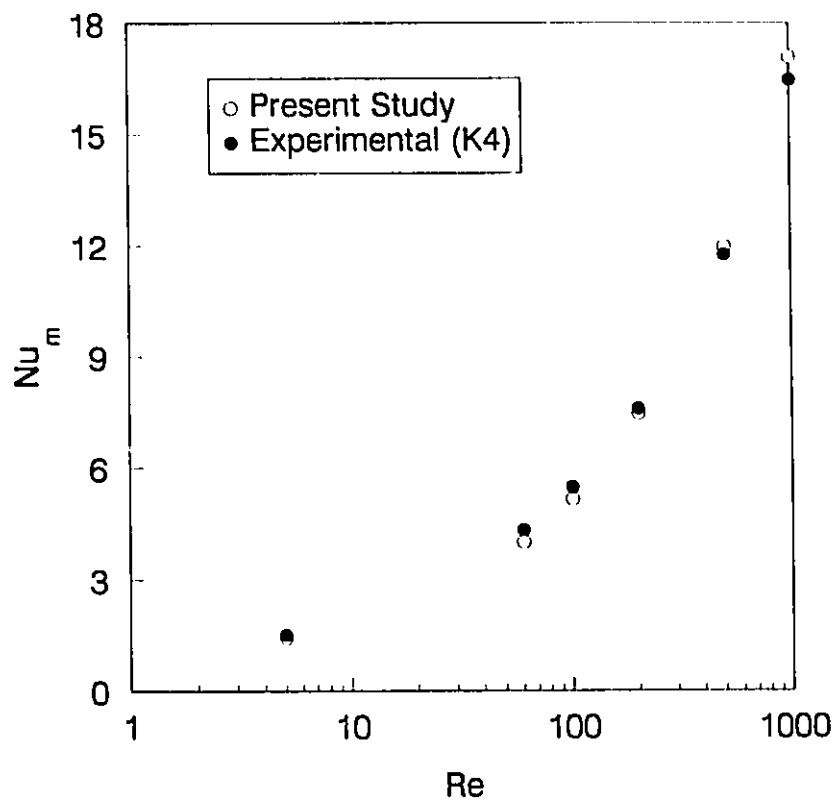


Figure 5.4 Mean Nusselt number at different Reynolds numbers

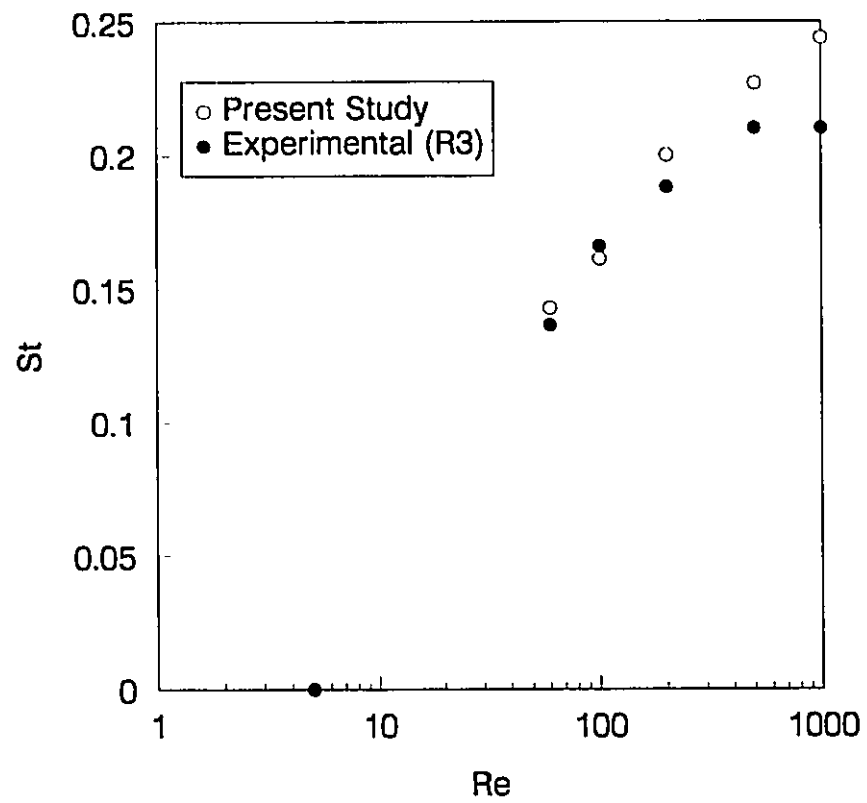


Figure 5.5 Strouhal number at different Reynolds numbers

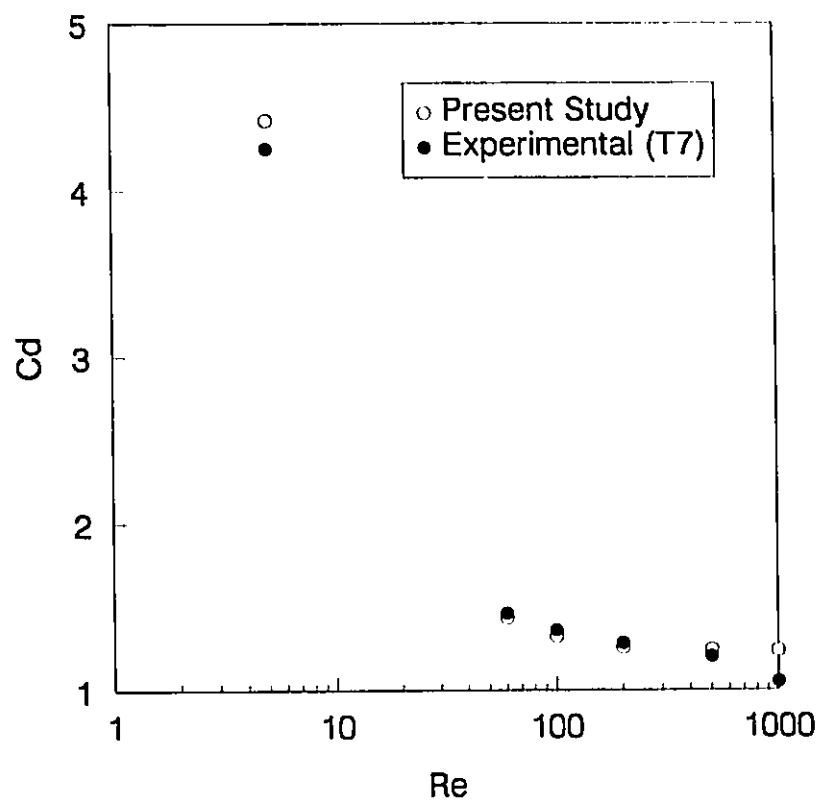


Figure 5.6 Mean drag coefficient at different Reynolds numbers

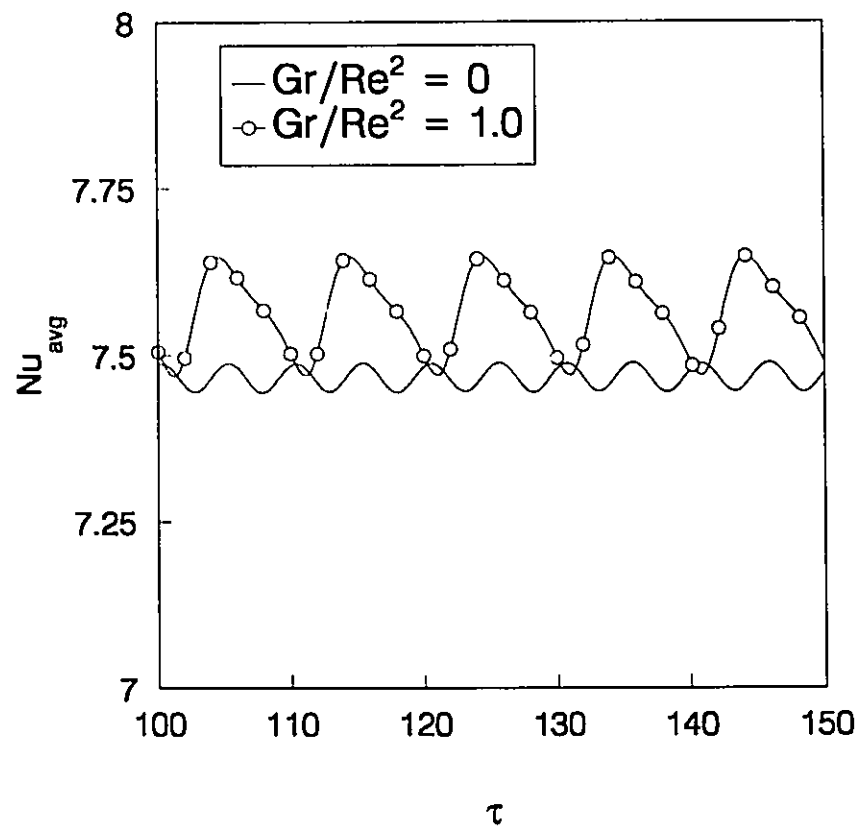


Figure 5.7 Time history of the average Nusselt number
(stationary cylinder, $Re = 200$)

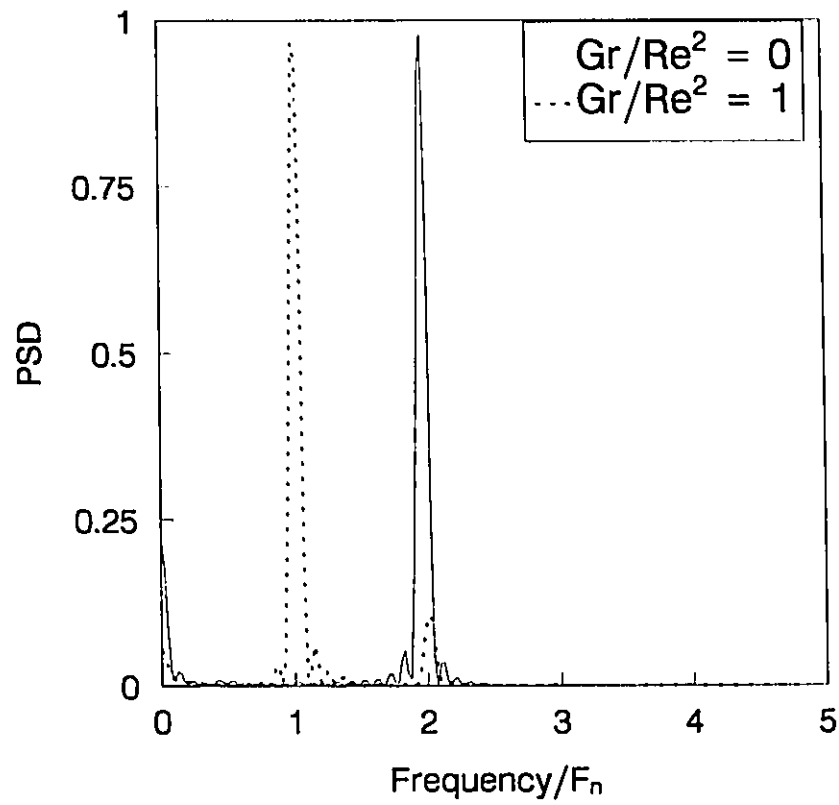


Figure 5.8 Power spectra of the average Nusselt number
(stationary cylinder, $Re = 200$)

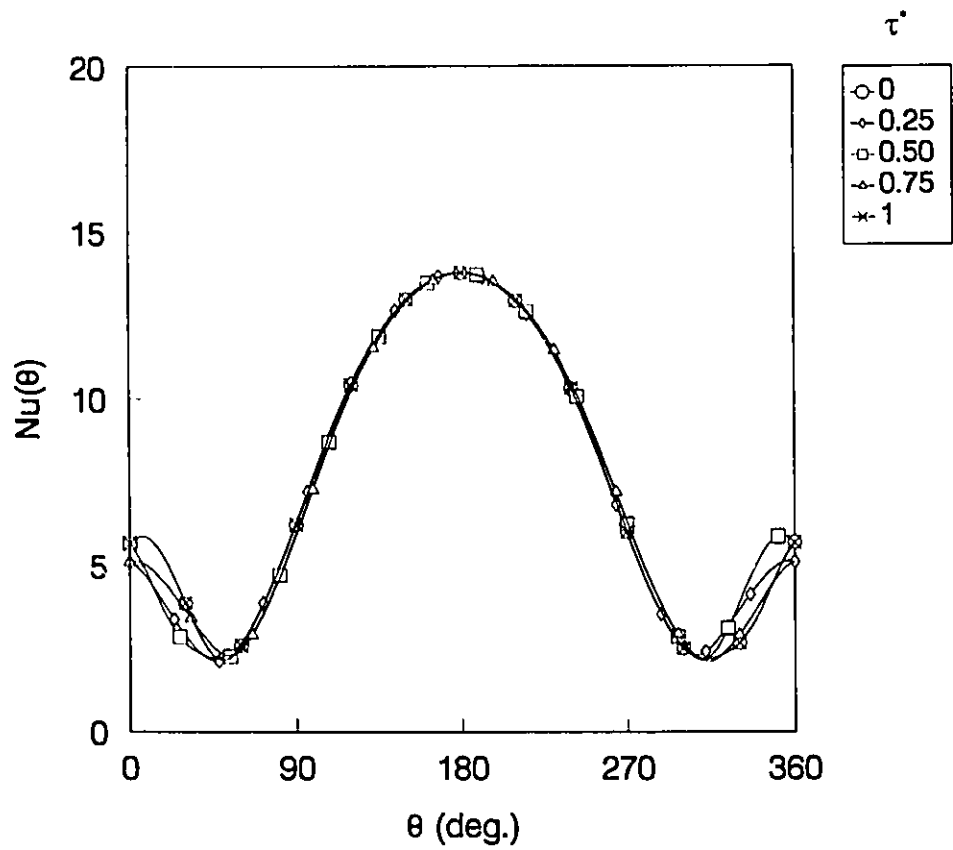


Figure 5.9 Local Nusselt number distribution in a full vortex shedding cycle (stationary cylinder, $Re = 200$, $Gr/Re^2 = 0$)

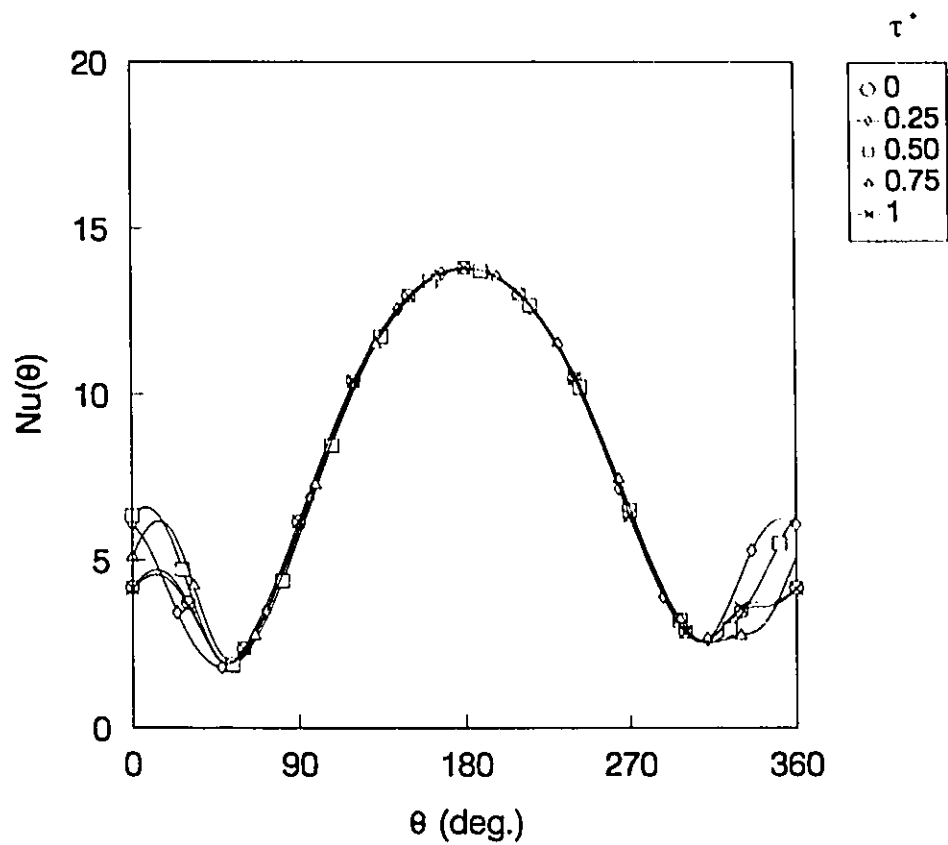


Figure 5.10 Local Nusselt number distribution in a full vortex shedding cycle (stationary cylinder, $Re = 200$, $Gr/Re^2 = 1$)

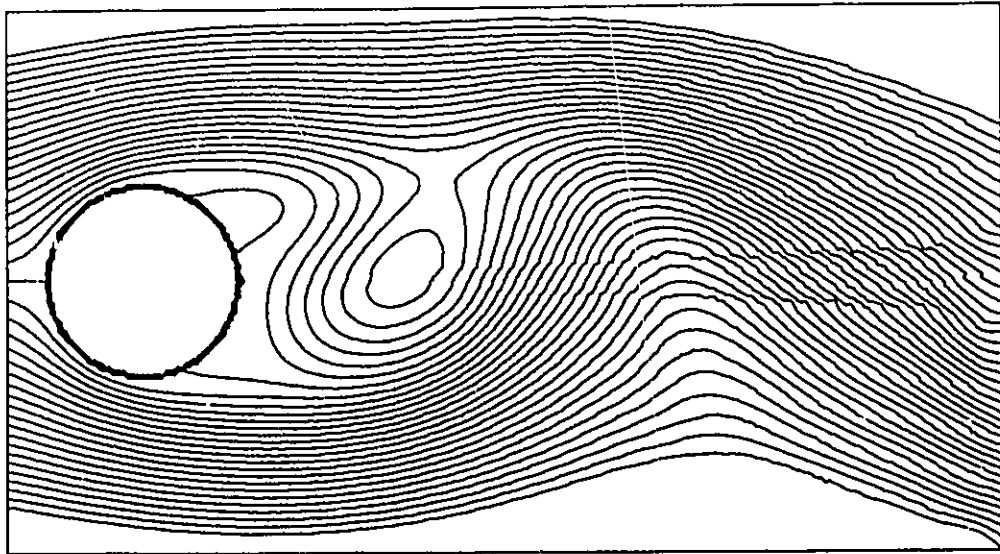


Figure 5.11 Streamline contour map for the case of forced convection
($Re = 200$, minimum and maximum contour level: -2 and 2,
contour interval: 0.1)

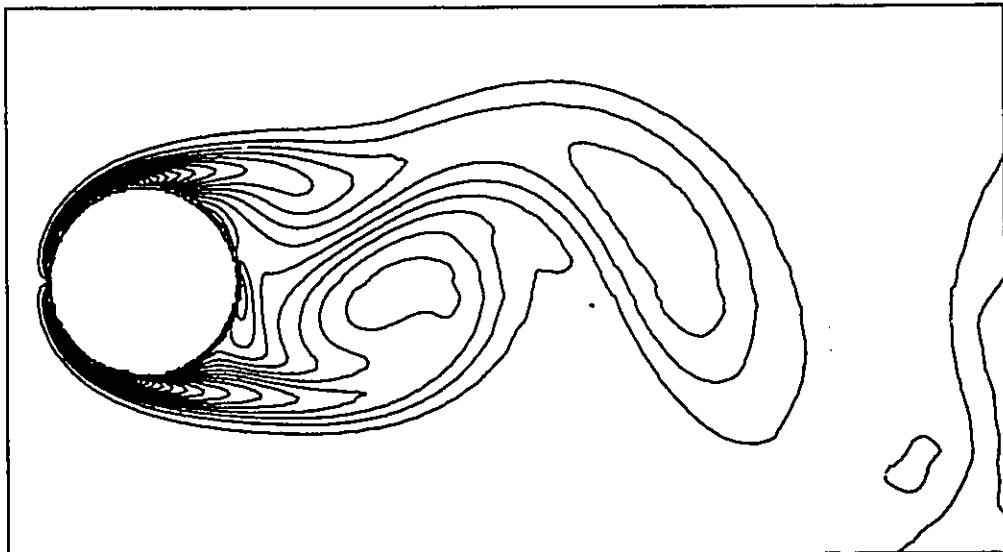


Figure 5.12 Vorticity contour map for the case of forced convection
($Re = 200$, minimum and maximum contour level: -10.25 and 10.25,
contour interval: 0.5)

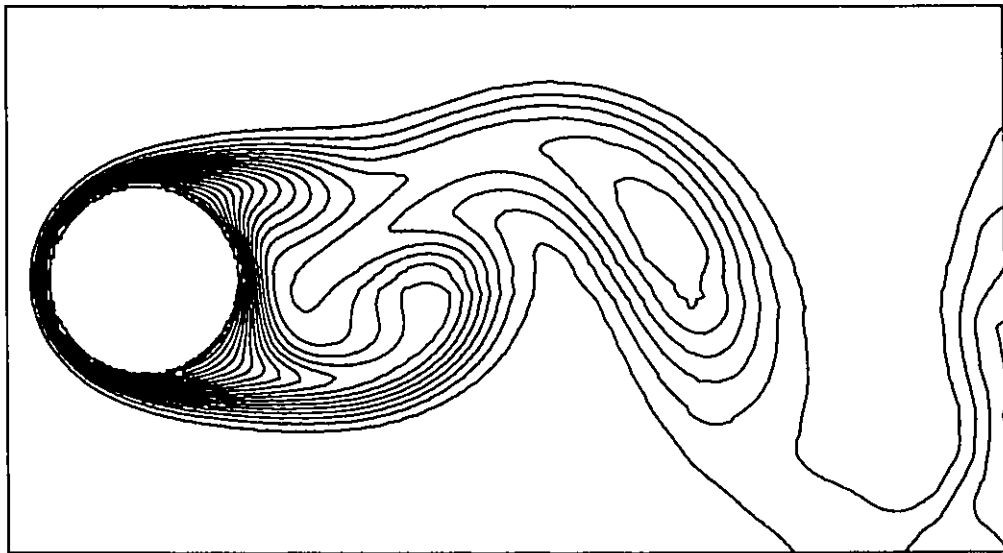


Figure 5.13 Isothermal contours for the case of forced convection
($Re = 200$, minimum and maximum contour level: 0.05 and 1,
contour interval: 0.05)

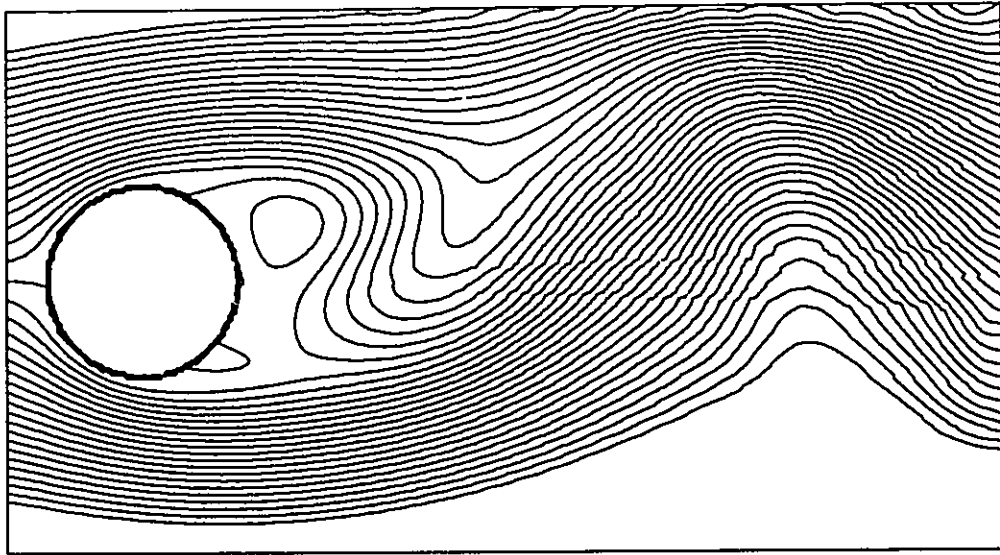


Figure 5.14 Streamline contour map for the case of mixed convection
($Re = 200$, minimum and maximum contour level: -2 and 2,
contour interval: 0.1)

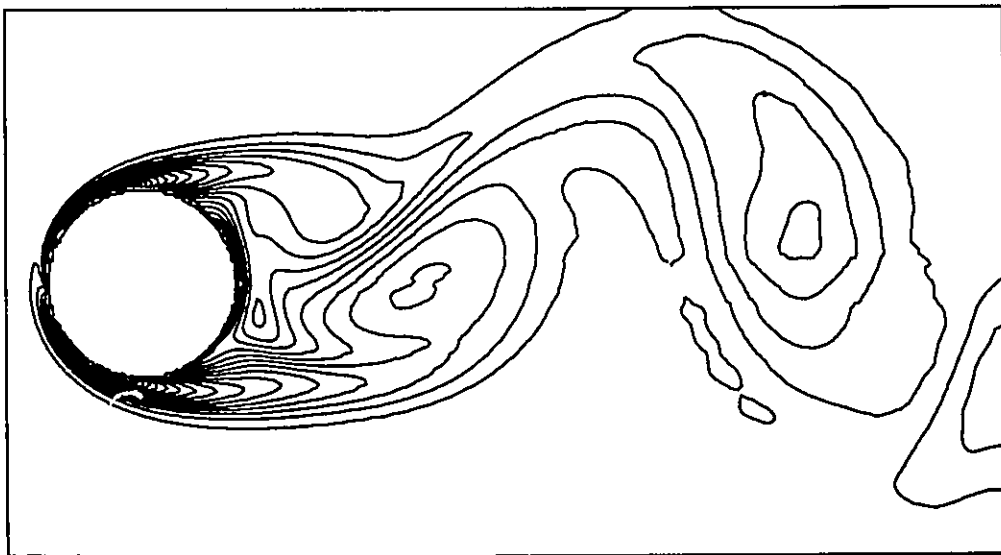


Figure 5.15 Vorticity contour map for the case of mixed convection
($Re = 200$, minimum and maximum contour level: -10.25 and 10.25,
contour interval: 0.5)

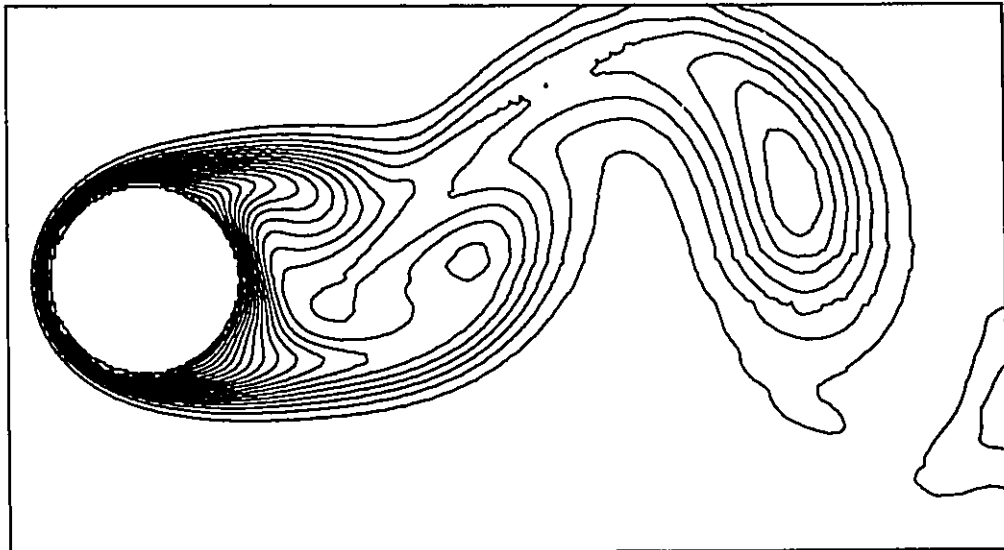


Figure 5.16 Isothermal contours for the case of mixed convection
($Re = 200$, minimum and maximum contour level: 0.05 and 1,
contour interval: 0.05)

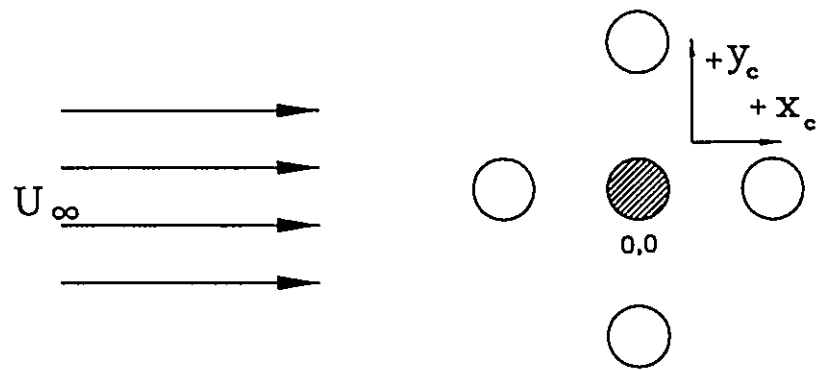


Figure 5.17 Schematic diagram of cylinder oscillation

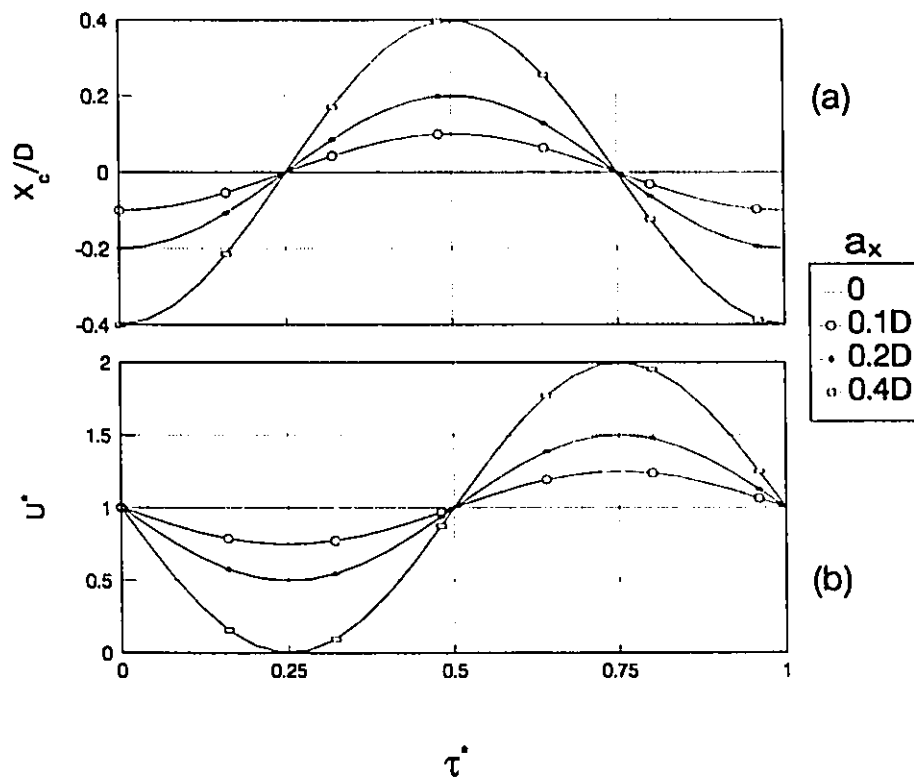


Figure 5.18 Details of forced oscillation of the cylinder (in-line oscillation, $F_x = 2F_n$) (a) position of the cylinder (b) magnitude of the relative free stream velocity

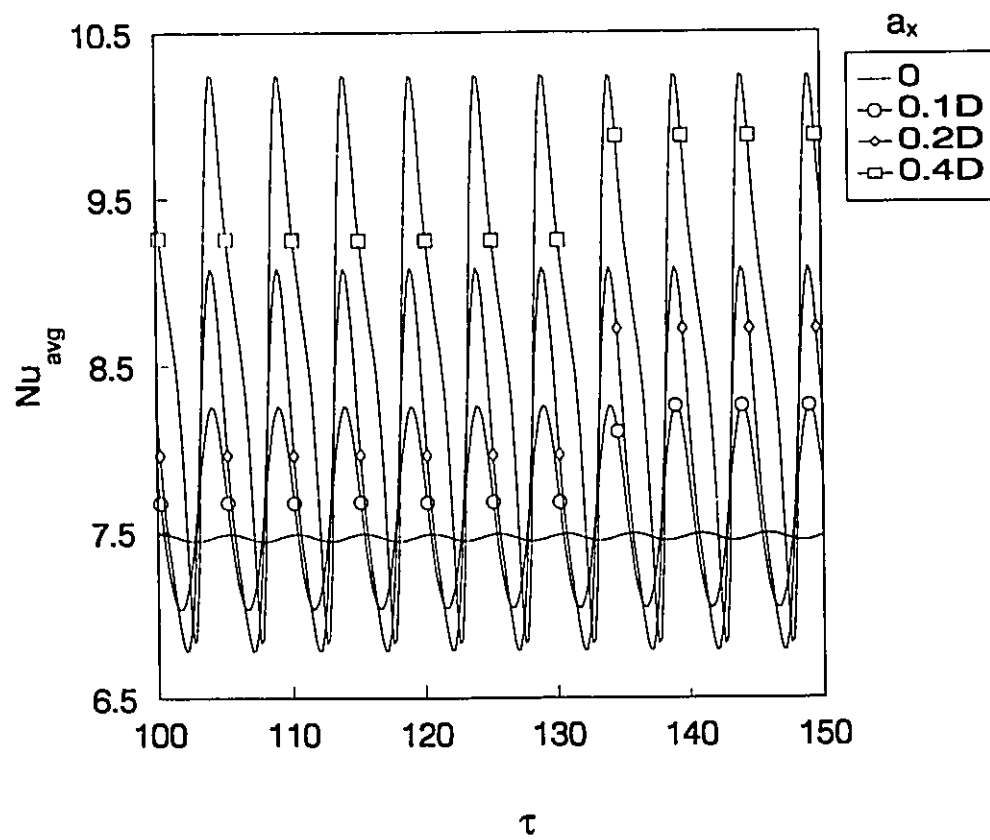


Figure 5.19 Time history of the average Nusselt number
(in-line oscillation, $F_x = 2F_n$, $Gr/Re^2 = 0$)

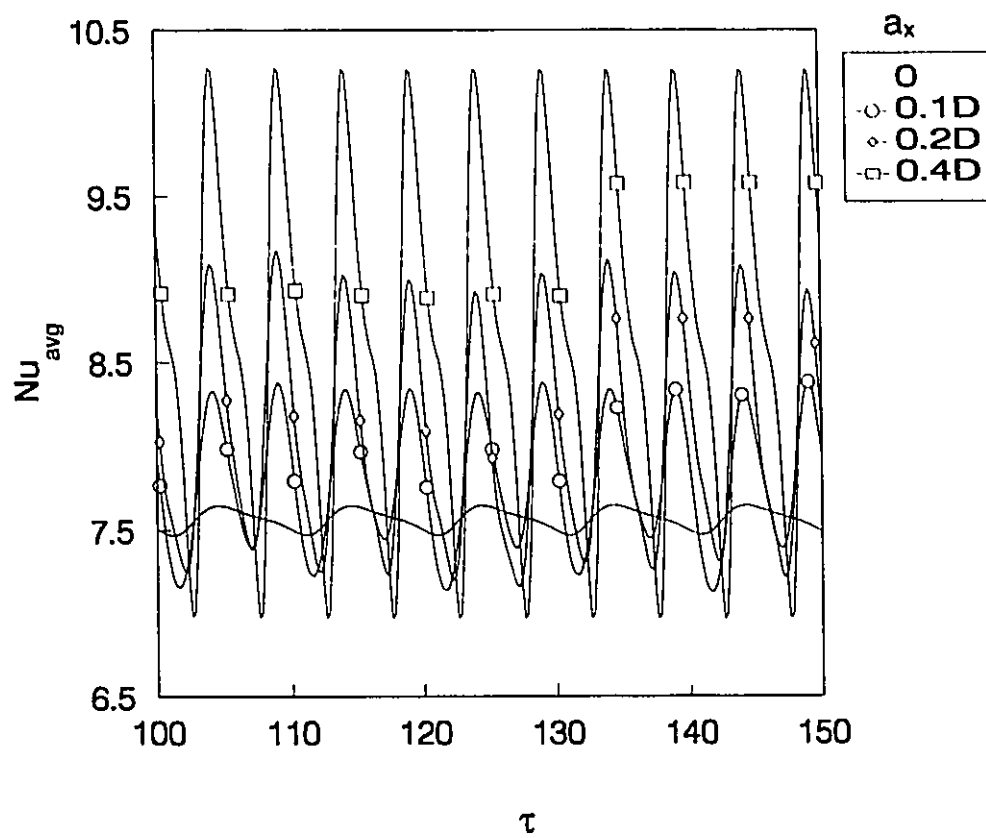


Figure 5.20 Time history of the average Nusselt number
(in-line oscillation, $F_x = 2F_n$, $Gr/Re^2 = 1$)

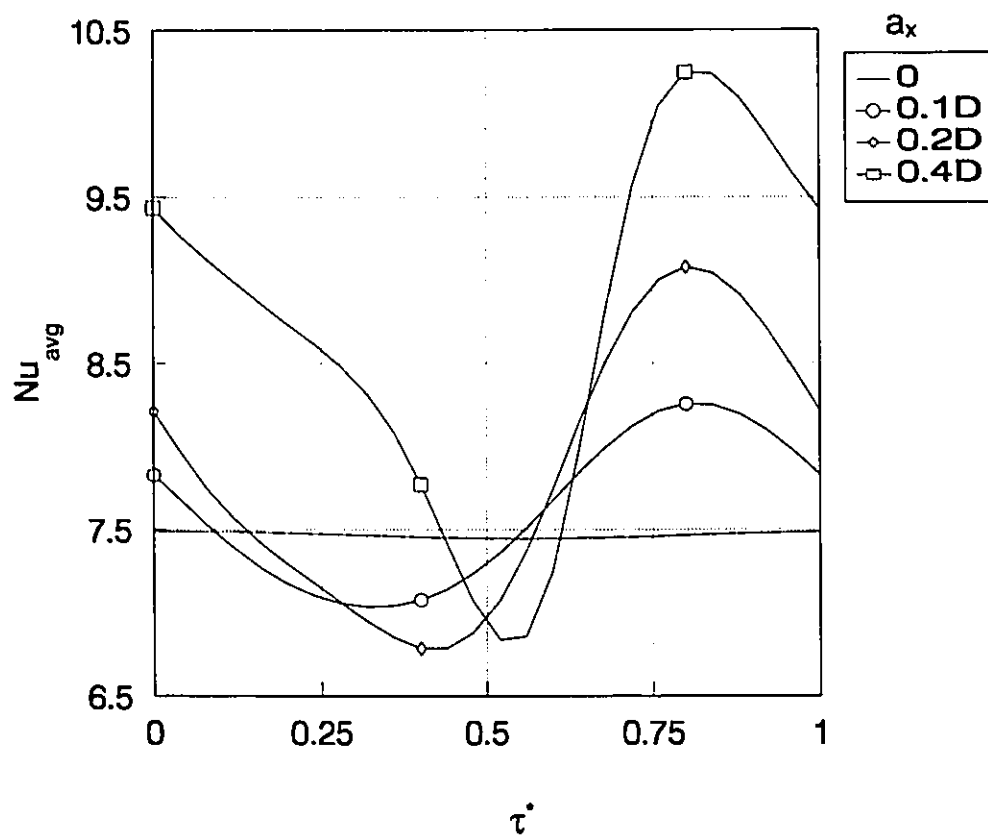


Figure 5.21 Average Nusselt number in a cycle of oscillation
(in-line oscillation, $F_x = 2F_n$, $Gr/Re^2 = 0$)

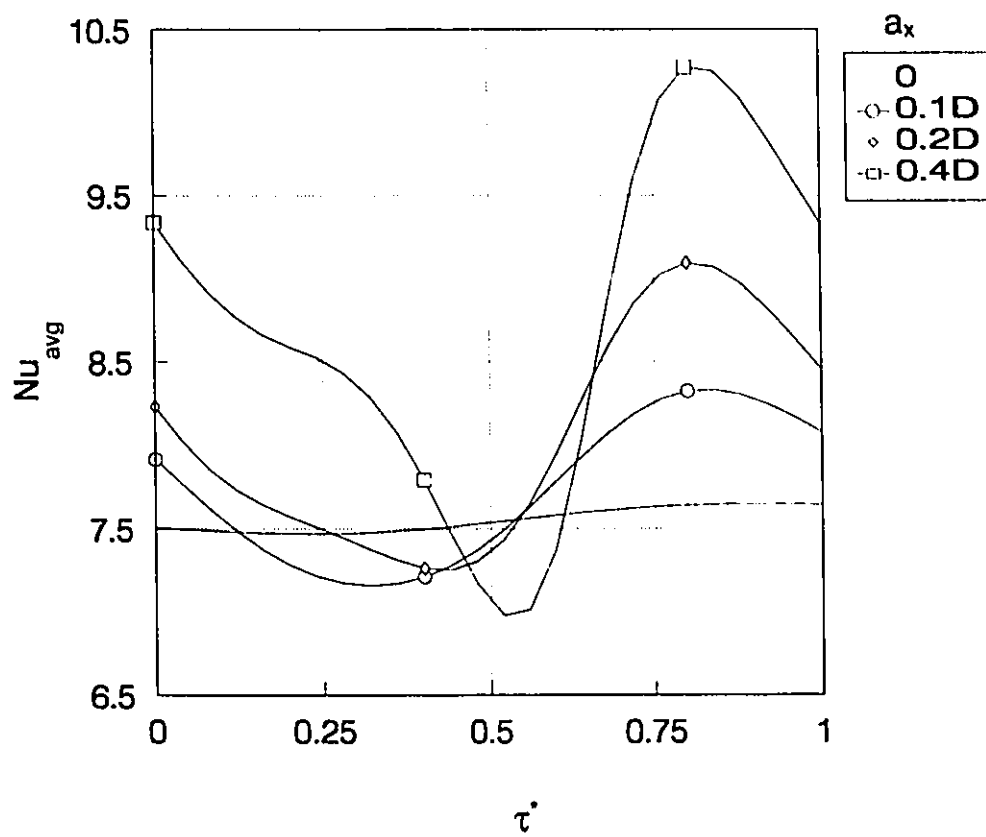


Figure 5.22 Average Nusselt number in a cycle of oscillation
(in-line oscillation, $F_x = 2F_n$, $Gr/Re^2 = 1$)

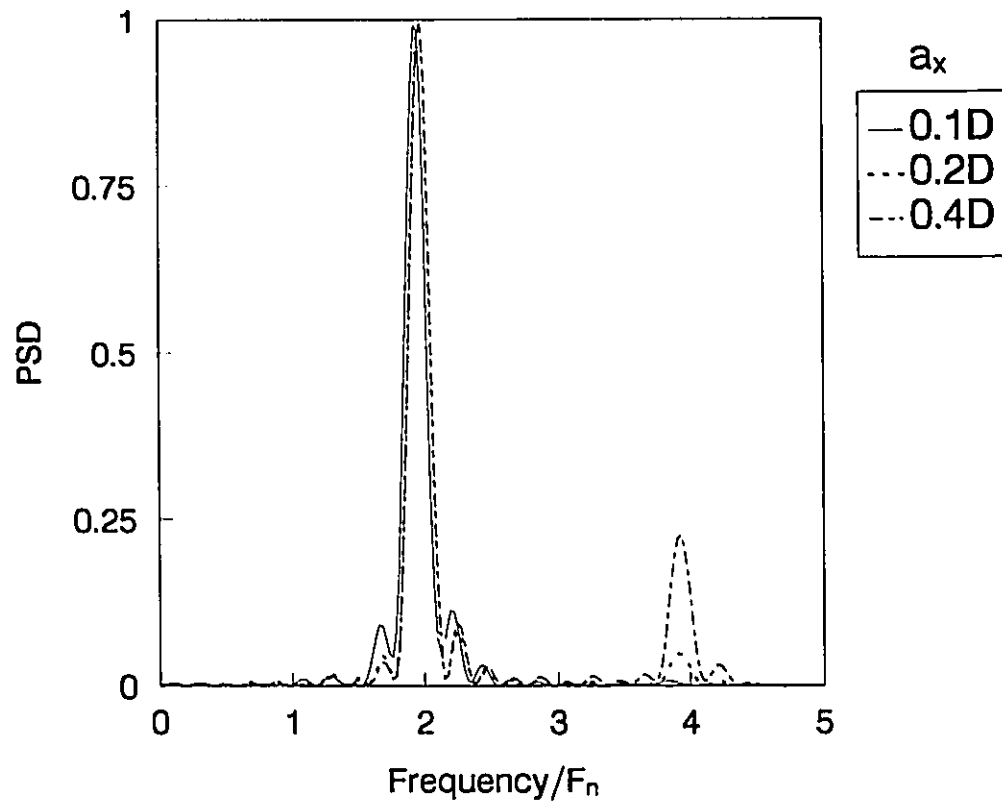


Figure 5.23 Power spectra of the average Nusselt number
(in-line oscillation, $F_x = 2F_n$, $Gr/Re^2 = 0$)

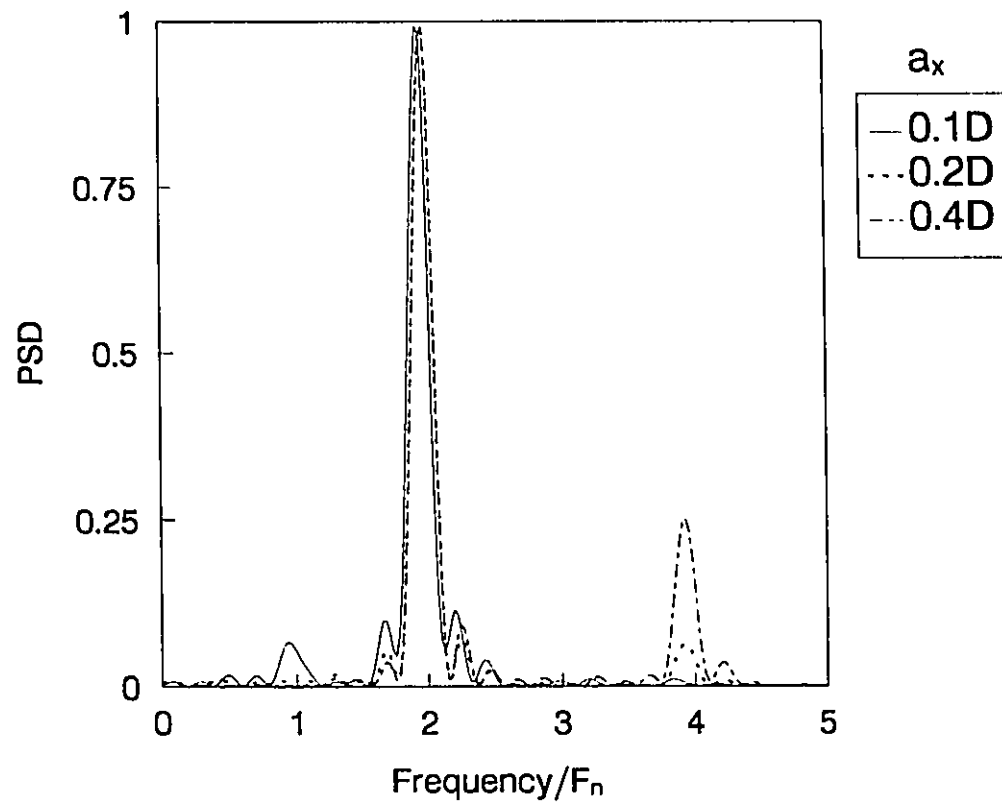


Figure 5.24 Power spectra of the average Nusselt number
(in-line oscillation, $F_x = 2F_n$, $Gr/Re^2 = 1$)

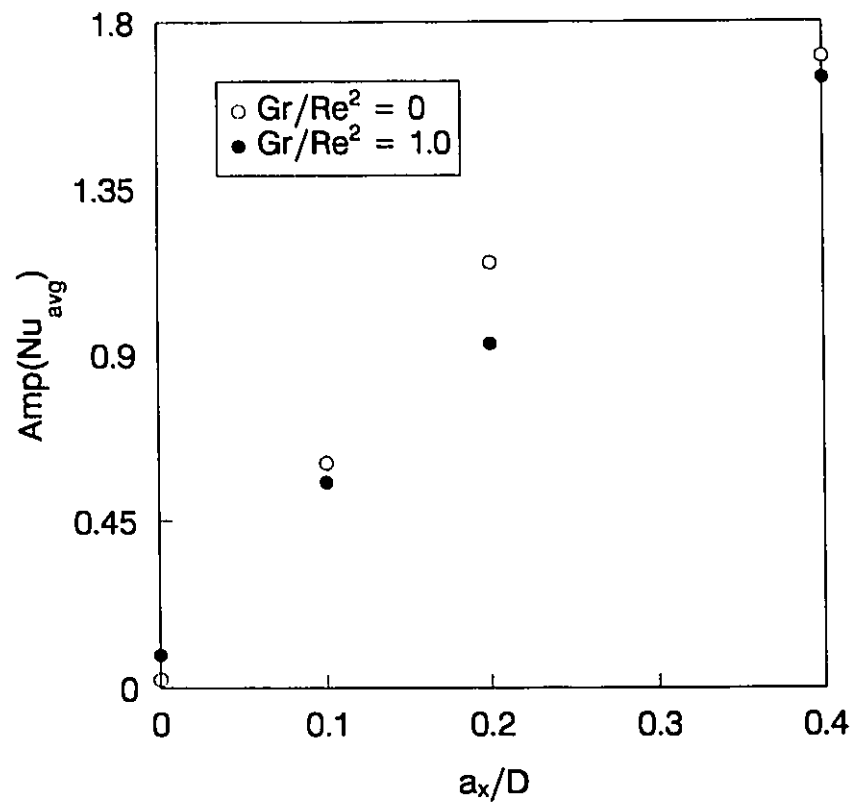


Figure 5.25 Amplitude of Nu_{avg} at different position amplitudes of oscillation (in-line oscillation, $F_x = 2F_n$)

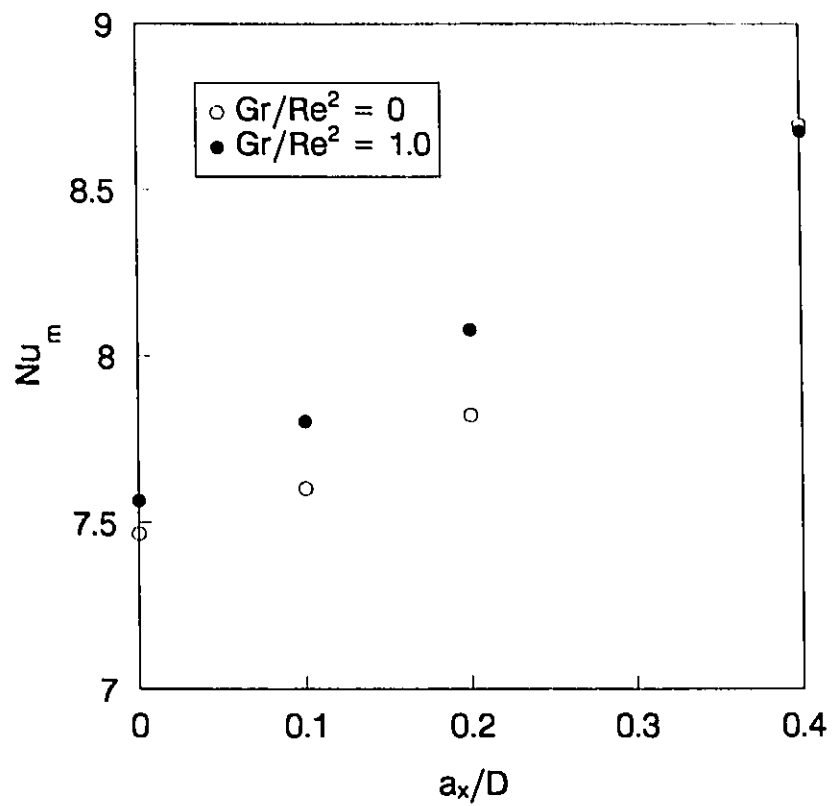


Figure 5.26 Mean Nusselt number at different position amplitudes of oscillation
(in-line oscillation, $F_x = 2F_n$)

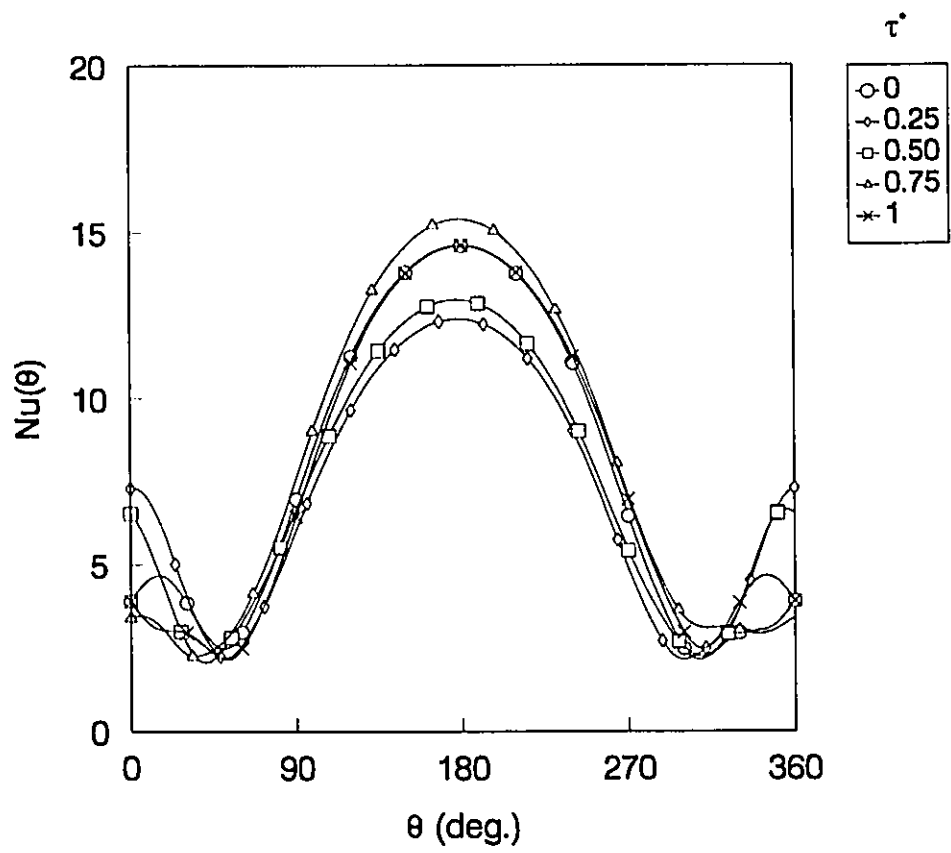


Figure 5.27 Local Nusselt number distribution in a full cycle of oscillation
(in-line oscillation, $F_x = 2F_n$, $a_x = 0.1D$, $Gr/Re^2 = 0$)

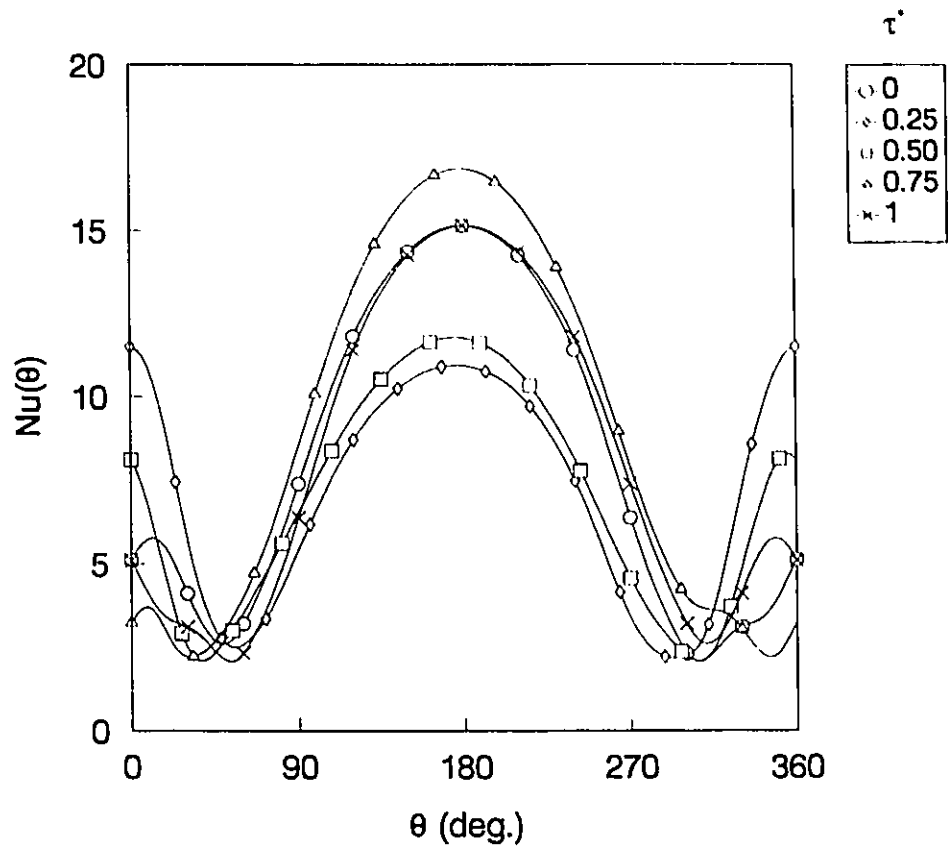


Figure 5.28 Local Nusselt number distribution in a full cycle of oscillation
(in-line oscillation, $F_x = 2F_n$, $a_y = 0.2D$, $Gr/Re^2 = 0$)

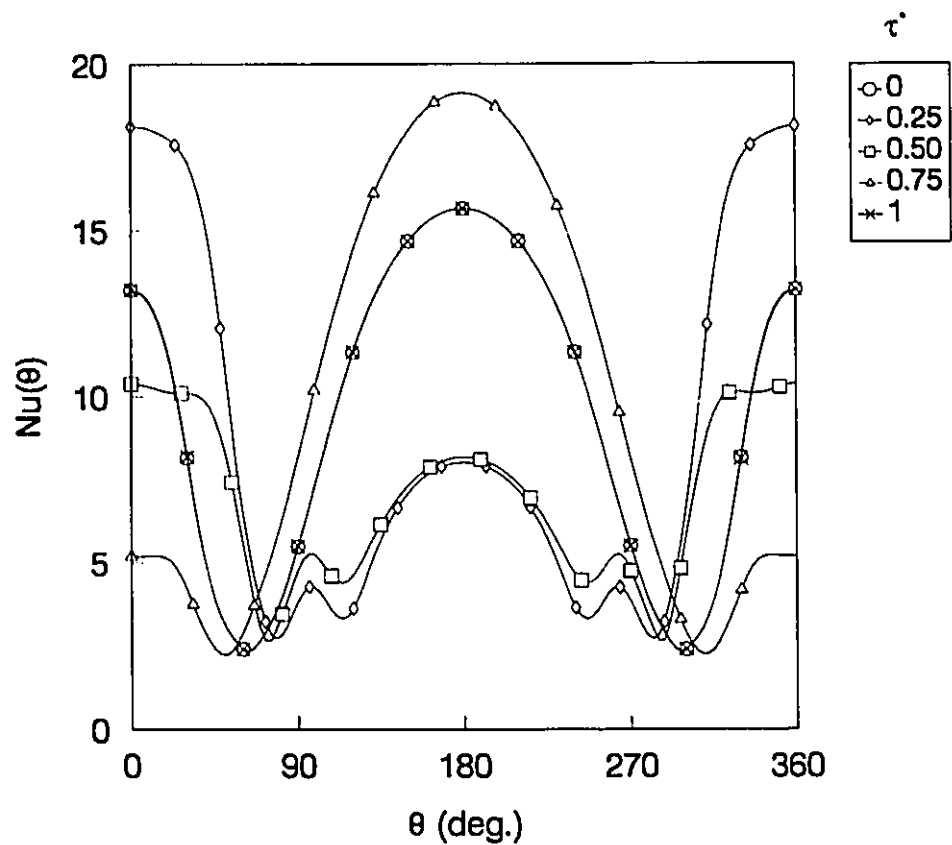


Figure 5.29 Local Nusselt number distribution in a full cycle of oscillation (in-line oscillation, $F_x = 2F_n$, $a_x = 0.4D$, $Gr/Re^2 = 0$)

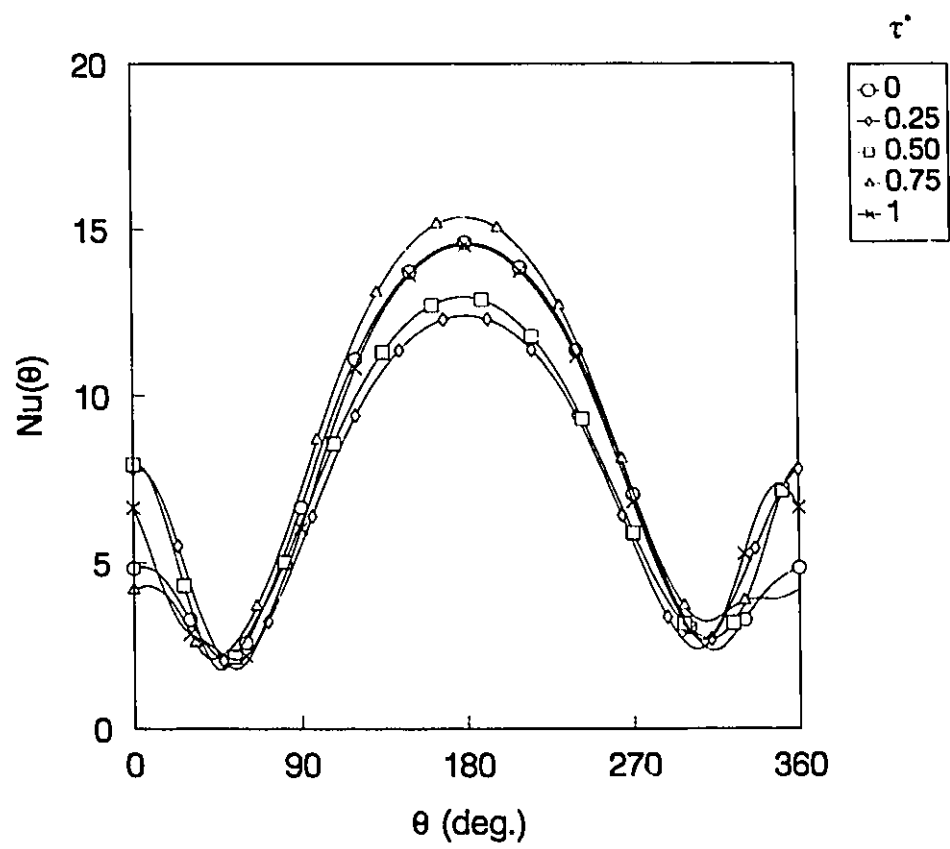


Figure 5.30 Local Nusselt number distribution in a full cycle of oscillation
(in-line oscillation, $F_x = 2F_n$, $a_x = 0.1D$, $Gr/Re^2 = 1$)

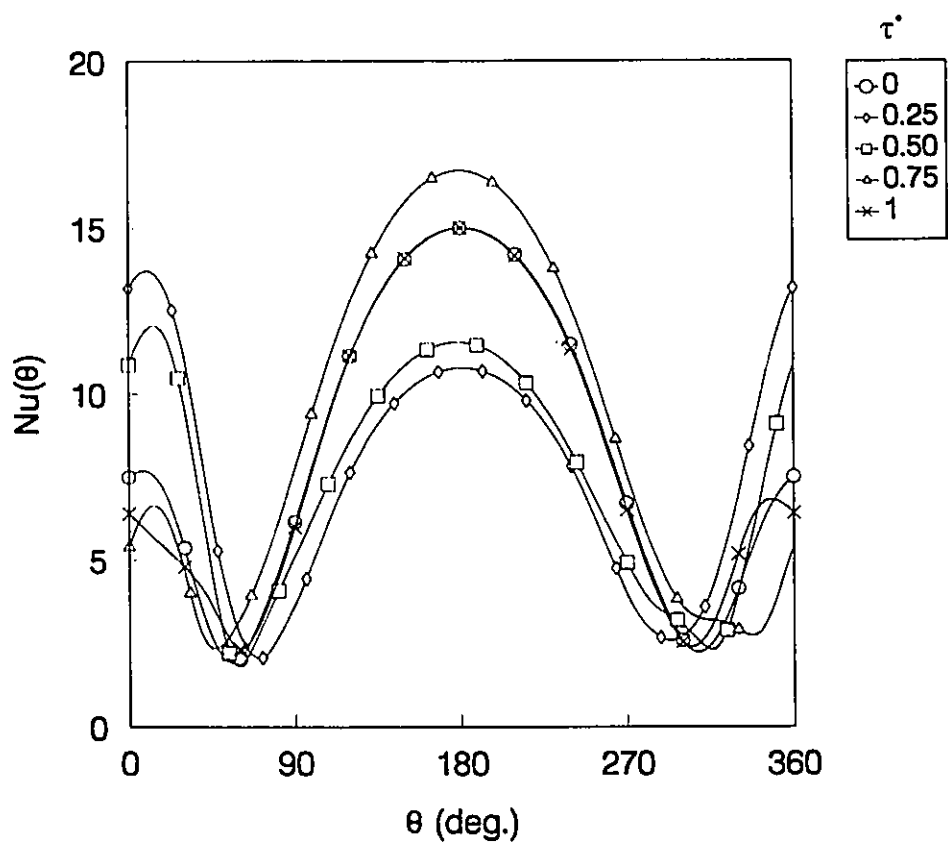


Figure 5.31 Local Nusselt number distribution in a full cycle of oscillation
(in-line oscillation, $F_x = 2F_n$, $a_x = 0.2D$, $Gr/Re^2 = 1$)

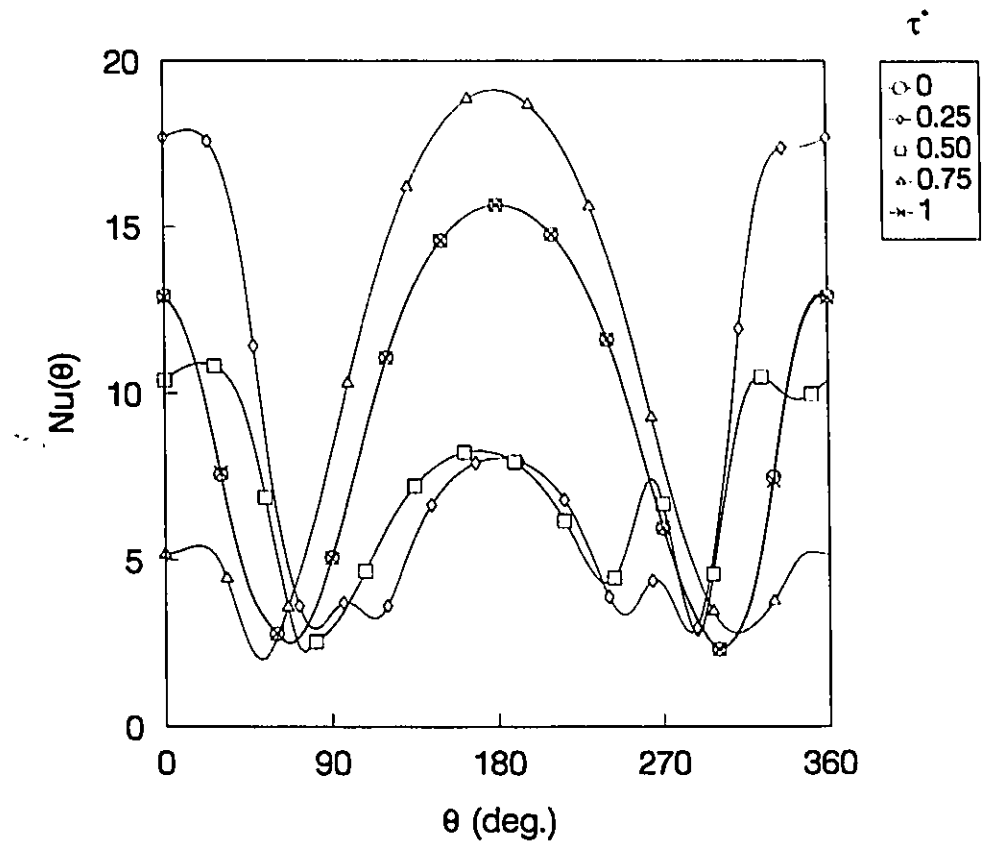


Figure 5.32 Local Nusselt number distribution in a full cycle of oscillation
(in-line oscillation, $F_x = 2F_n$, $a_x = 0.4D$, $Gr/Re^2 = 1$)

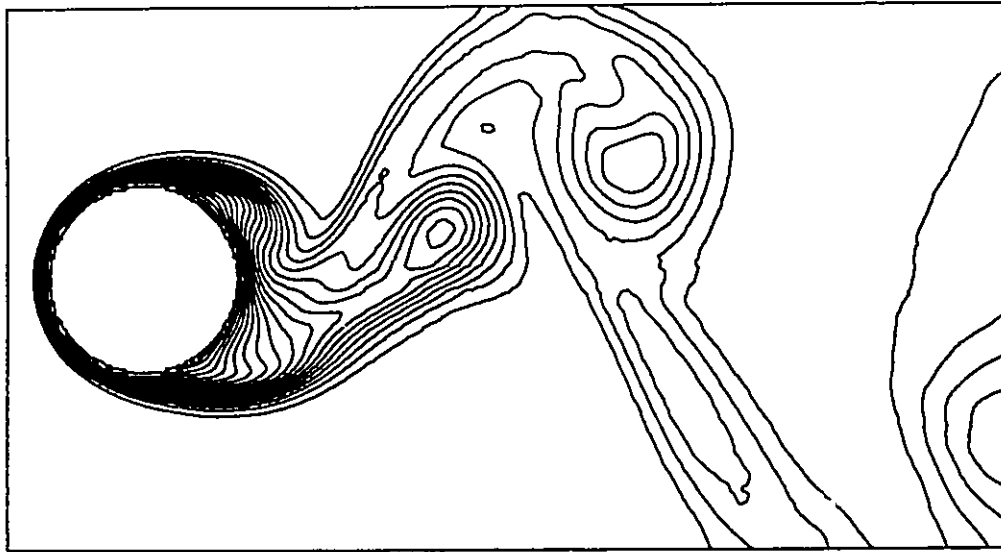


Figure 5.33 Isothermal contours for the case of forced convection (in-line oscillation, $\tau^* = 0$, $a_x = 0.2D$, minimum and maximum contour level: 0.05 and 1, contour interval: 0.05)

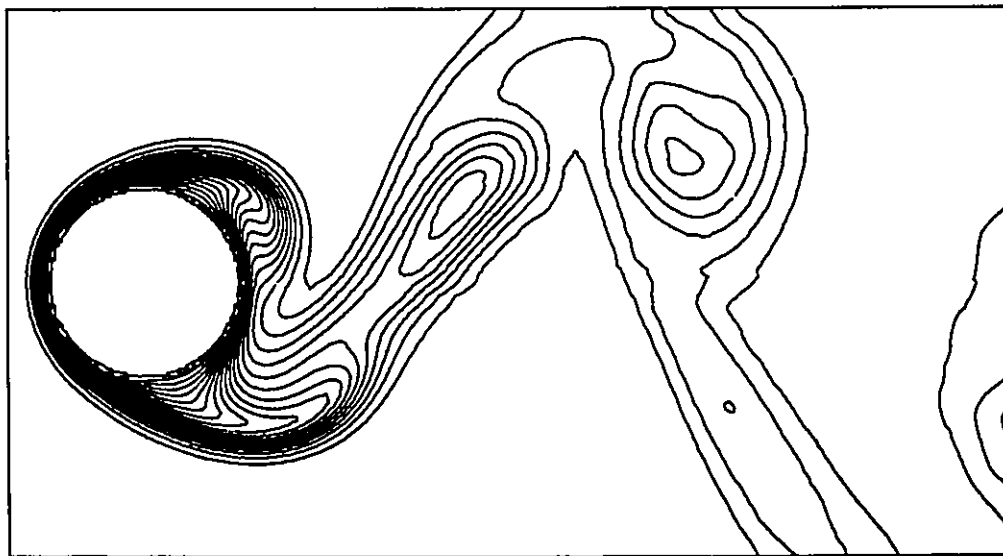


Figure 5.34 Isothermal contours for the case of forced convection (in-line oscillation, $\tau^* = 0.25$, $a_x = 0.2D$, minimum and maximum contour level: 0.05 and 1, contour interval: 0.05)

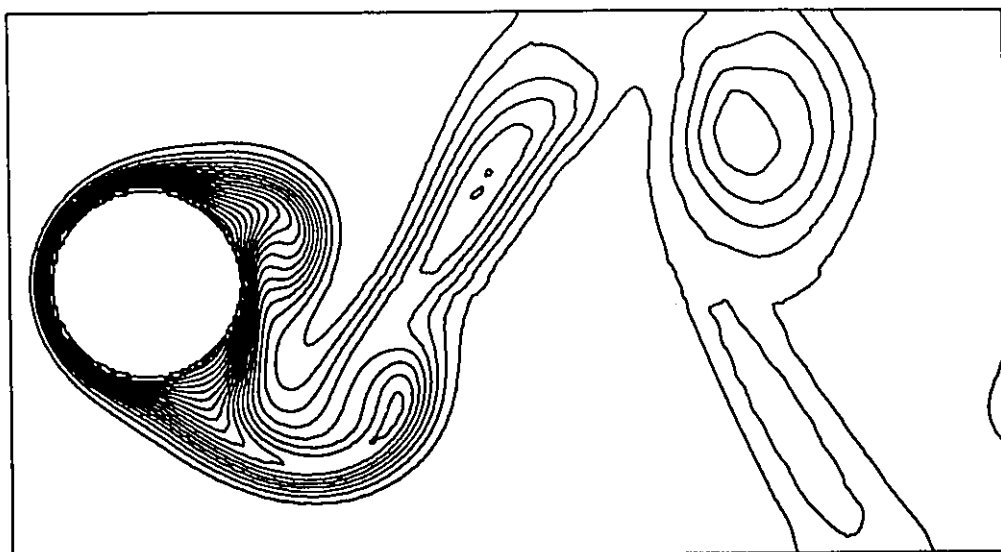


Figure 5.35 Isothermal contours for the case of forced convection (in-line oscillation, $\tau^* = 0.50$, $a_x = 0.2D$, minimum and maximum contour level: 0.05 and 1, contour interval: 0.05)

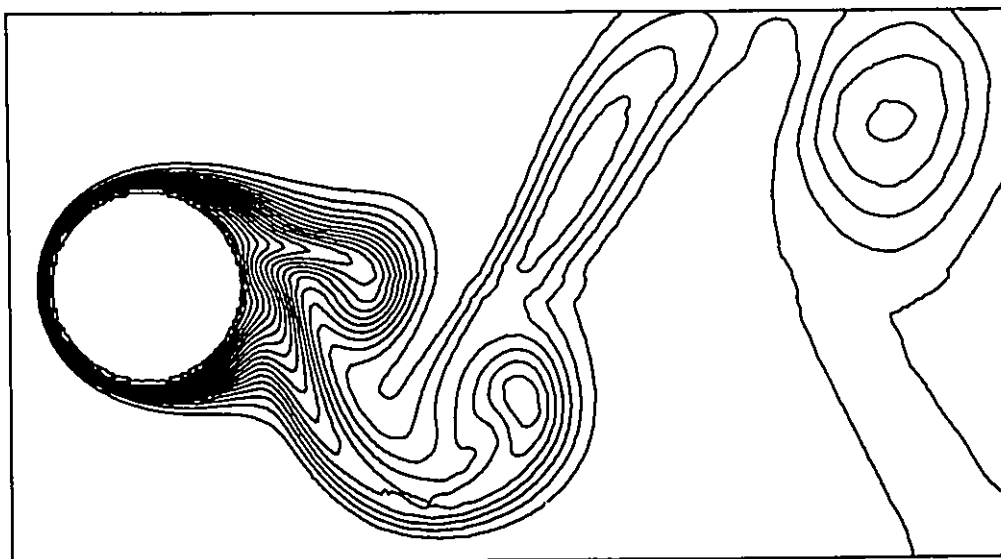


Figure 5.36 Isothermal contours for the case of forced convection (in-line oscillation, $\tau^* = 0.75$, $a_x = 0.2D$, minimum and maximum contour level: 0.05 and 1, contour interval: 0.05)

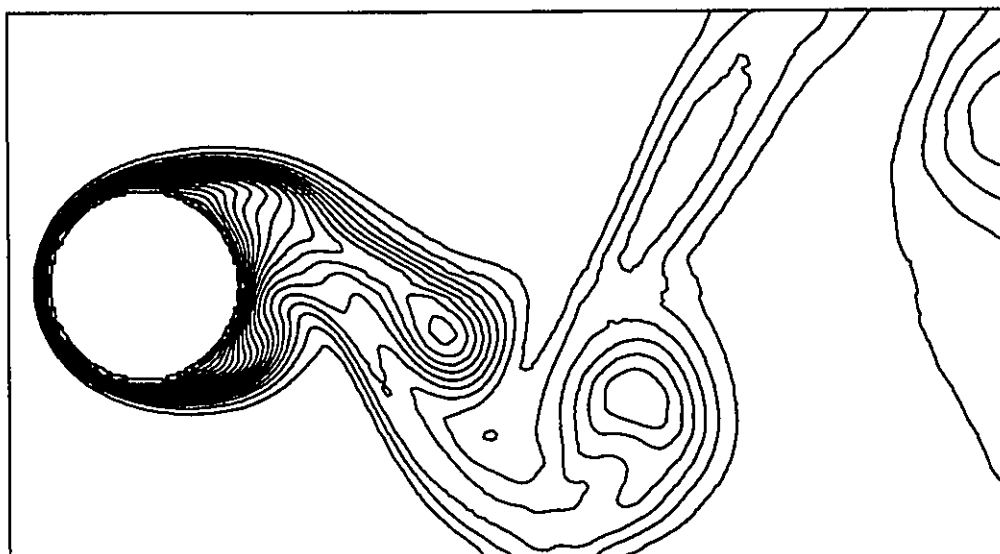


Figure 5.37 Isothermal contours for the case of forced convection (in-line oscillation, $\tau^* = 1$, $a_x = 0.2D$, minimum and maximum contour level: 0.05 and 1, contour interval: 0.05)

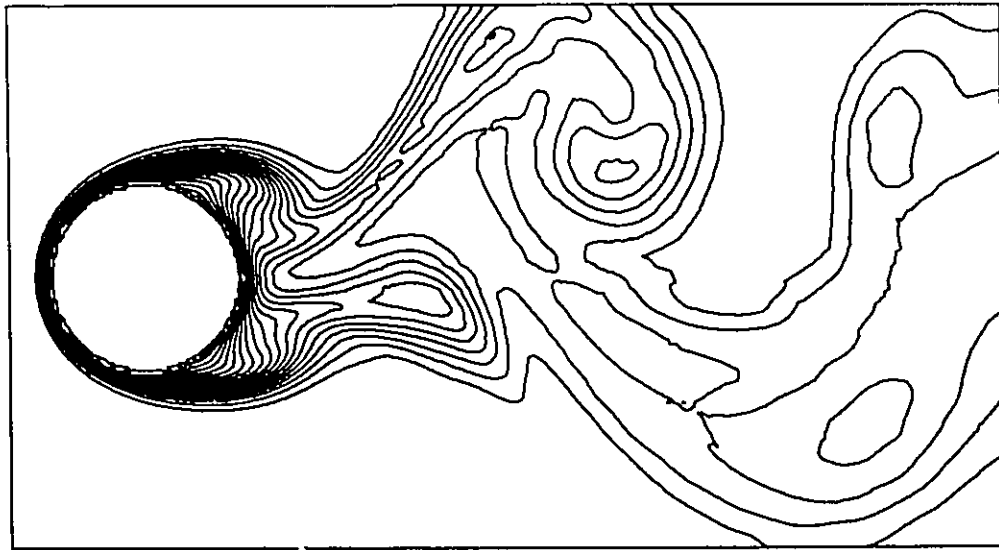


Figure 5.38 Isothermal contours for the case of mixed convection (in-line oscillation, $\tau^* = 0$, $a_x = 0.2D$, minimum and maximum contour level: 0.05 and 1, contour interval: 0.05)

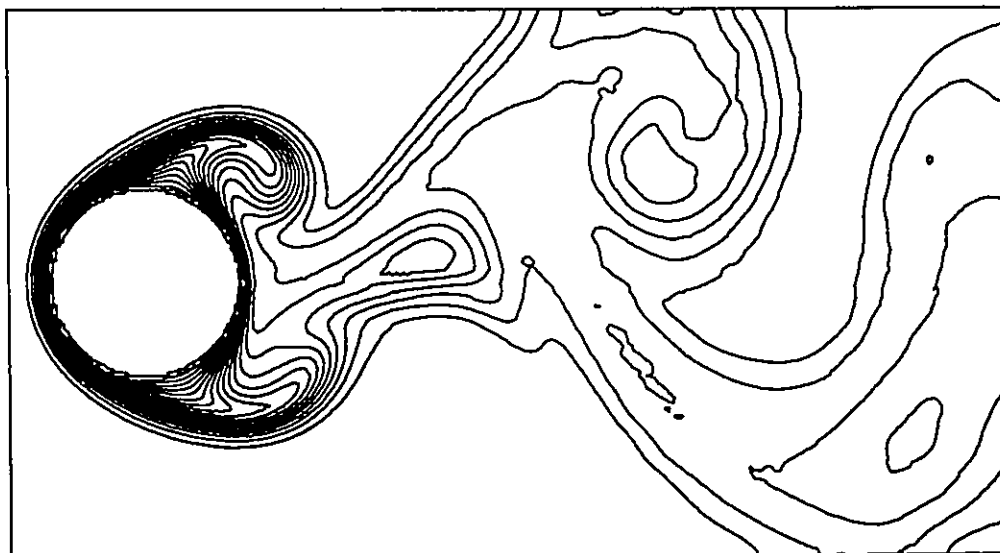


Figure 5.39 Isothermal contours for the case of mixed convection (in-line oscillation, $\tau^* = 0.25$, $a_x = 0.2D$, minimum and maximum contour level: 0.05 and 1, contour interval: 0.05)

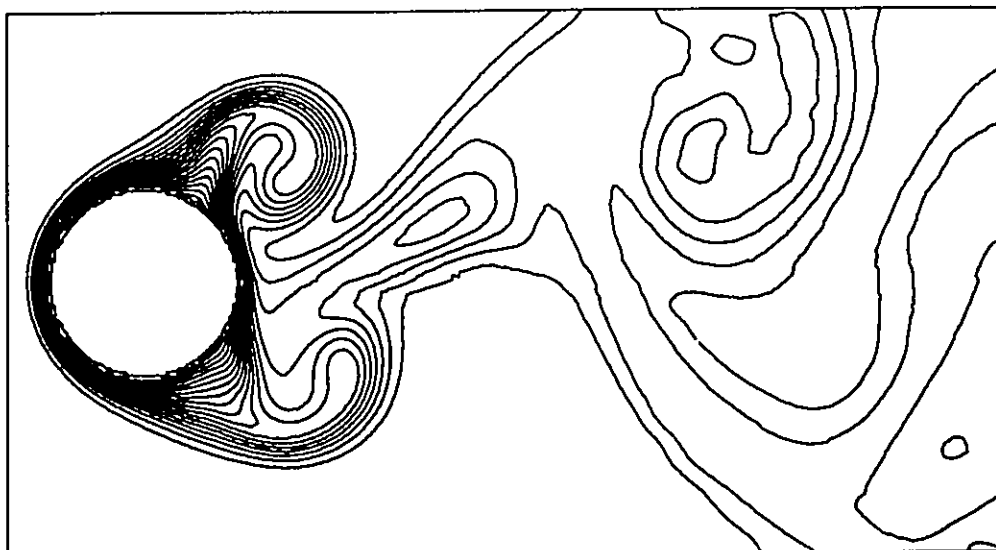


Figure 5.40 Isothermal contours for the case of mixed convection (in-line oscillation, $\tau' = 0.50$, $a_x = 0.2D$, minimum and maximum contour level: 0.05 and 1, contour interval: 0.05)

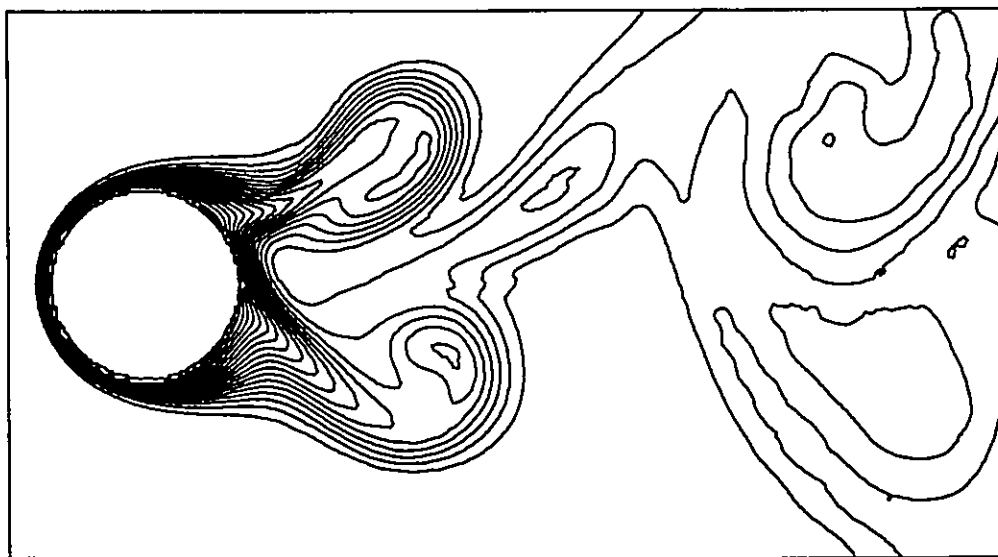


Figure 5.41 Isothermal contours for the case of mixed convection (in-line oscillation, $\tau' = 0.75$, $a_x = 0.2D$, minimum and maximum contour level: 0.05 and 1, contour interval: 0.05)

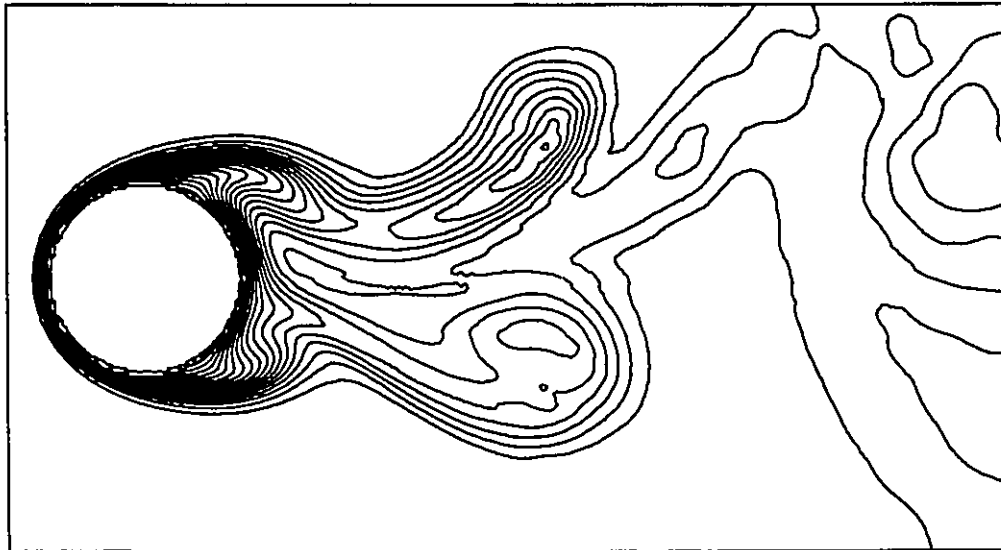


Figure 5.42 Isothermal contours for the case of mixed convection (in-line oscillation, $\tau' = 1$, $a_x = 0.2D$, minimum and maximum contour level: 0.05 and 1, contour interval: 0.05)

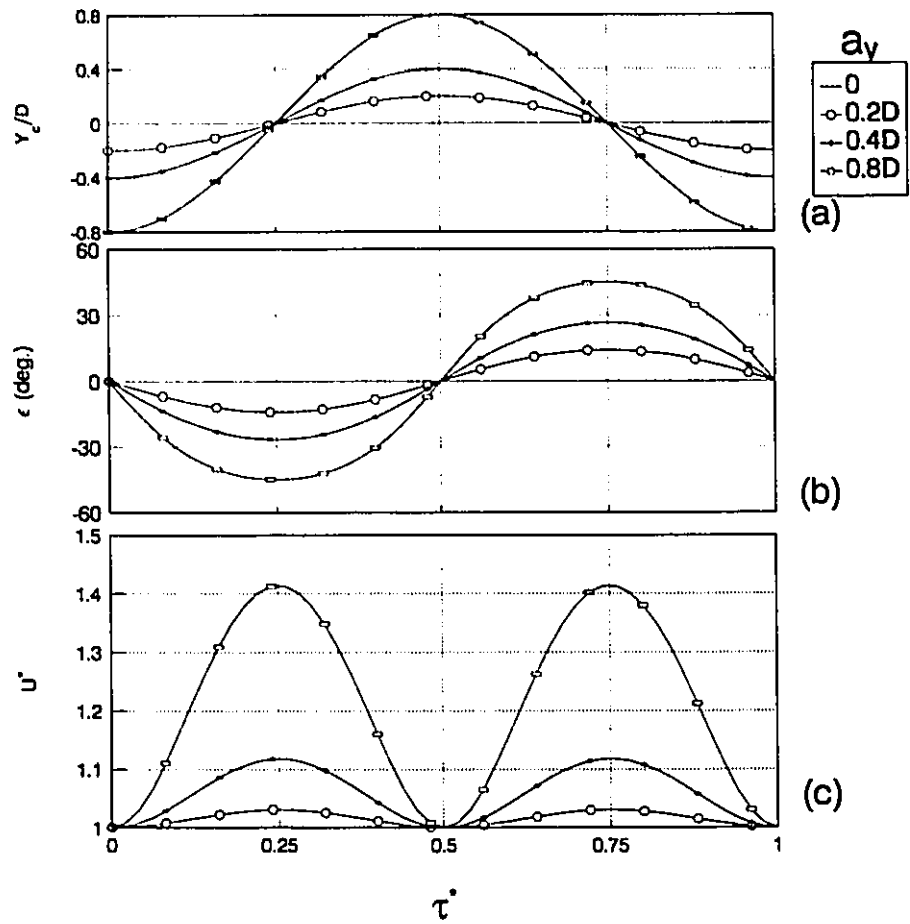


Figure 5.43 Details of forced oscillation of the cylinder
(transverse oscillation , $F_y = F_n$) (a) position of the cylinder (b) incident angle of
the relative free stream velocity (c) magnitude of the relative free stream
velocity

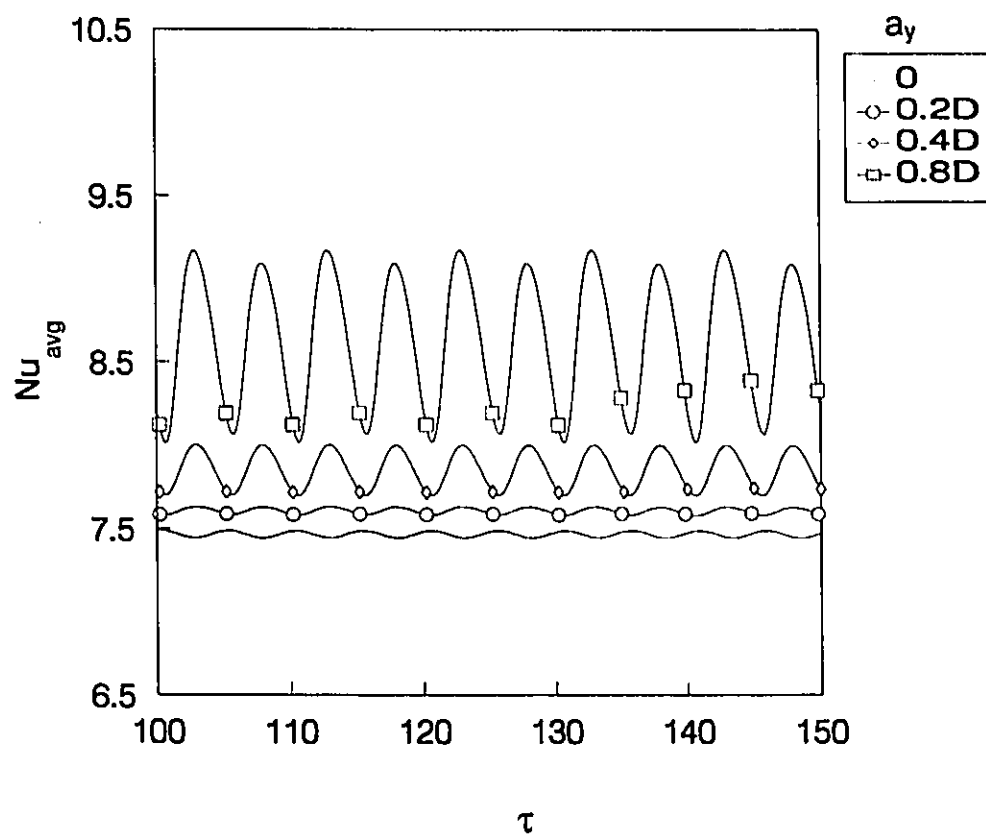


Figure 5.44 Time history of the average Nusselt number
(transverse oscillation, $F_y = F_n$, $Gr/Re^2 = 0$)

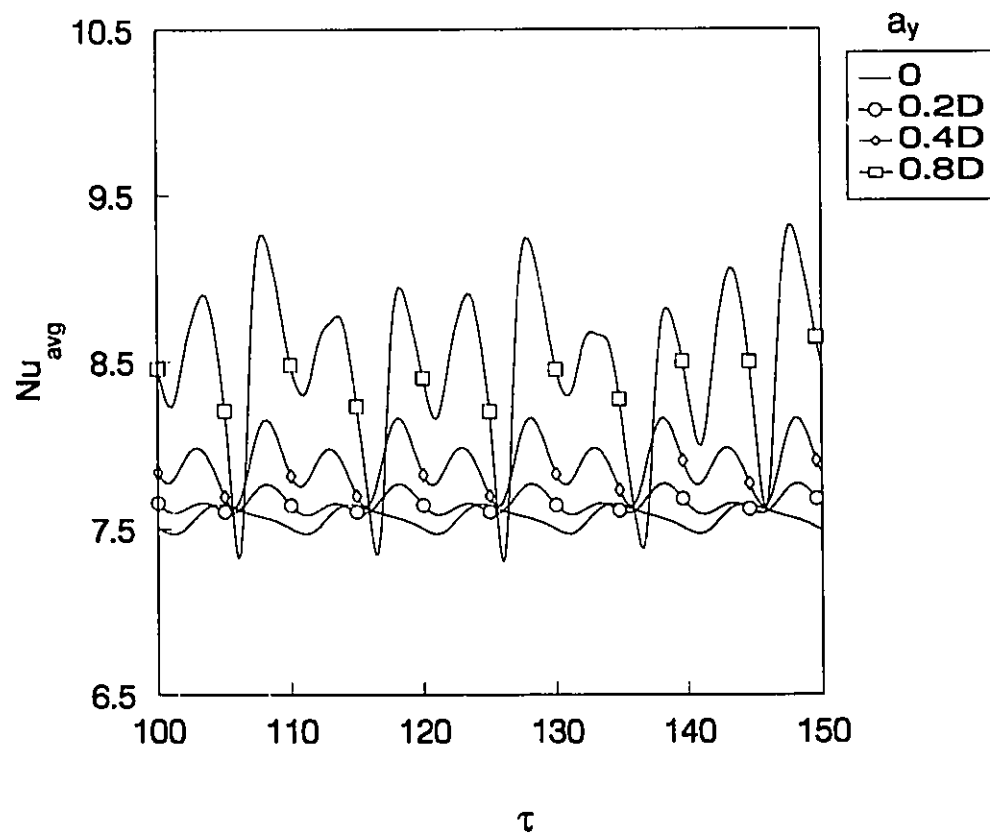


Figure 5.45 Time history of the average Nusselt number
(transverse oscillation, $F_y = F_n$, $Gr/Re^2 = 1$)

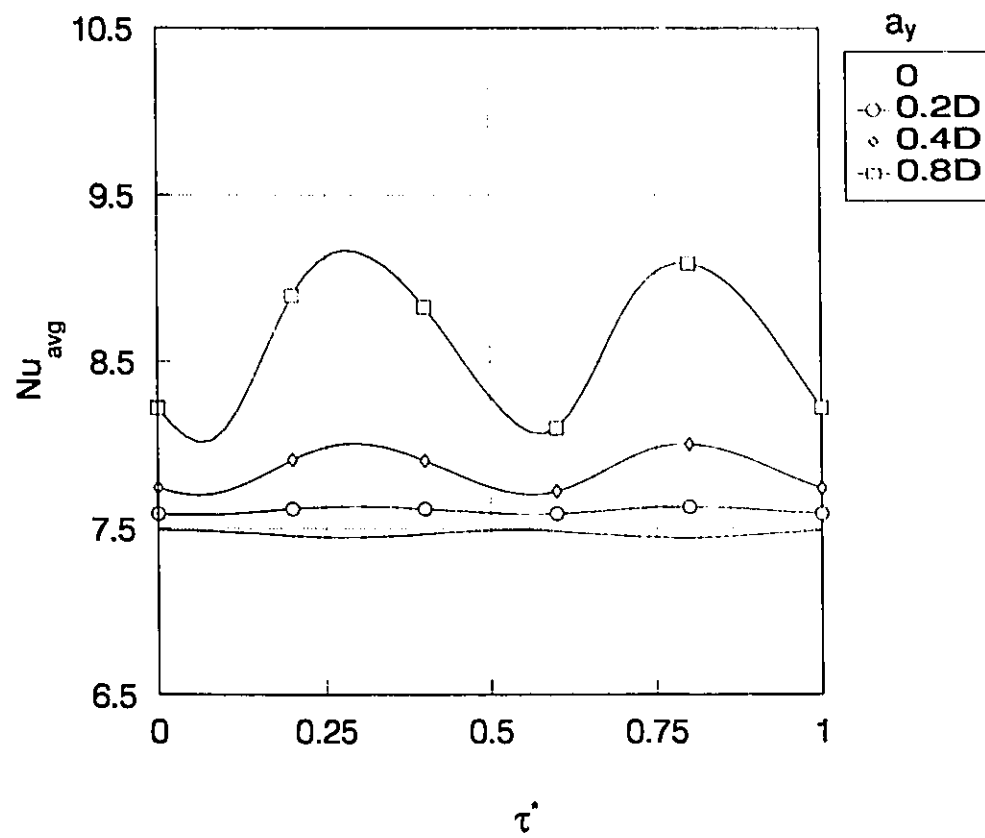


Figure 5.46 Average Nusselt number in a cycle of oscillation
(transverse oscillation, $F_y = F_n$, $Gr/Re^2 = 0$)

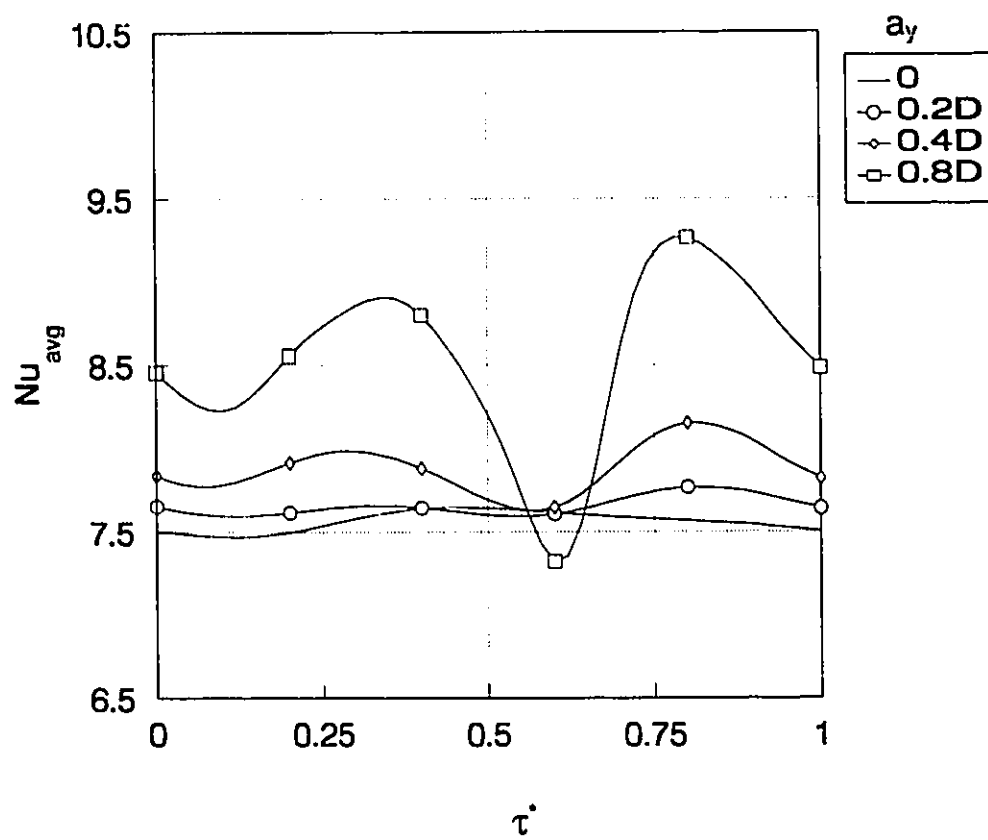


Figure 5.47 Average Nusselt number in a cycle of oscillation
(transverse oscillation, $F_y = F_n$, $Gr/Re^2 = 1$)

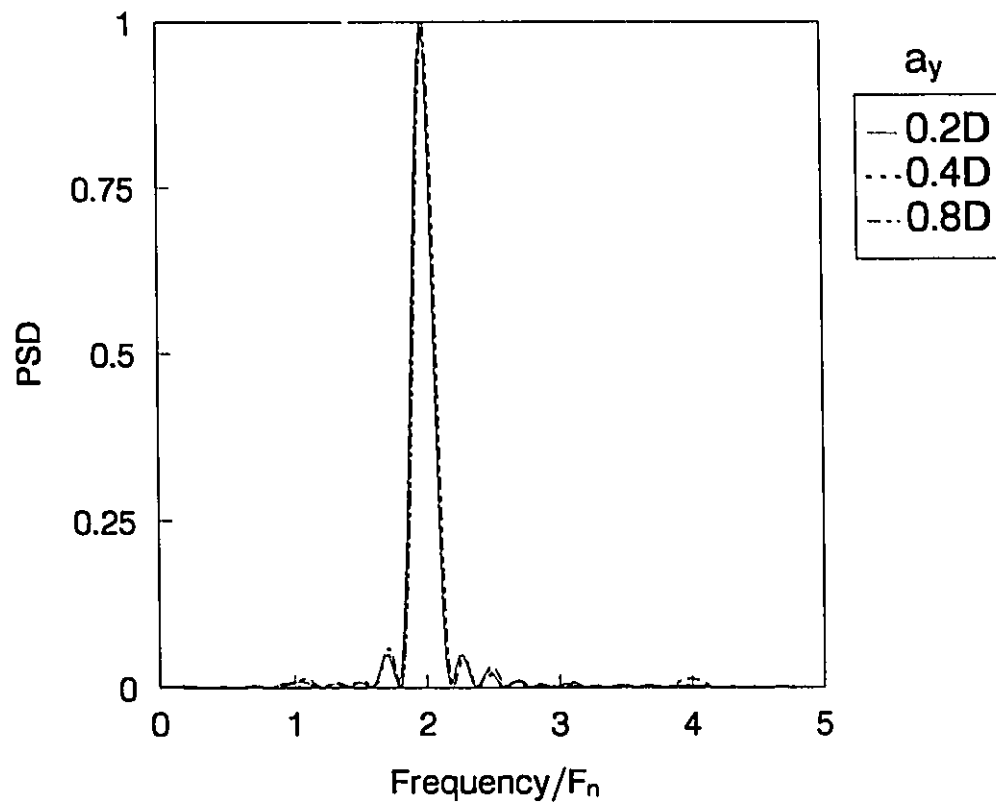


Figure 5.48 Power spectra of the average Nusselt number
(transverse oscillation, $F_y = F_n$, $Gr/Re^2 = 0$)

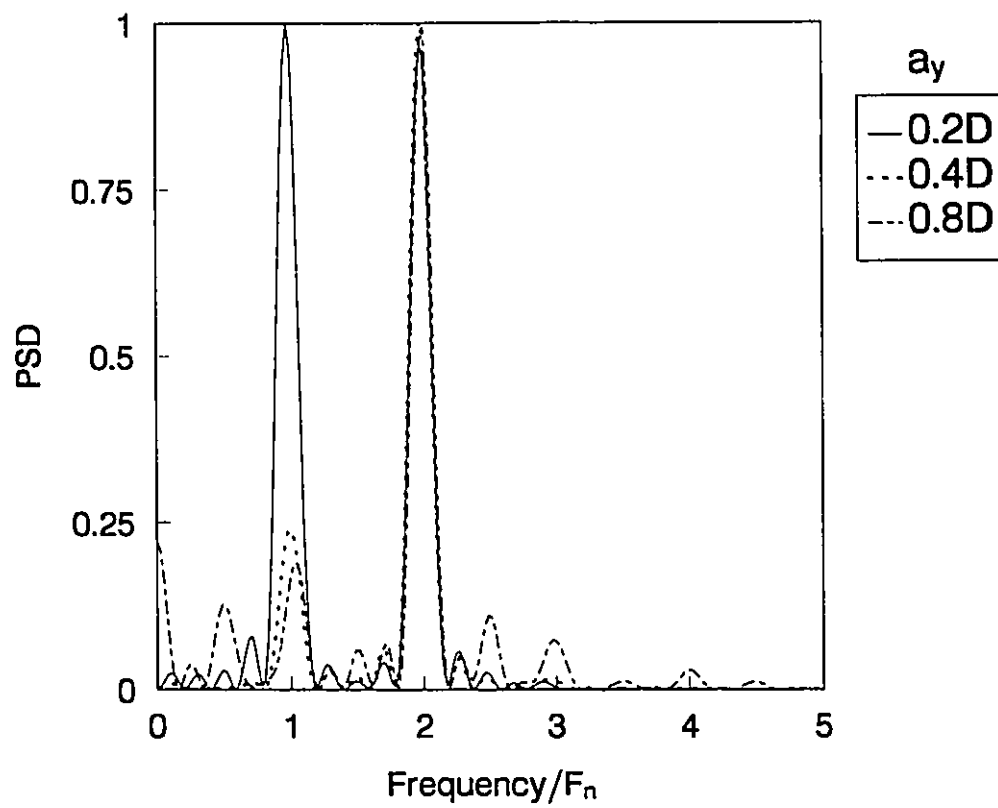


Figure 5.49 Power spectra of the average Nusselt number
(transverse oscillation, $F_y = F_n$, $Gr/Re^2 = 1$)

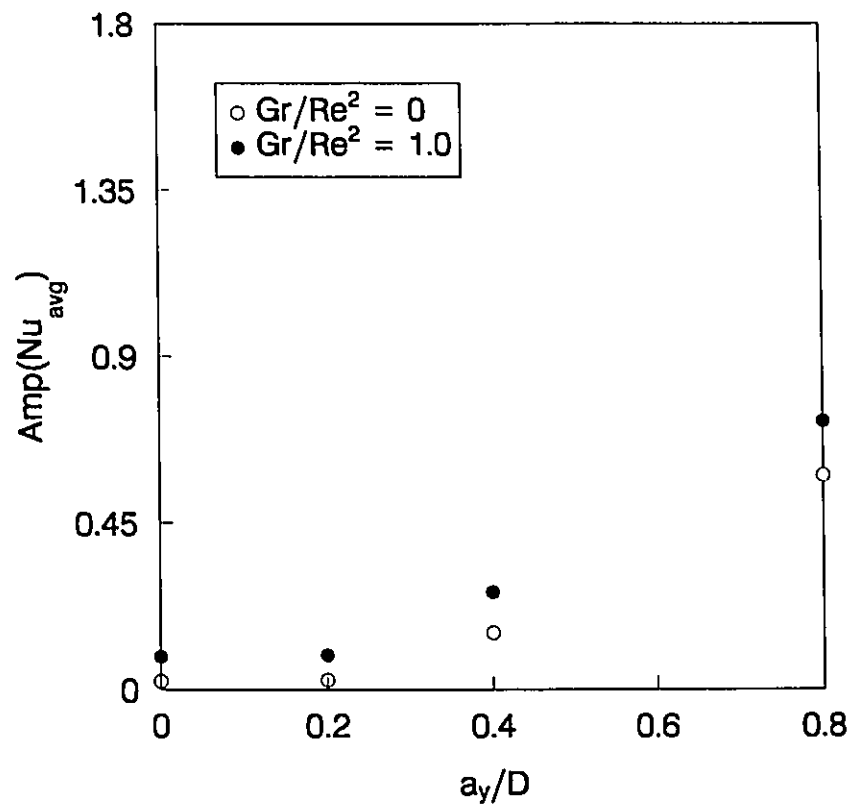


Figure 5.50 Amplitude of Nu_{avg} at different position amplitudes of oscillation (transverse oscillation, $F_y = F_n$)

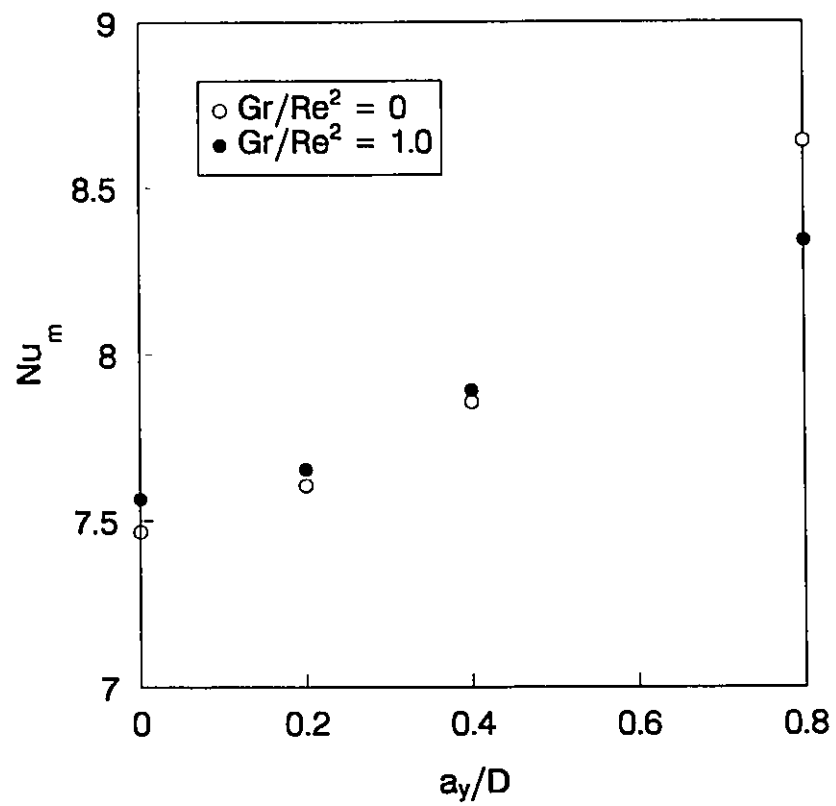


Figure 5.51 Mean Nusselt number at different position amplitudes of oscillation
(transverse oscillation, $F_y = F_n$)

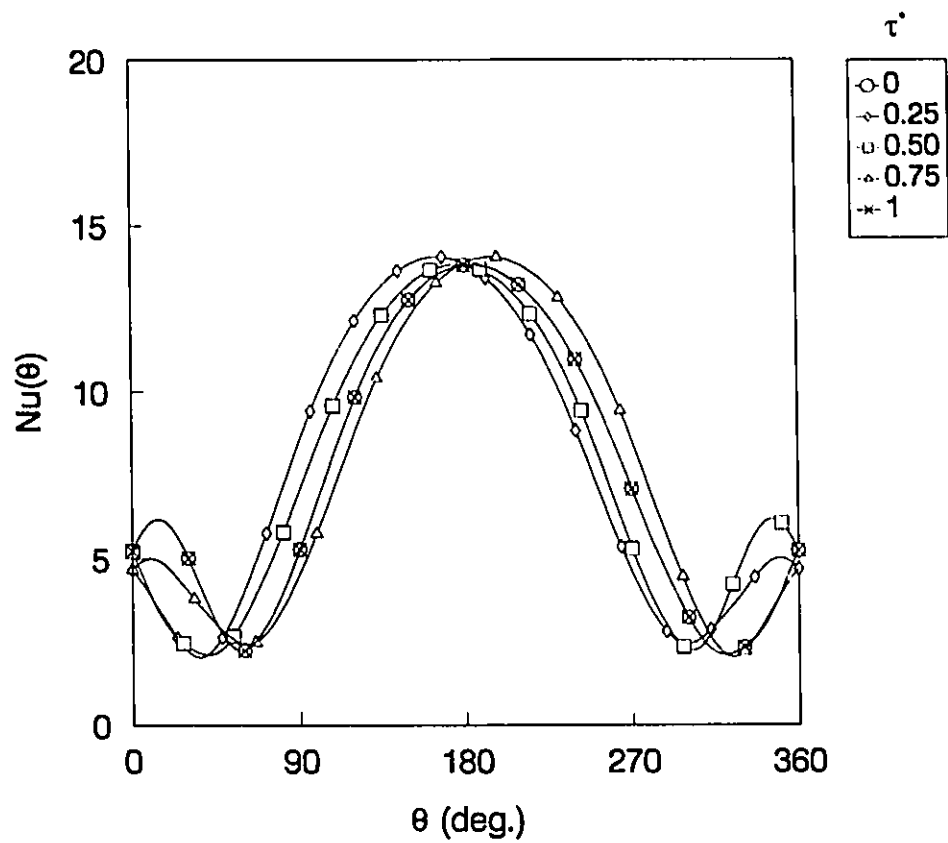


Figure 5.52 Local Nusselt number distribution in a full cycle of oscillation
(transverse oscillation, $F_y = F_n$, $a_y = 0.2D$, $Gr/Re^2 = 0$)

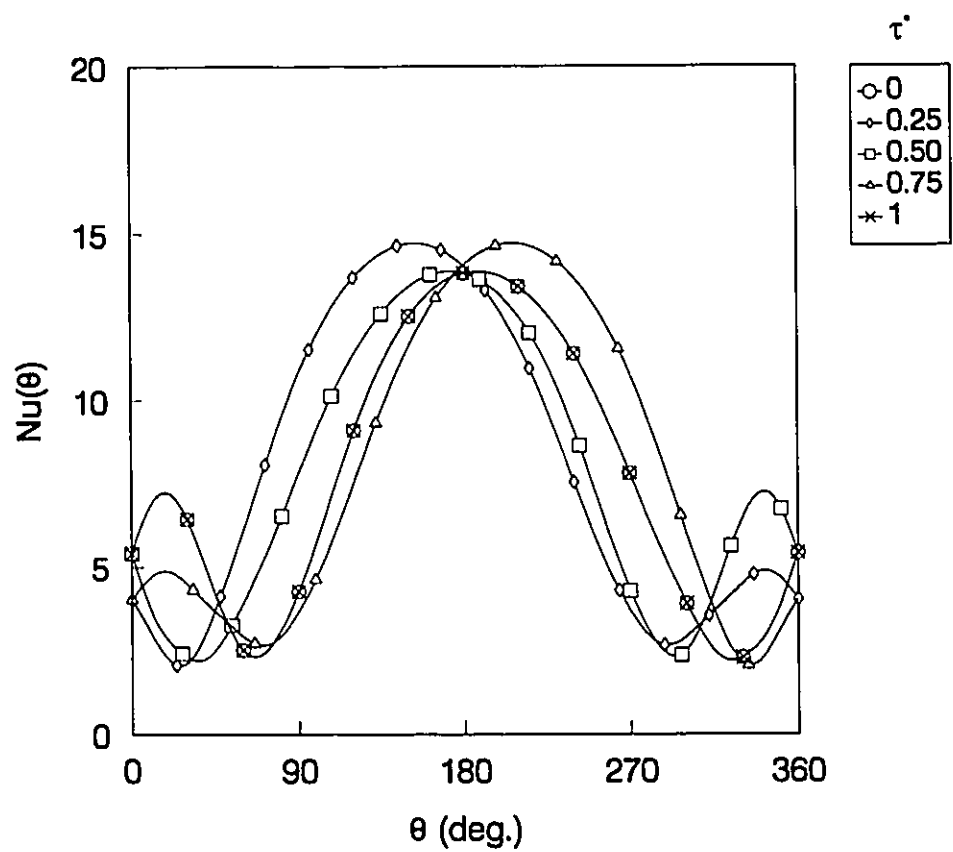


Figure 5.53 Local Nusselt number distribution in a full cycle of oscillation
(transverse oscillation, $F_y = F_n$, $a_y = 0.4D$, $Gr/Re^2 = 0$)

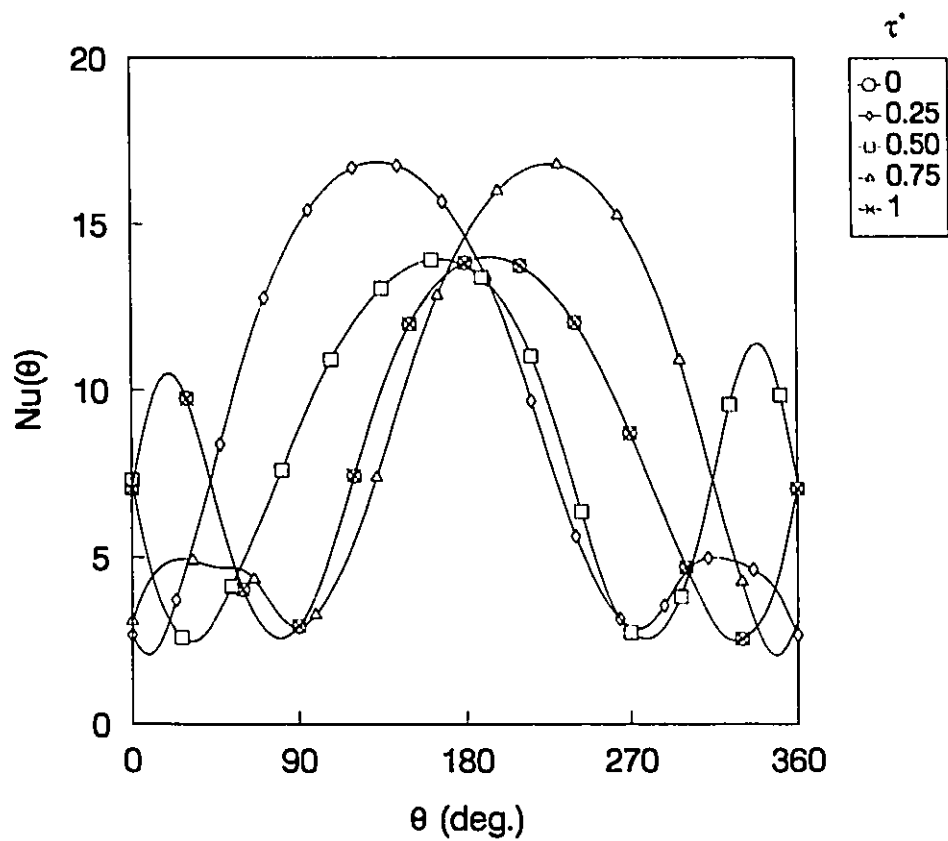


Figure 5.54 Local Nusselt number distribution in a full cycle of oscillation
(transverse oscillation, $F_y = F_n$, $a_y = 0.8D$, $Gr/Re^2 = 0$)

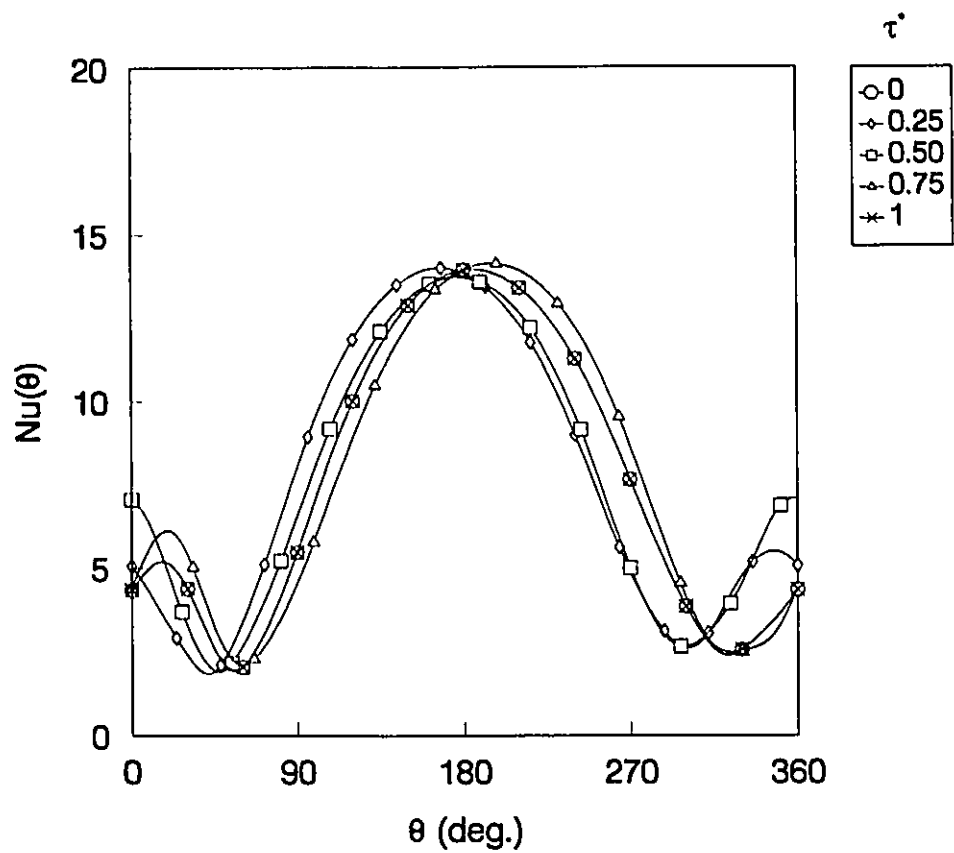


Figure 5.55 Local Nusselt number distribution in a full cycle of oscillation
(transverse oscillation, $F_y = F_n$, $a_y = 0.2D$, $Gr/Re^2 = 1$)

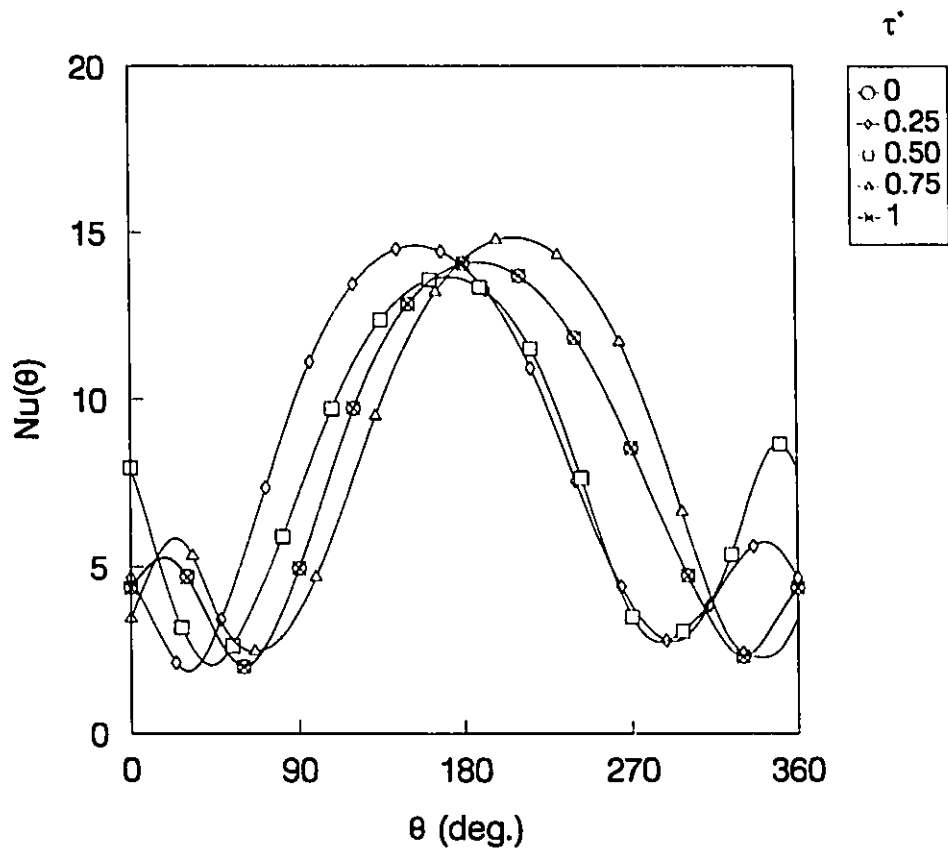


Figure 5.56 Local Nusselt number distribution in a full cycle of oscillation
(transverse oscillation, $F_y = F_n$, $a_y = 0.4D$, $Gr/Re^2 = 1$)

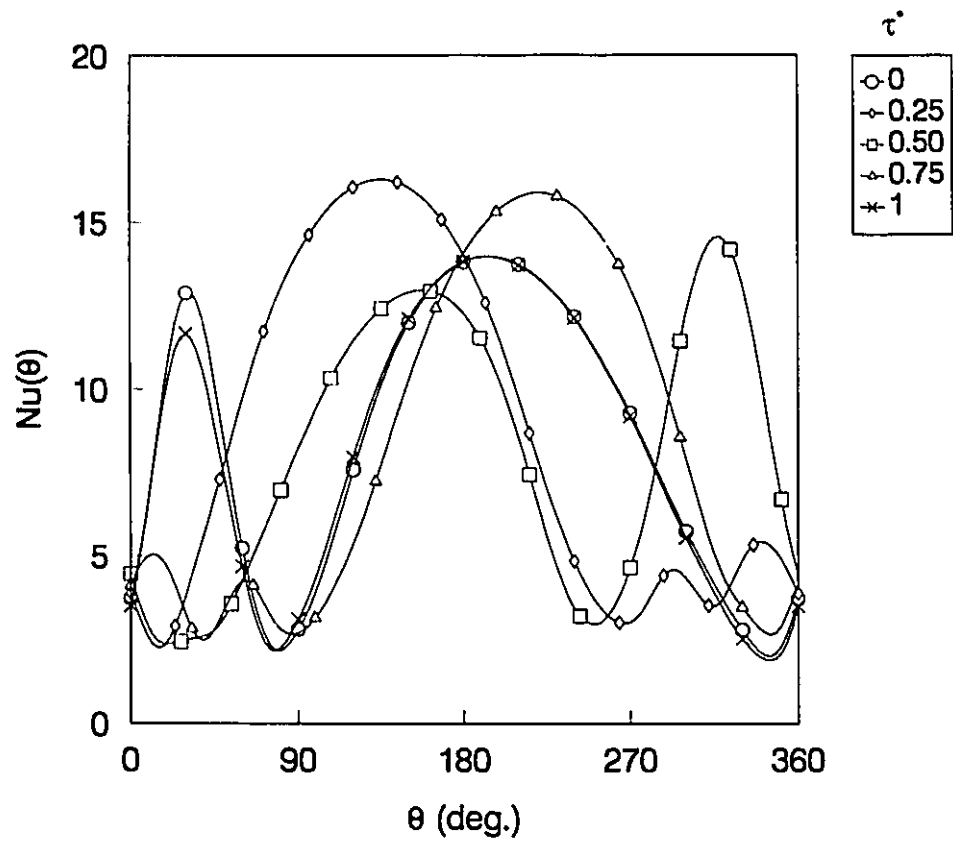


Figure 5.57 Local Nusselt number distribution in a full cycle of oscillation
(transverse oscillation, $F_y = F_n$, $a_y = 0.8D$, $Gr/Re^2 = 1$)

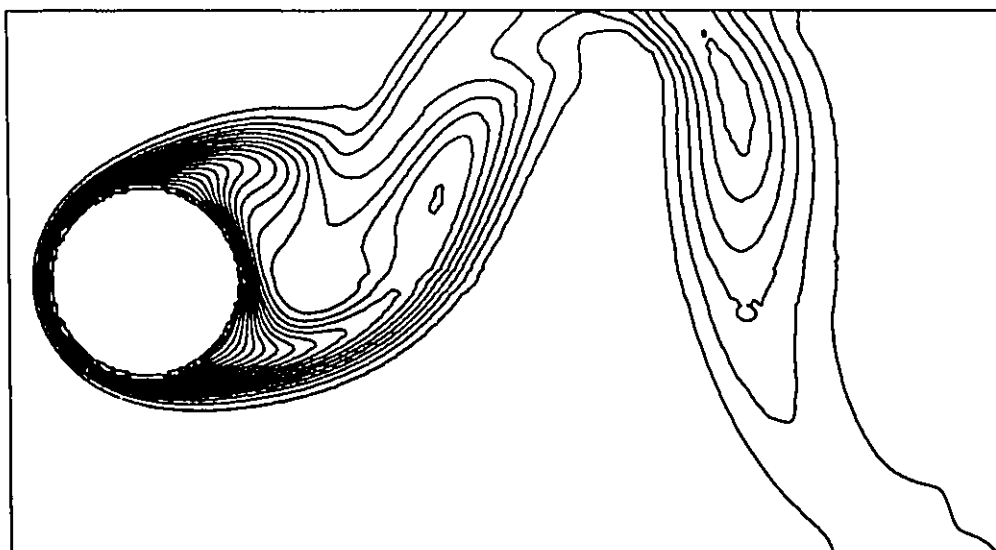


Figure 5.58 Isothermal contours for the case of forced convection (transverse oscillation, $\tau^* = 0$, $a_y = 0.4D$, minimum and maximum contour level: 0.05 and 1, contour interval: 0.05)

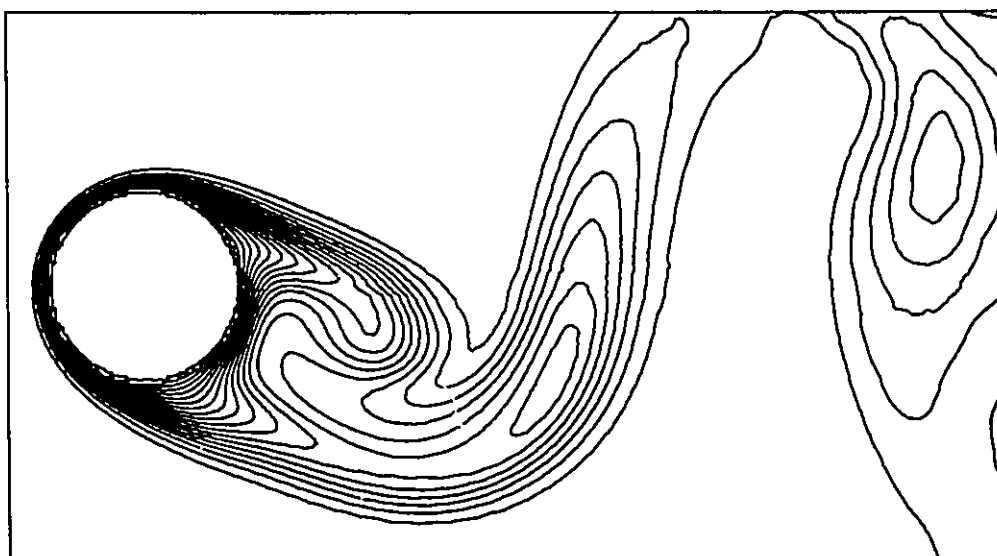


Figure 5.59 Isothermal contours for the case of forced convection (transverse oscillation, $\tau^* = 0.25$, $a_y = 0.4D$, minimum and maximum contour level: 0.05 and 1, contour interval: 0.05)

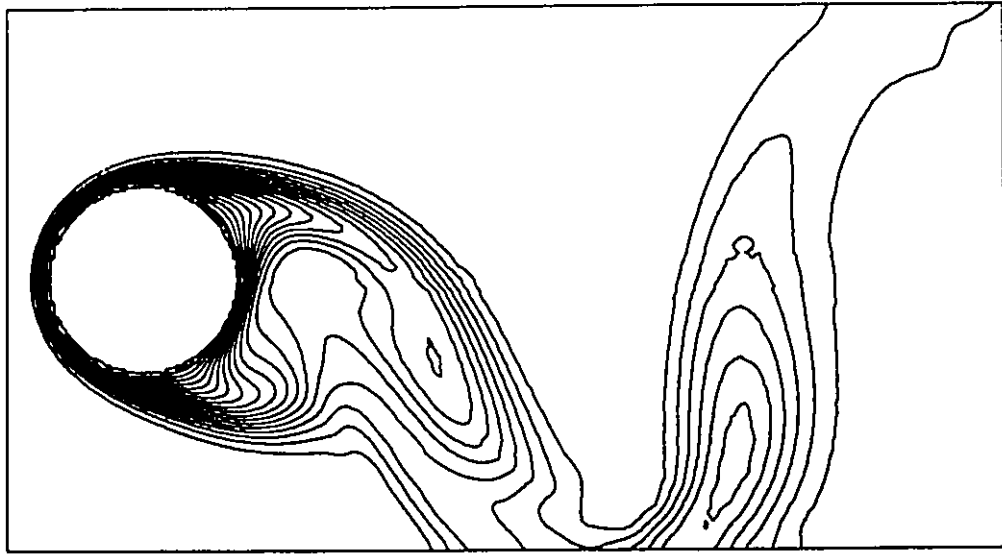


Figure 5.60 Isothermal contours for the case of forced convection (transverse oscillation, $\tau^* = 0.50$, $a_y = 0.4D$, minimum and maximum contour level: 0.05 and 1, contour interval: 0.05)

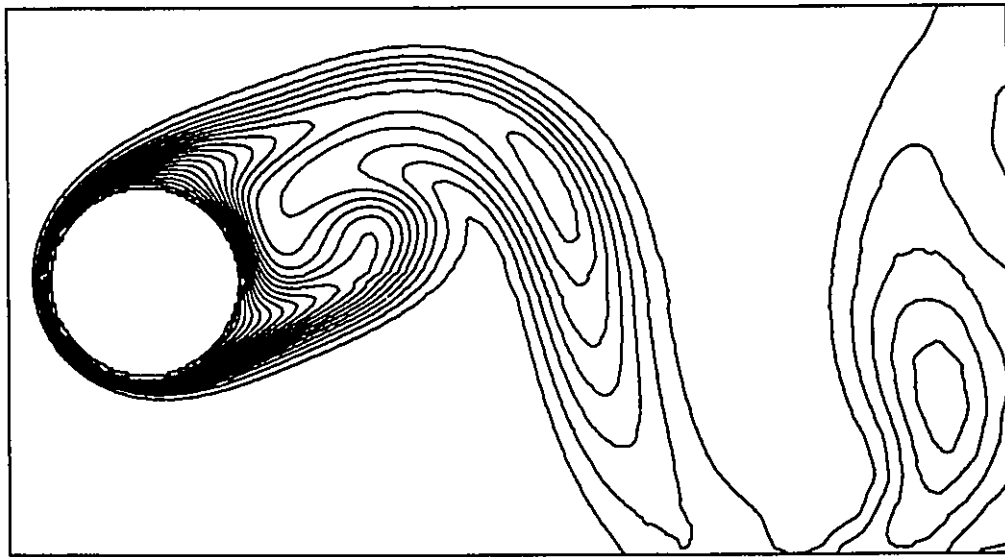


Figure 5.61 Isothermal contours for the case of forced convection (transverse oscillation, $\tau^* = 0.75$, $a_y = 0.4D$, minimum and maximum contour level: 0.05 and 1, contour interval: 0.05)

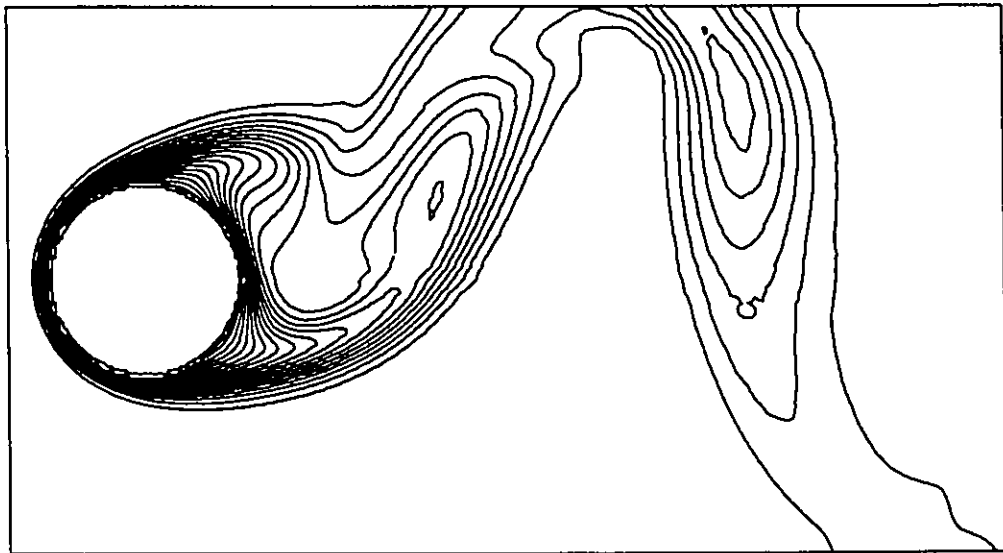


Figure 5.62 Isothermal contours for the case of forced convection (transverse oscillation, $\tau = 1$, $a_y = 0.4D$, minimum and maximum contour level: 0.05 and 1, contour interval: 0.05)

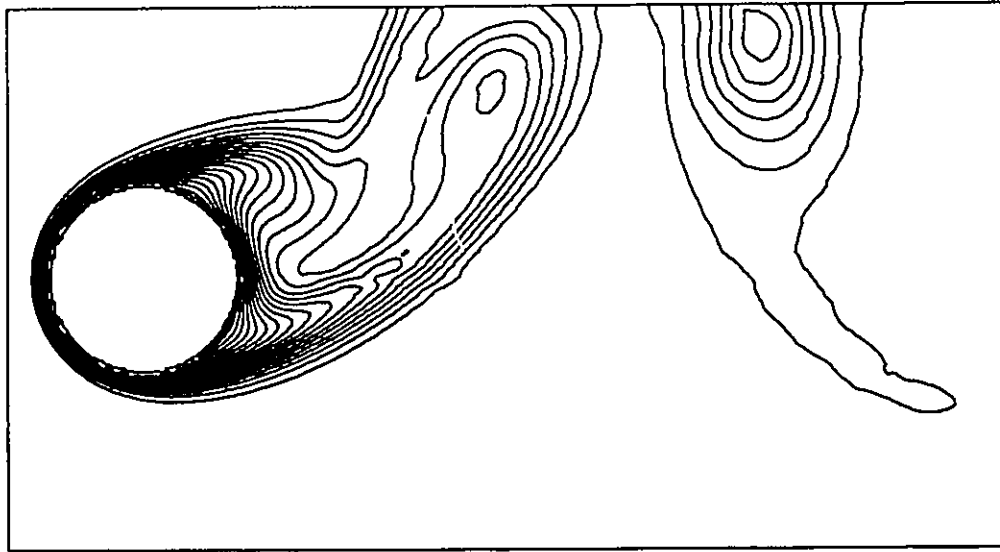


Figure 5.63 Isothermal contours for the case of mixed convection (transverse oscillation, $\tau^* = 0$, $a_y = 0.4D$, minimum and maximum contour level: 0.05 and 1, contour interval: 0.05)

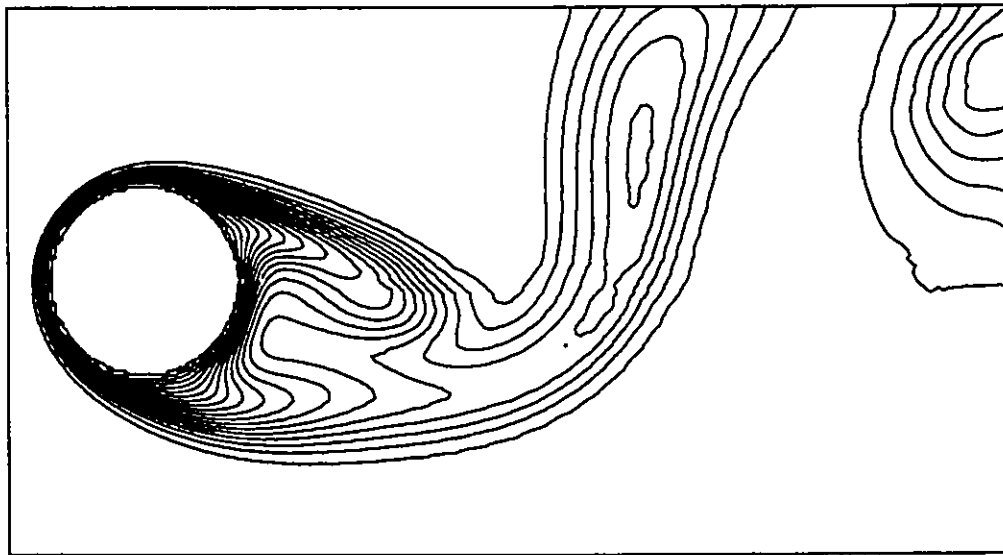


Figure 5.64 Isothermal contours for the case of mixed convection (transverse oscillation, $\tau^* = 0.25$, $a_y = 0.4D$, minimum and maximum contour level: 0.05 and 1, contour interval: 0.05)

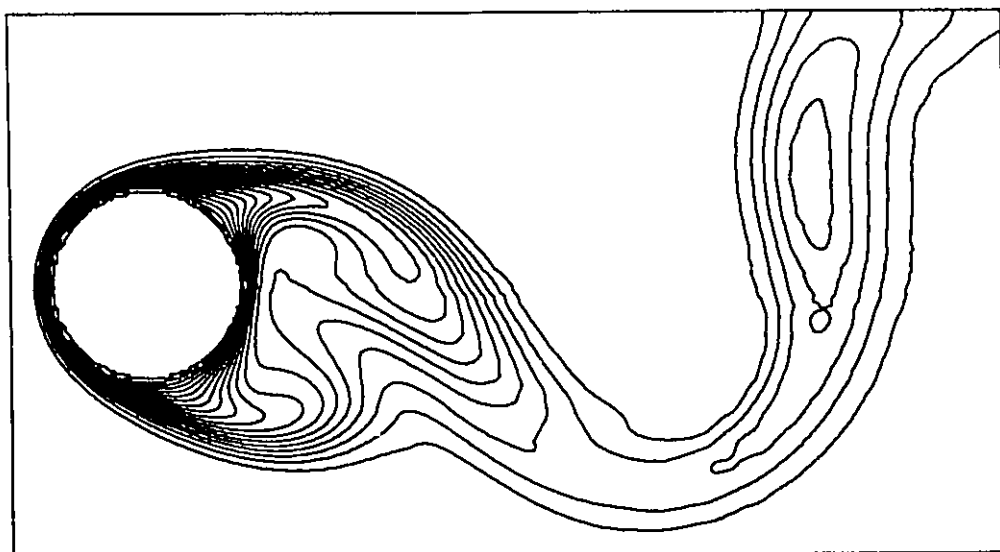


Figure 5.65 Isothermal contours for the case of mixed convection (transverse oscillation, $\tau^* = 0.50$, $a_y = 0.4D$, minimum and maximum contour level: 0.05 and 1, contour interval: 0.05)

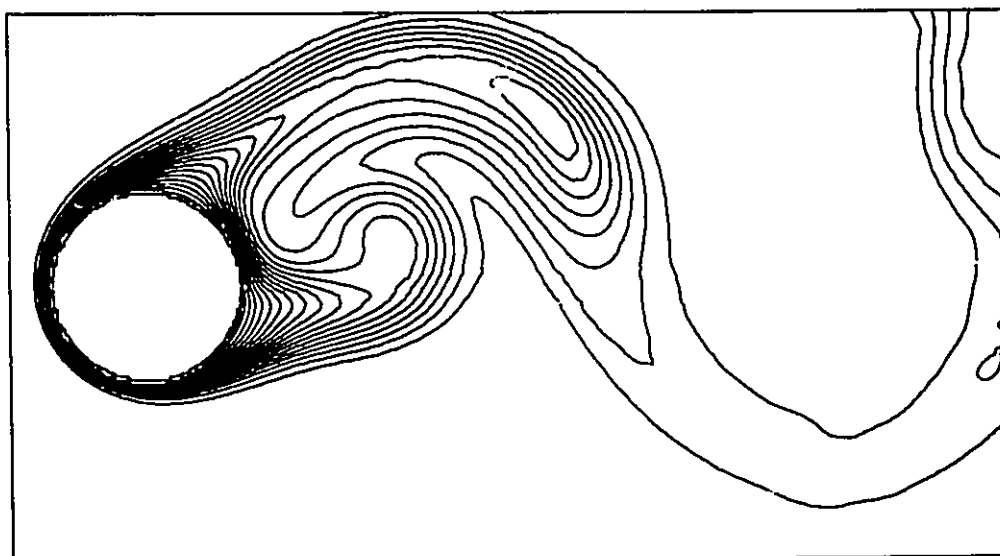


Figure 5.66 Isothermal contours for the case of mixed convection (transverse oscillation, $\tau^* = 0.75$, $a_y = 0.4D$, minimum and maximum contour level: 0.05 and 1, contour interval: 0.05)

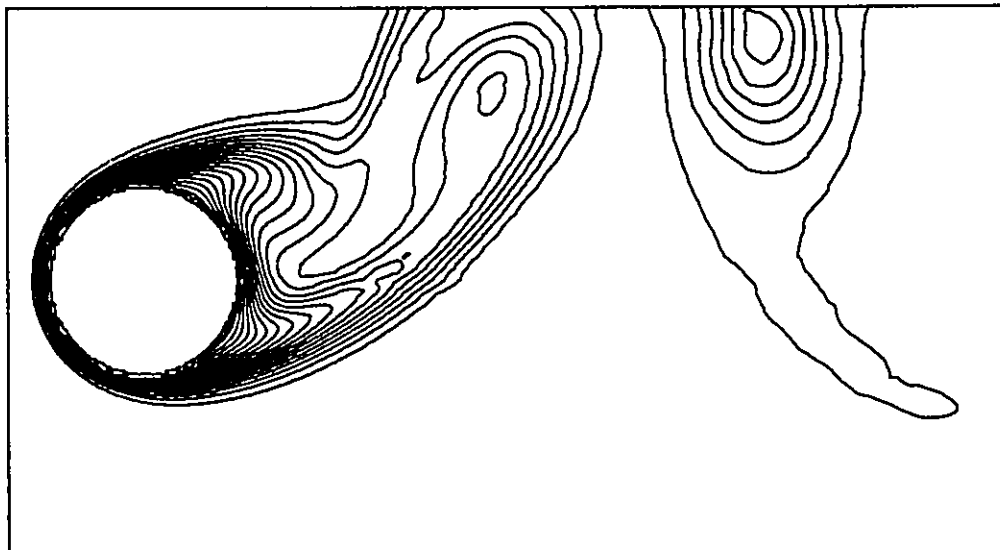


Figure 5.67 Isothermal contours for the case of mixed convection (transverse oscillation, $\tau^* = 1$, $a_y = 0.4D$, minimum and maximum contour level: 0.05 and 1, contour interval: 0.05)

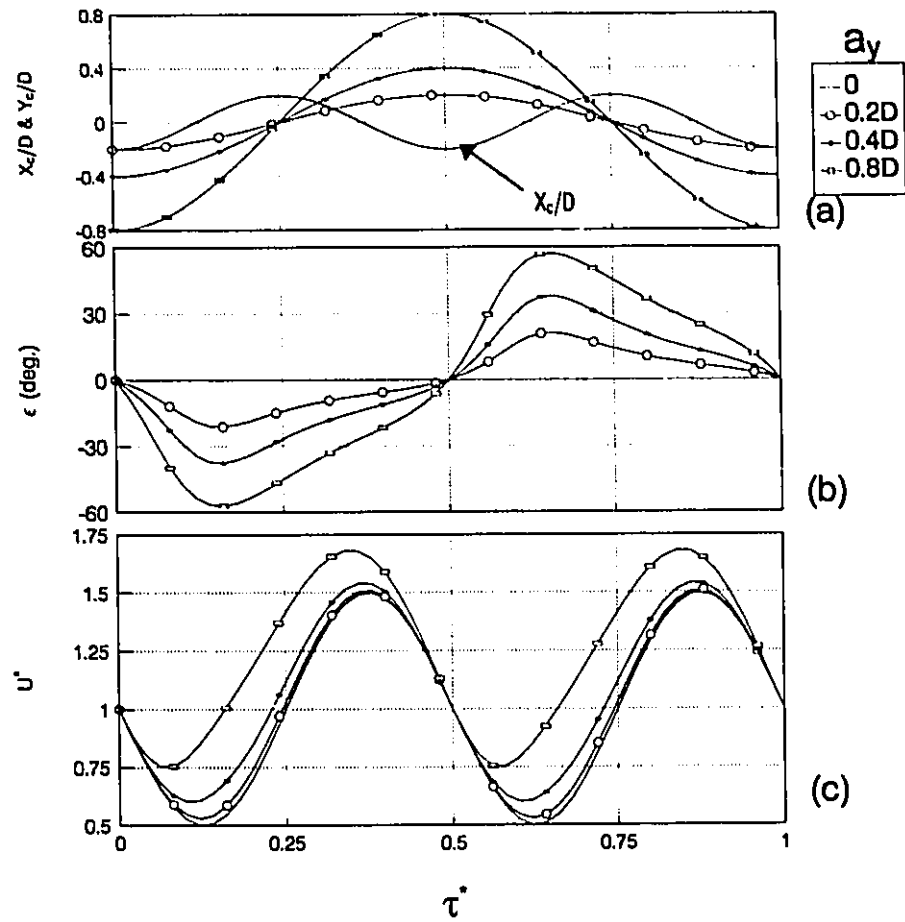


Figure 5.68 Details of forced oscillation of the cylinder
(combined oscillation , $F_x = 2F_n$, $F_y = F_n$, $a_x = 0.2D$) (a) position of the cylinder
(b) incident angle of the relative free stream velocity (c) magnitude of the
relative free stream velocity

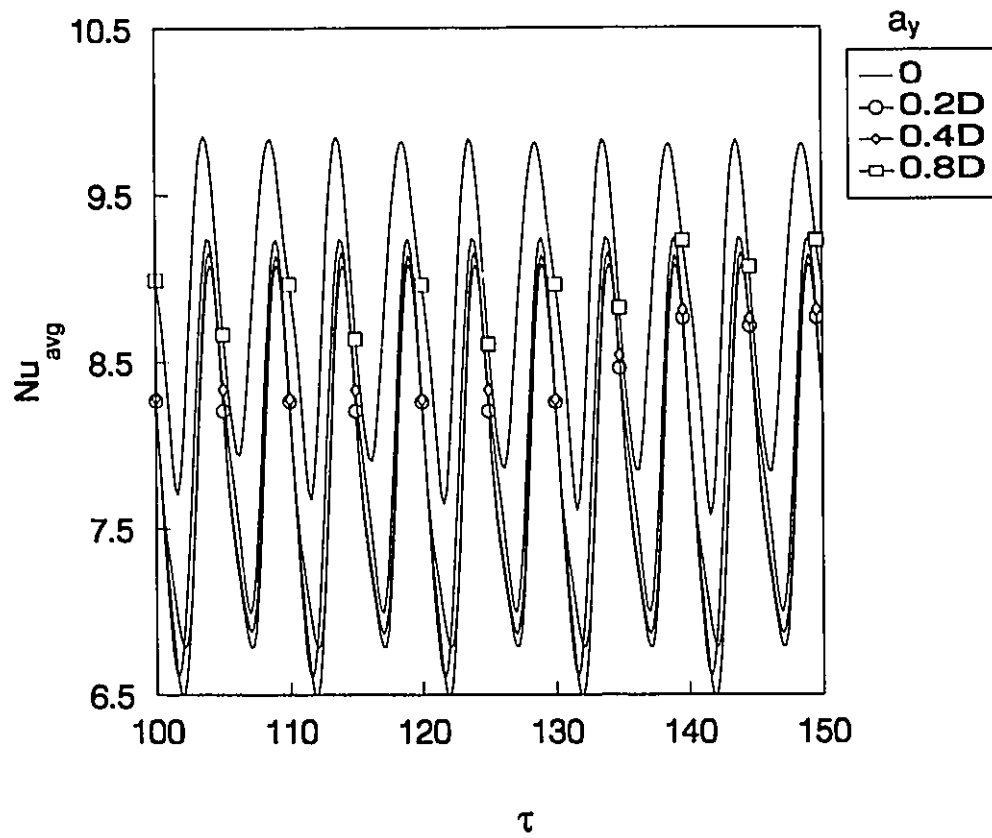


Figure 5.69 Time history of the average Nusselt number (combined oscillation, $F_x = 2F_n$, $F_y = F_n$, $a_x = 0.2D$, $Gr/Re^2 = 0$)

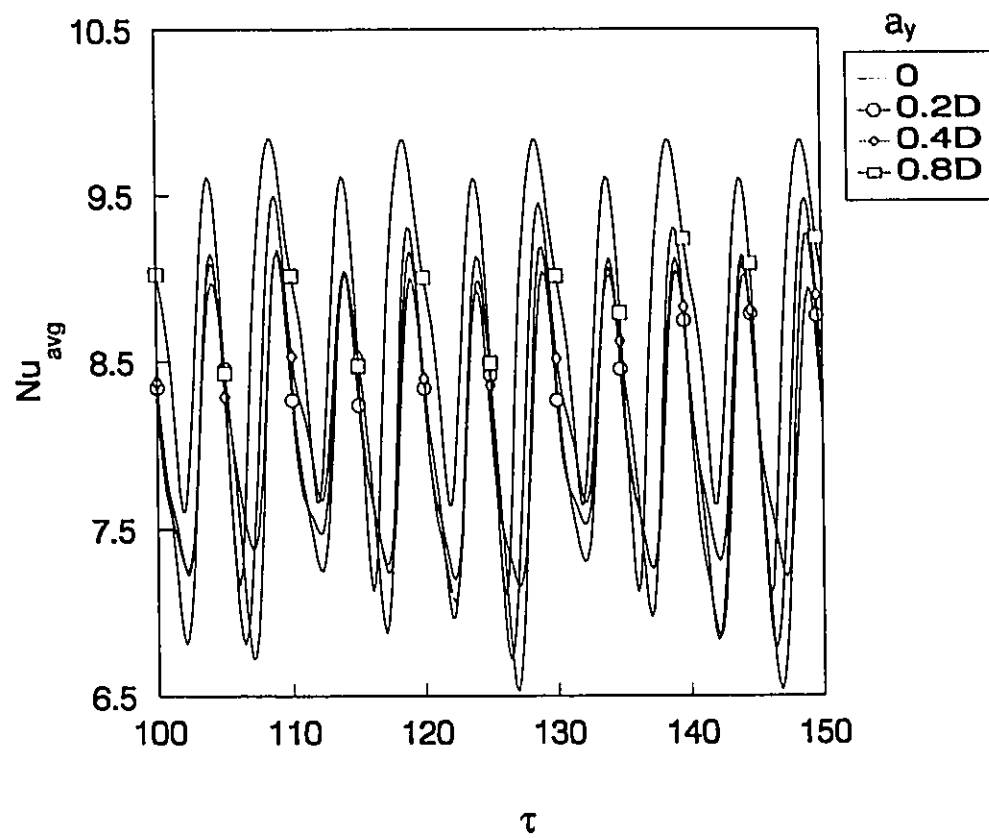


Figure 5.70 Time history of the average Nusselt number
(combined oscillation, $F_x = 2F_n$, $F_y = F_n$, $a_x = 0.2D$, $Gr/Re^2 = 1$)

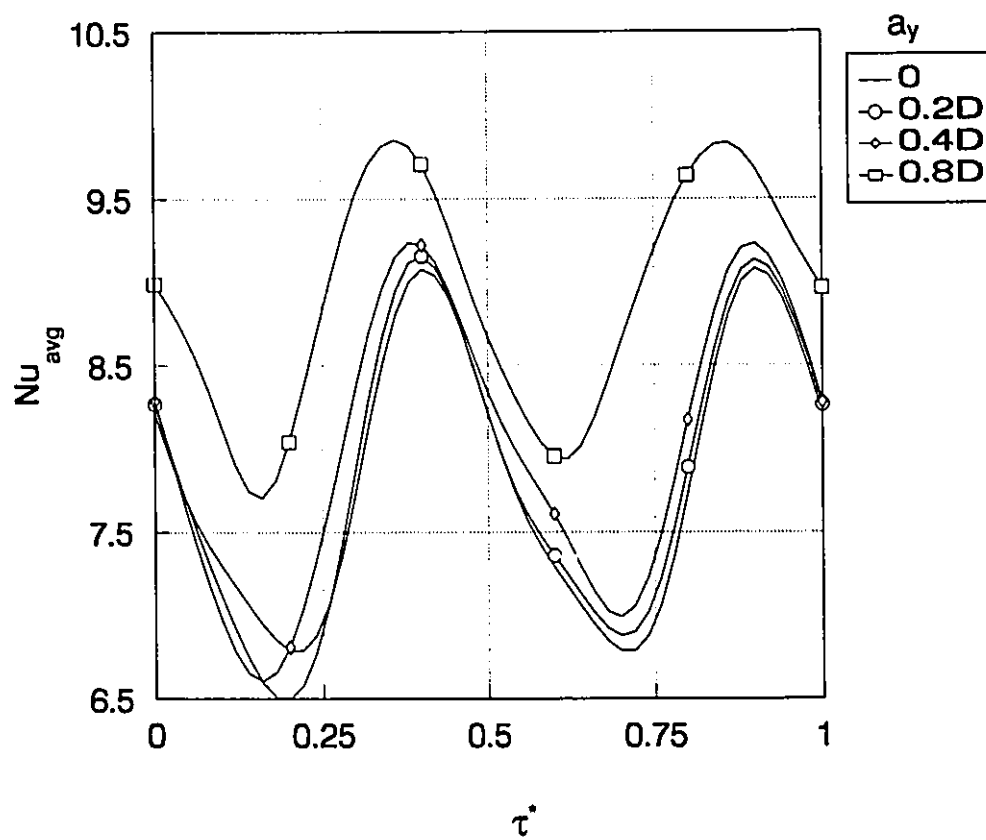


Figure 5.71 Average Nusselt number in a cycle of oscillation (combined oscillation, $F_x = 2F_n$, $F_y = F_n$, $a_x = 0.2D$, $Gr/Re^2 = 0$)

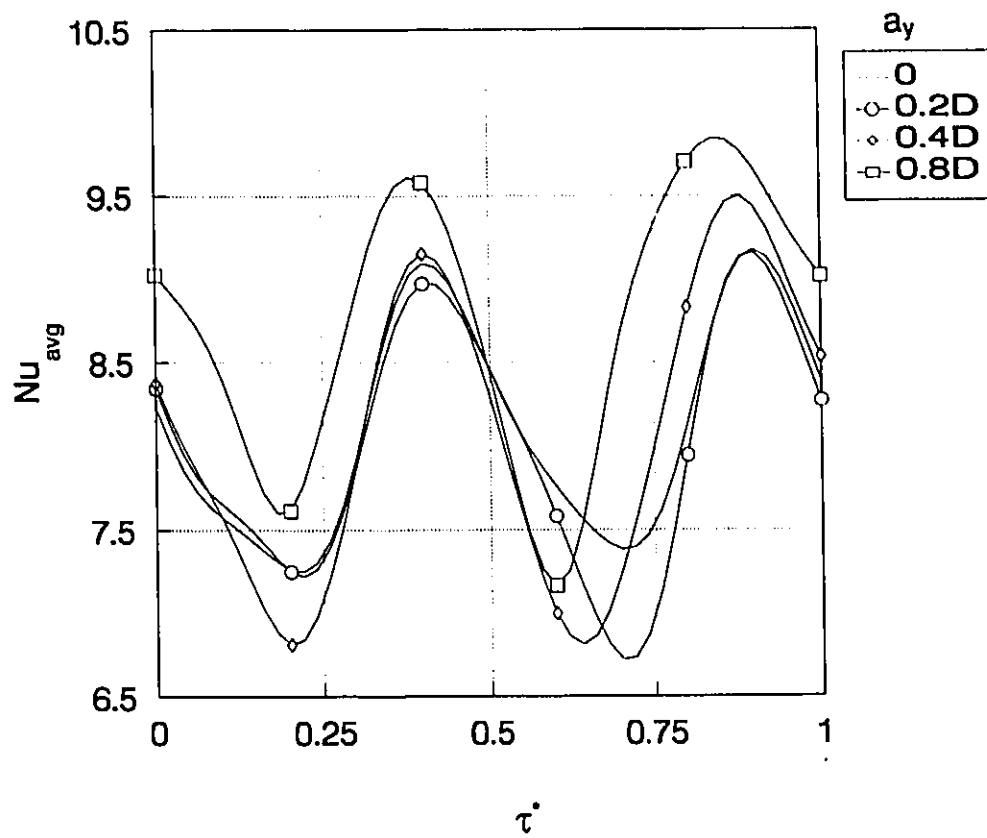


Figure 5.72 Average Nusselt number in a cycle of oscillation (combined oscillation, $F_x = 2F_n$, $F_y = F_n$, $a_x = 0.2D$, $Gr/Re^2 = 1$)

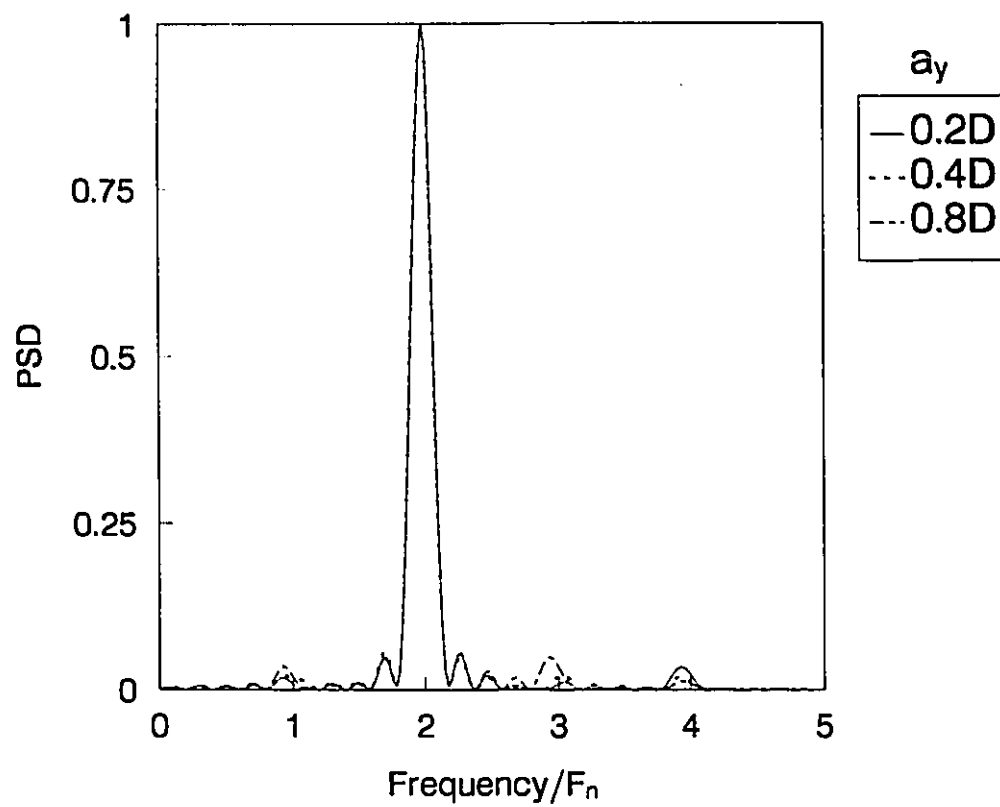


Figure 5.73 Power spectra of the average Nusselt number
(combined oscillation, $F_x = 2F_n$, $F_y = F_n$, $a_x = 0.2D$, $Gr/Re^2 = 0$)

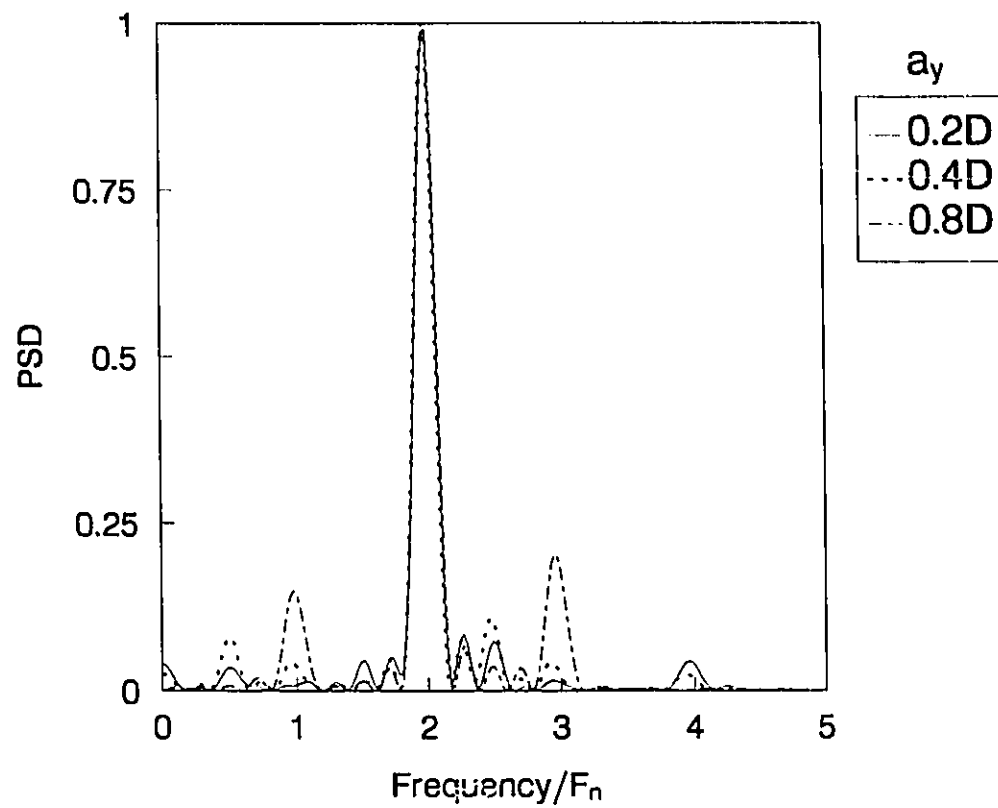


Figure 5.74 Power spectra of the average Nusselt number
(combined oscillation, $F_x = 2F_n$, $F_y = F_n$, $a_x = 0.2D$, $Gr/Re^2 = 1$)

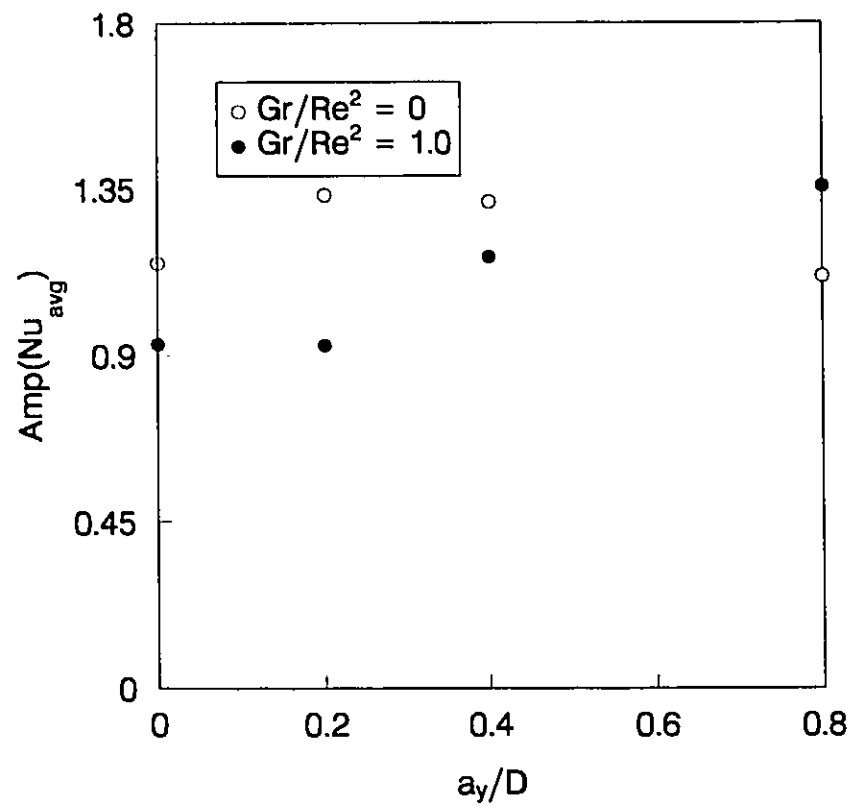


Figure 5.75 Amplitude of Nu_{avg} at different position amplitudes of oscillation (combined oscillation, $F_x = 2F_n$, $F_y = F_n$, $a_x = 0.2D$)

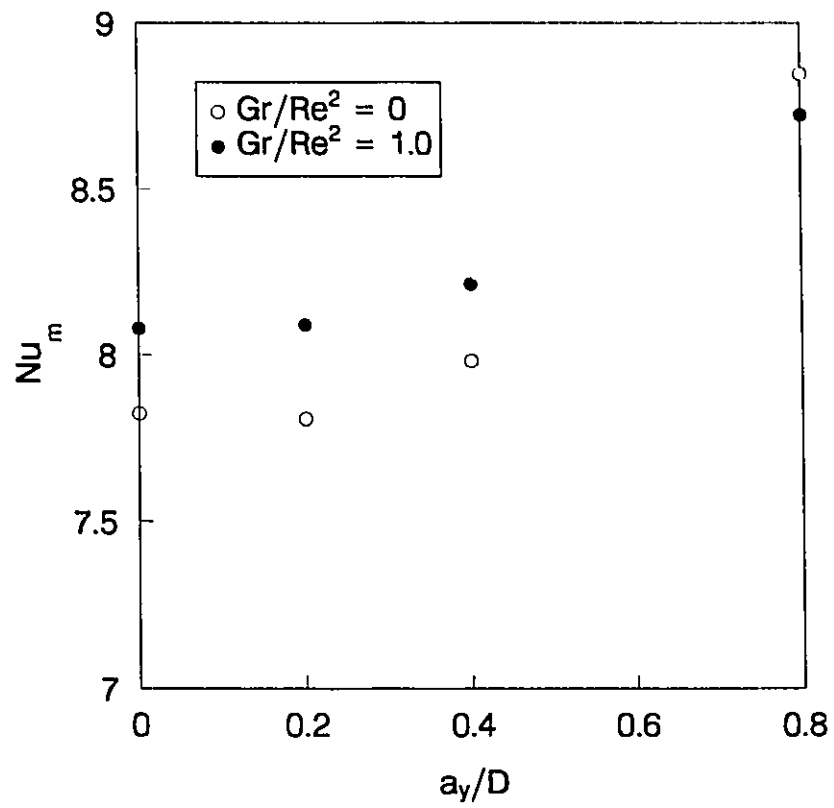


Figure 5.76 Mean Nusselt number at different position amplitudes of oscillation
(combined oscillation, $F_x = 2F_n$, $F_y = F_n$, $a_x = 0.2D$)

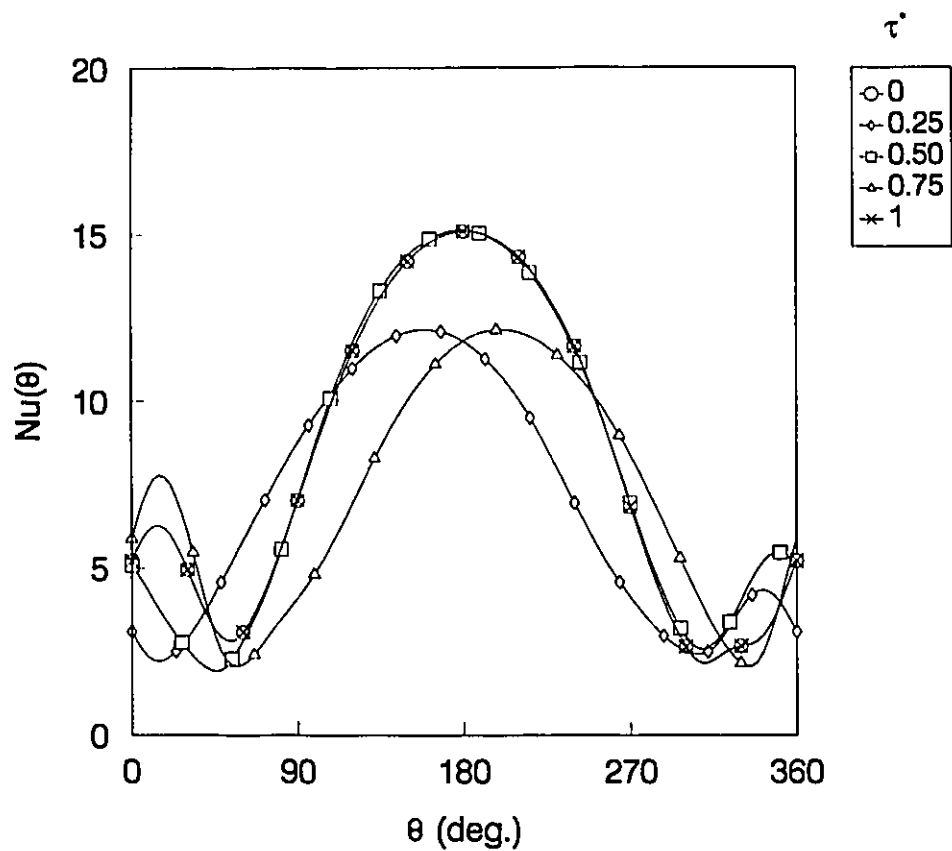


Figure 5.77 Local Nusselt number distribution in a full cycle of oscillation (combined oscillation, $F_x = 2F_n$, $F_y = F_n$, $a_x = a_y = 0.2D$, $Gr/Re^2 = 0$)

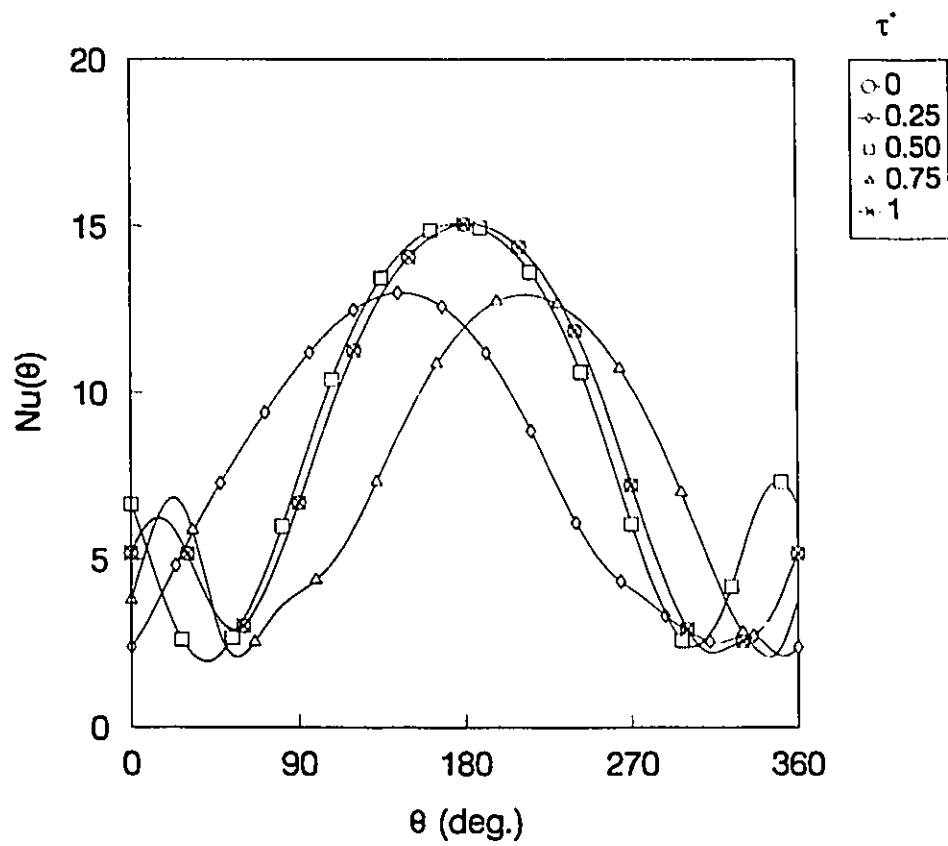


Figure 5.78 Local Nusselt number distribution in a full cycle of oscillation (combined oscillation, $F_x = 2F_n$, $F_y = F_n$, $a_x = 0.2D$, $a_y = 0.4D$, $Gr/Re^2 = 0$)

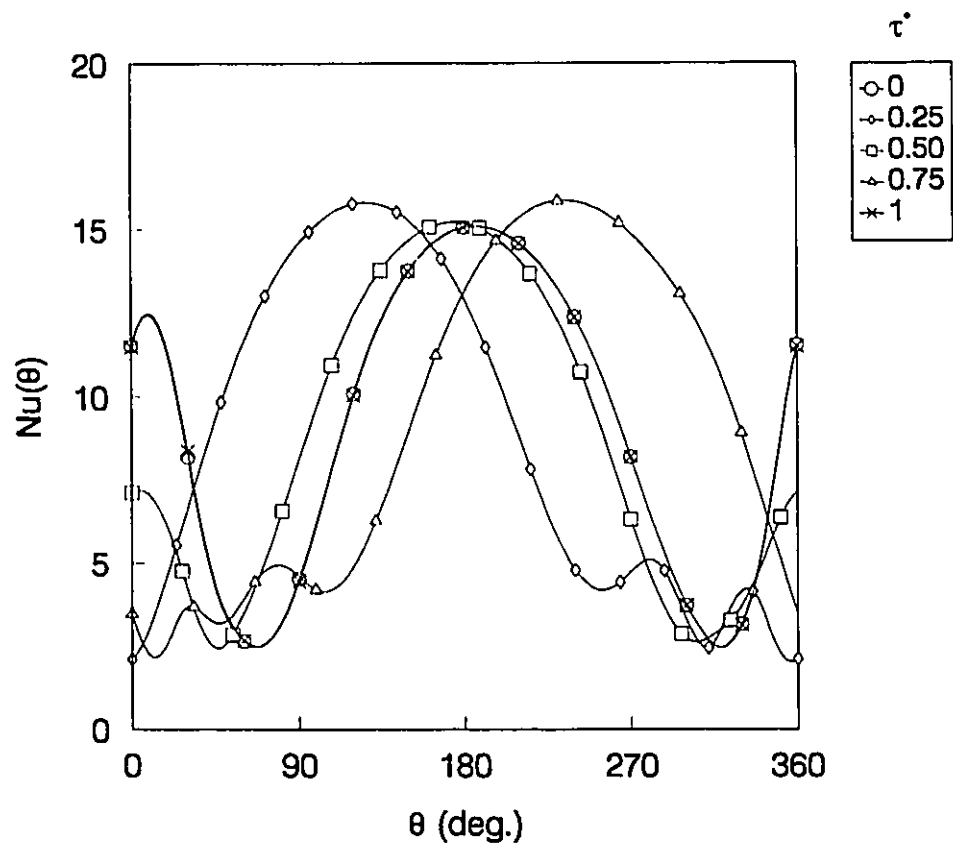


Figure 5.79 Local Nusselt number distribution in a full cycle of oscillation (combined oscillation, $F_x = 2F_n$, $F_y = F_n$, $a_x = 0.2D$, $a_y = 0.8D$, $Gr/Re^2 = 0$)

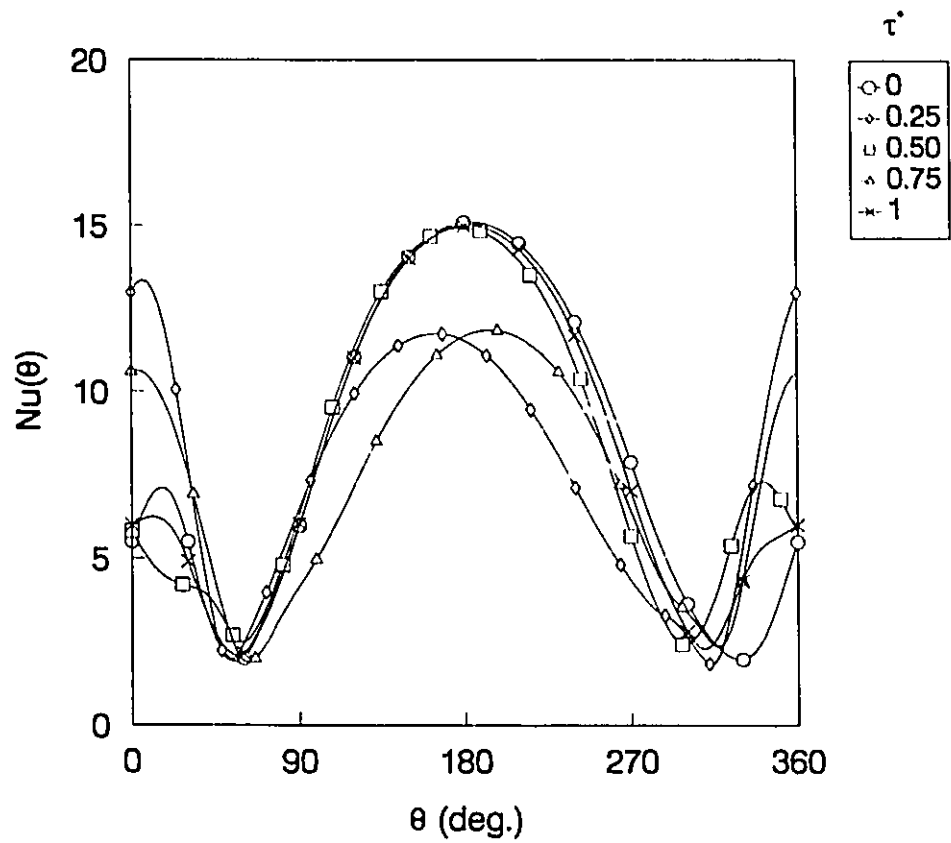


Figure 5.80 Local Nusselt number distribution in a full cycle of oscillation
(combined oscillation, $F_x = 2F_n$, $F_y = F_n$, $a_x = a_y = 0.2D$, $Gr/Re^2 = 1$)

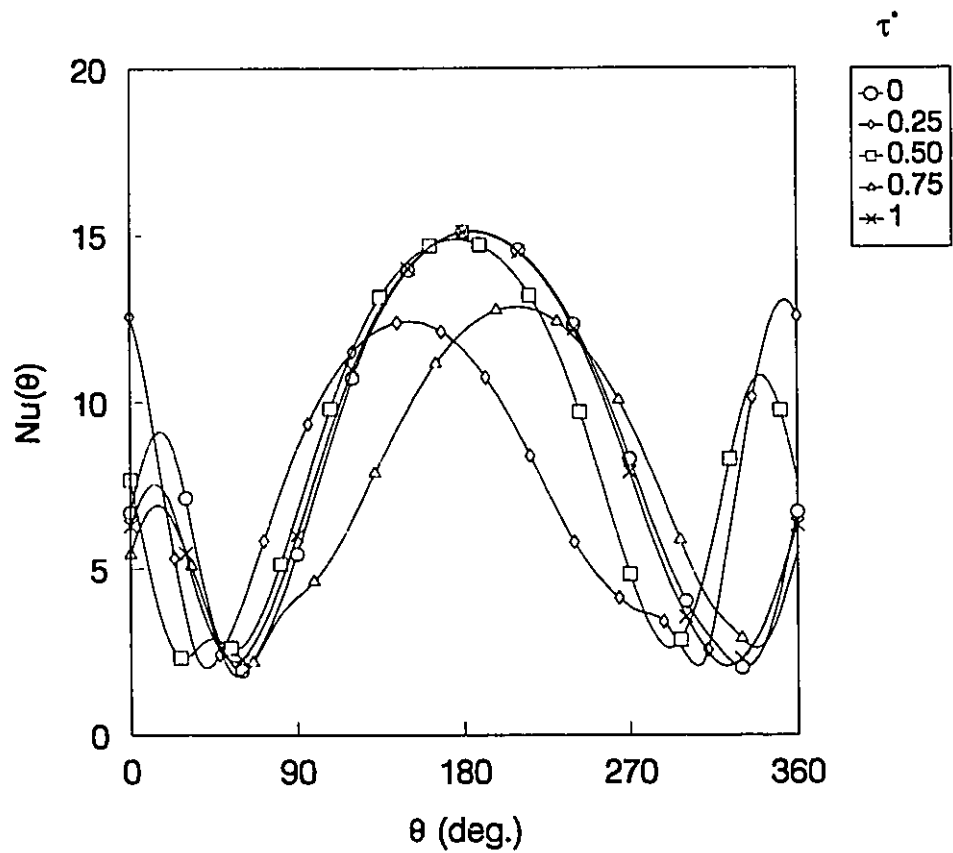


Figure 5.81 Local Nusselt number distribution in a full cycle of oscillation (combined oscillation, $F_x = 2F_n$, $F_y = F_n$, $a_x = 0.2D$, $a_y = 0.4D$, $Gr/Re^2 = 1$)

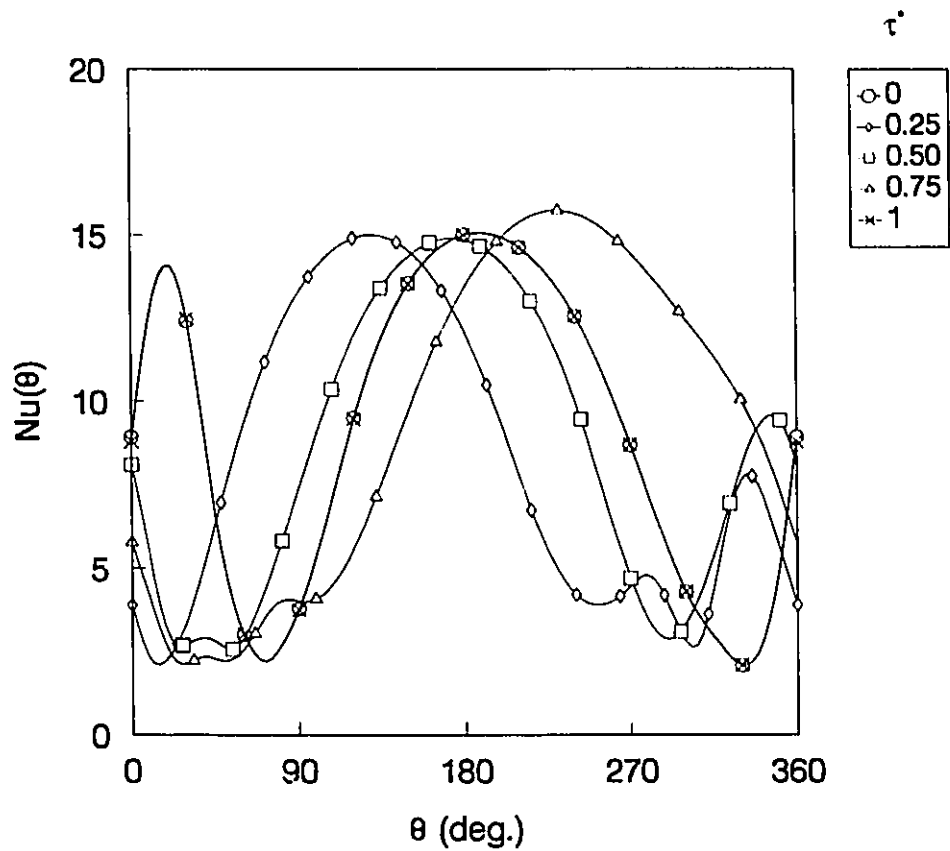


Figure 5.82 Local Nusselt number distribution in a full cycle of oscillation (combined oscillation, $F_x = 2F_n$, $F_y = F_n$, $a_x = 0.2D$, $a_y = 0.8D$, $Gr/Re^2 = 1$)



Figure 5.83 Isothermal contours for the case of forced convection (combined oscillation, $\tau^* = 0$, $a_x = 0.2D$, $a_y = 0.4D$, minimum and maximum contour level: 0.05 and 1, contour interval: 0.05)

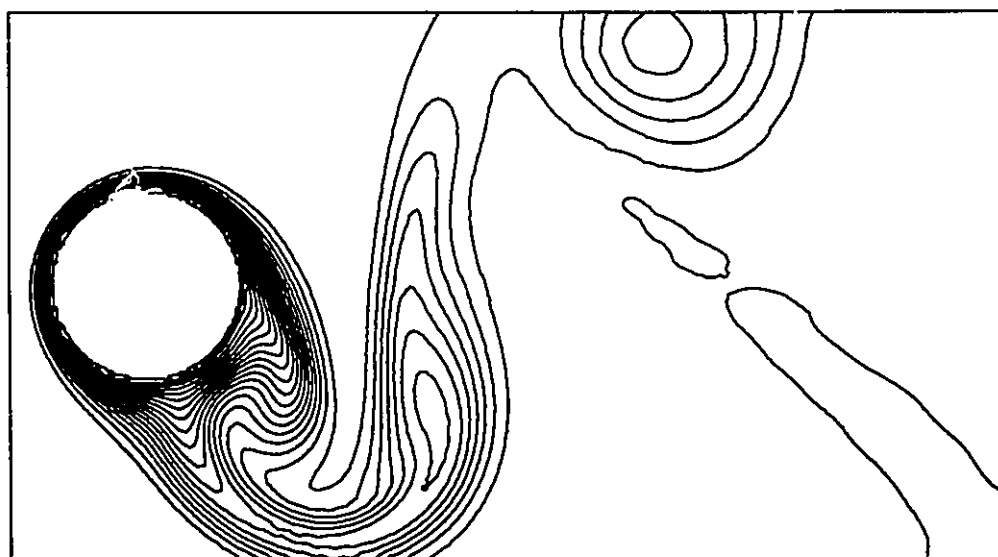


Figure 5.84 Isothermal contours for the case of forced convection (combined oscillation, $\tau^* = 0.25$, $a_x = 0.2D$, $a_y = 0.4D$, minimum and maximum contour level: 0.05 and 1, contour interval: 0.05)

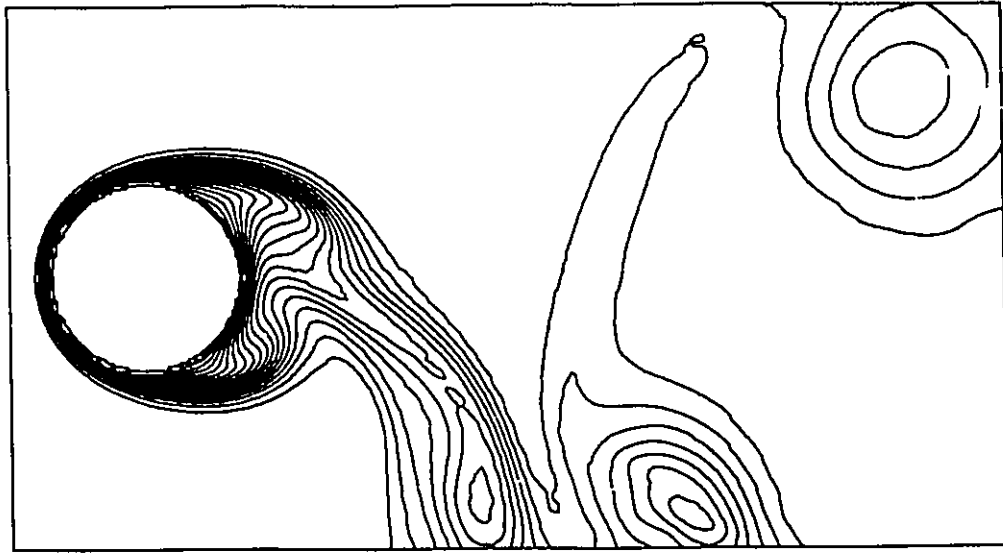


Figure 5.85 Isothermal contours for the case of forced convection (combined oscillation, $\tau^* = 0.50$, $a_x = 0.2D$, $a_y = 0.4D$, minimum and maximum contour level: 0.05 and 1, contour interval: 0.05)

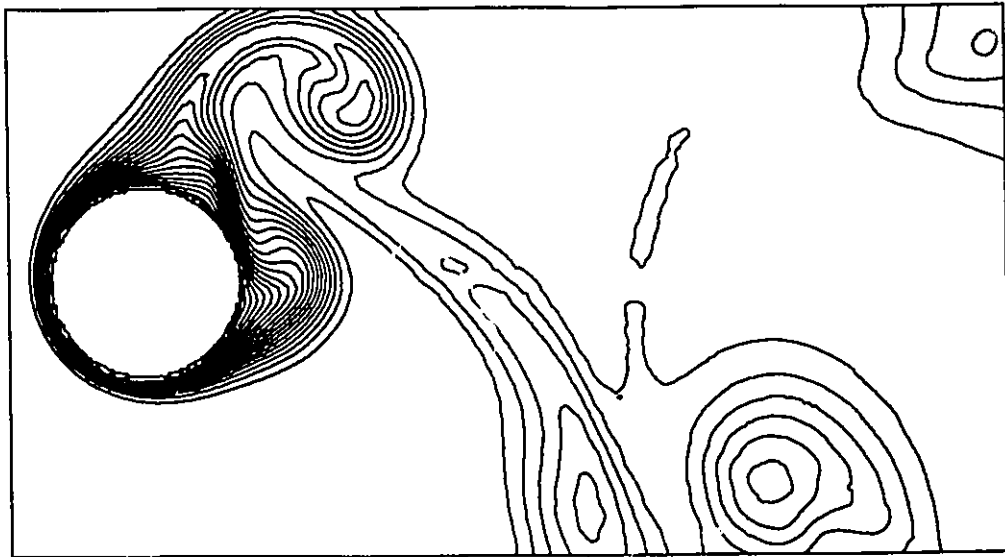


Figure 5.86 Isothermal contours for the case of forced convection (combined oscillation, $\tau^* = 0.75$, $a_x = 0.2D$, $a_y = 0.4D$, minimum and maximum contour level: 0.05 and 1, contour interval: 0.05)



Figure 5.87 Isothermal contours for the case of forced convection (combined oscillation, $\tau = 1$, $a_x = 0.2D$, $a_y = 0.4D$, minimum and maximum contour level: 0.05 and 1, contour interval: 0.05)



Figure 5.88 Isothermal contours for the case of mixed convection (combined oscillation, $\tau^* = 0$, $a_x = 0.2D$, $a_y = 0.4D$, minimum and maximum contour level: 0.05 and 1, contour interval: 0.05)

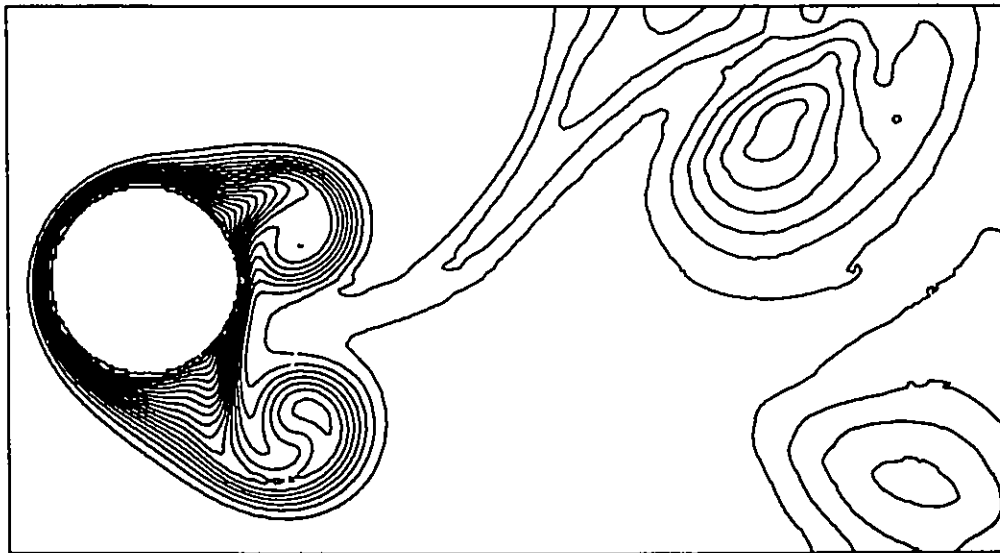


Figure 5.89 Isothermal contours for the case of mixed convection (combined oscillation, $\tau^* = 0.25$, $a_x = 0.2D$, $a_y = 0.4D$, minimum and maximum contour level: 0.05 and 1, contour interval: 0.05)

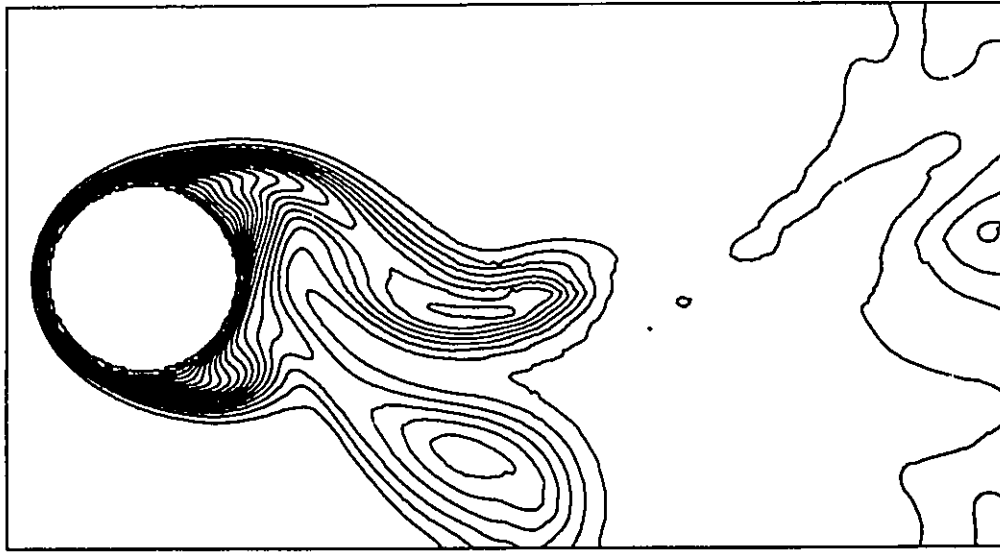


Figure 5.90 Isothermal contours for the case of mixed convection (combined oscillation, $\tau^* = 0.50$, $a_x = 0.2D$, $a_y = 0.4D$, minimum and maximum contour level: 0.05 and 1, contour interval: 0.05)

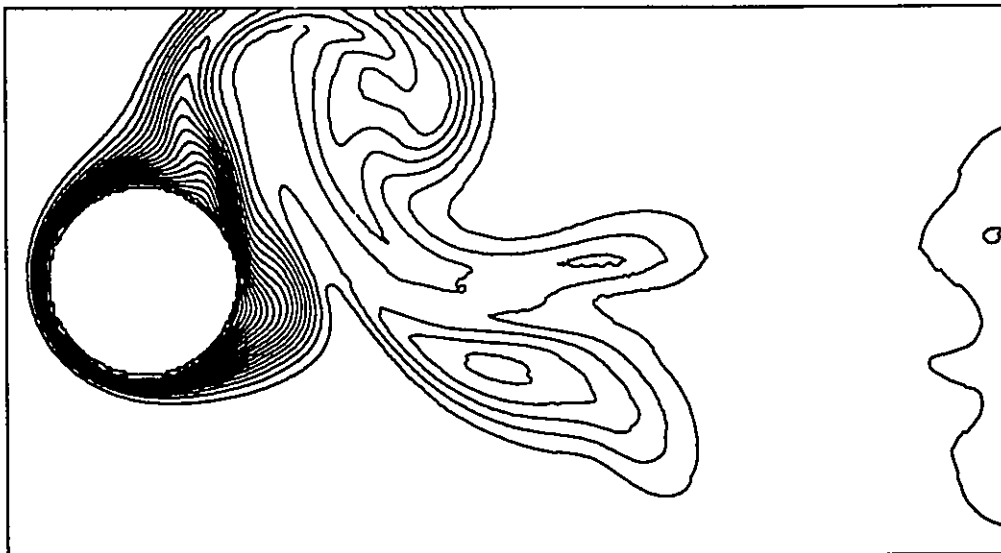


Figure 5.91 Isothermal contours for the case of mixed convection (combined oscillation, $\tau^* = 0.75$, $a_x = 0.2D$, $a_y = 0.4D$, minimum and maximum contour level: 0.05 and 1, contour interval: 0.05)

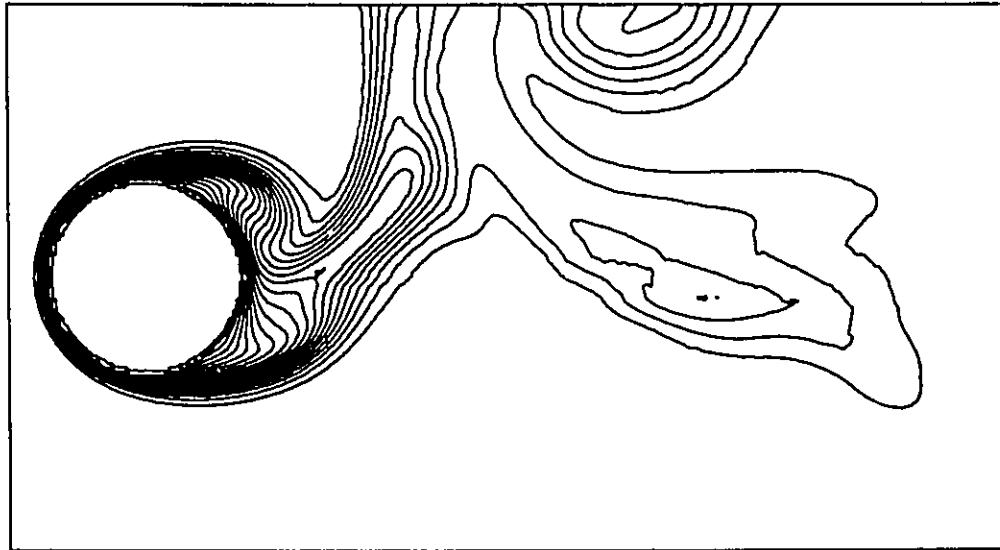


Figure 5.92 Isothermal contours for the case of mixed convection (combined oscillation, $\tau^* = 1$, $a_x = 0.2D$, $a_y = 0.4D$, minimum and maximum contour level: 0.05 and 1, contour interval: 0.05)

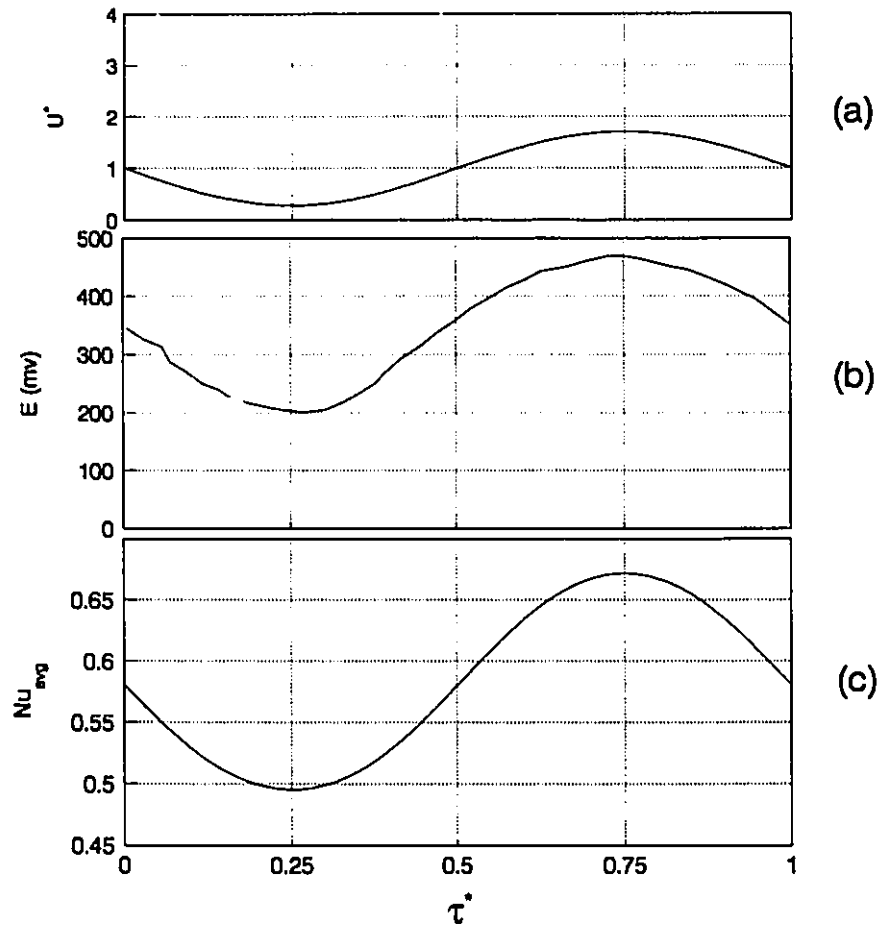


Figure 5.93 Oscillating hot-wire response ($Re = 0.25$, $Gr = 3.988 \times 10^{-6}$, $A_x = 0.712$, $F_x = 4.48 \times 10^{-3}$) (a) magnitude of the relative free stream velocity (b) experimental hot-wire response (H3) (c) computed Nu_{avg} in a cycle of oscillation

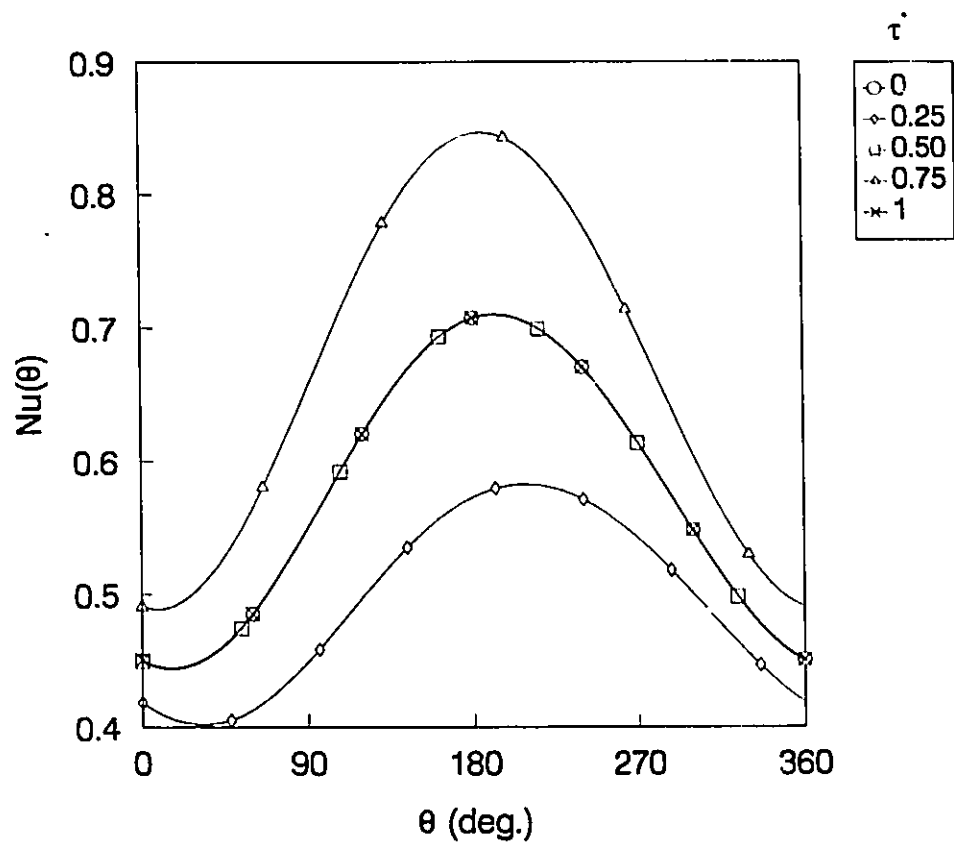


Figure 5.94 Local Nusselt number distribution in a full cycle of oscillation (oscillating hot-wire, $Re = 0.25$, $Gr = 3.988 \times 10^{-6}$, $A_x = 0.712$, $F_x = 4.48 \times 10^{-3}$)

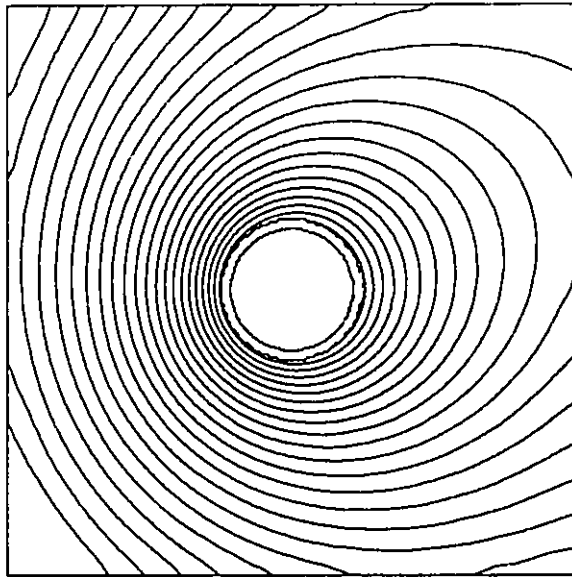


Figure 5.95 Isothermal contours surrounding the oscillating hot-wire
($\tau = 0$, $A_x = 0.712$, minimum and maximum contour levels: 0.4 and 1, contour interval: 0.025)

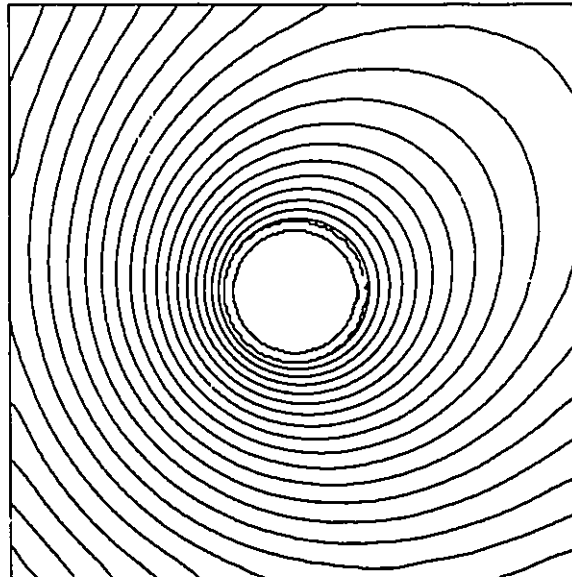


Figure 5.96 Isothermal contours surrounding the oscillating hot-wire
($\tau = 0.25$, $A_x = 0.712$, minimum and maximum contour levels: 0.4 and 1, contour interval: 0.025)

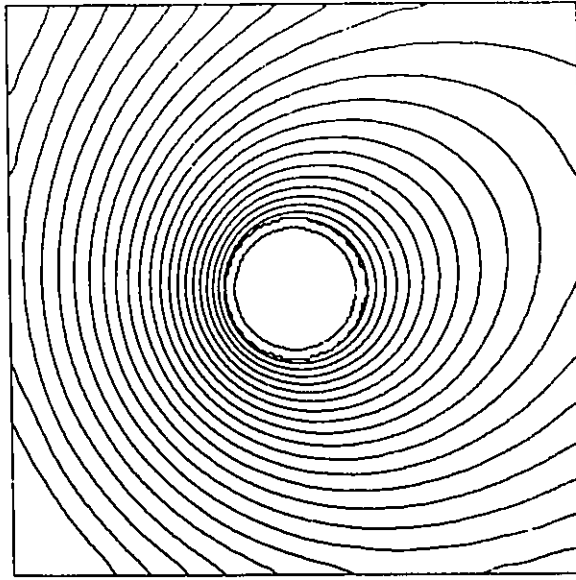


Figure 5.97 Isothermal contours surrounding the oscillating hot-wire ($\tau^* = 0.50$, $A_x = 0.712$, minimum and maximum contour levels: 0.4 and 1, contour interval: 0.025)

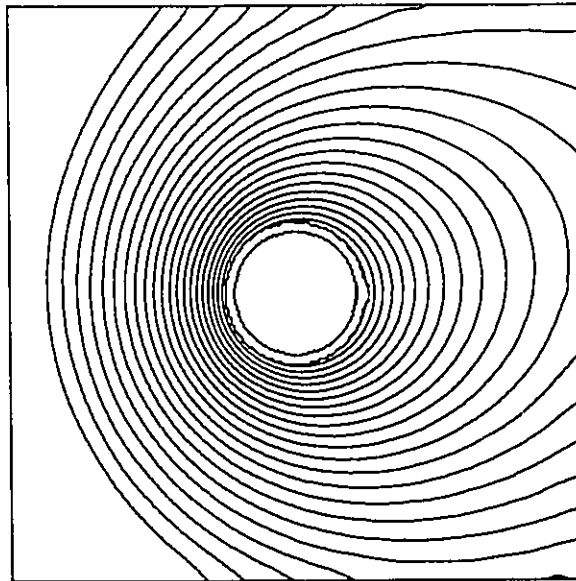


Figure 5.98 Isothermal contours surrounding the oscillating hot-wire ($\tau^* = 0.75$, $A_x = 0.712$, minimum and maximum contour levels: 0.4 and 1, contour interval: 0.025)

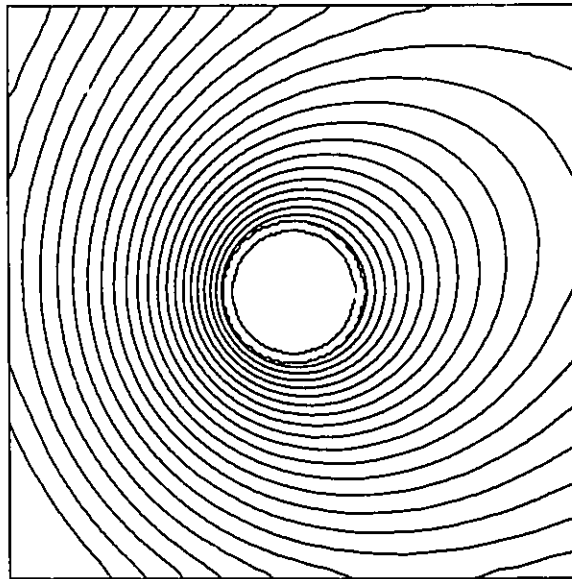


Figure 5.99 Isothermal contours surrounding the oscillating hot-wire ($\tau = 1$, $A_x = 0.712$, minimum and maximum contour levels: 0.4 and 1, contour interval: 0.025)

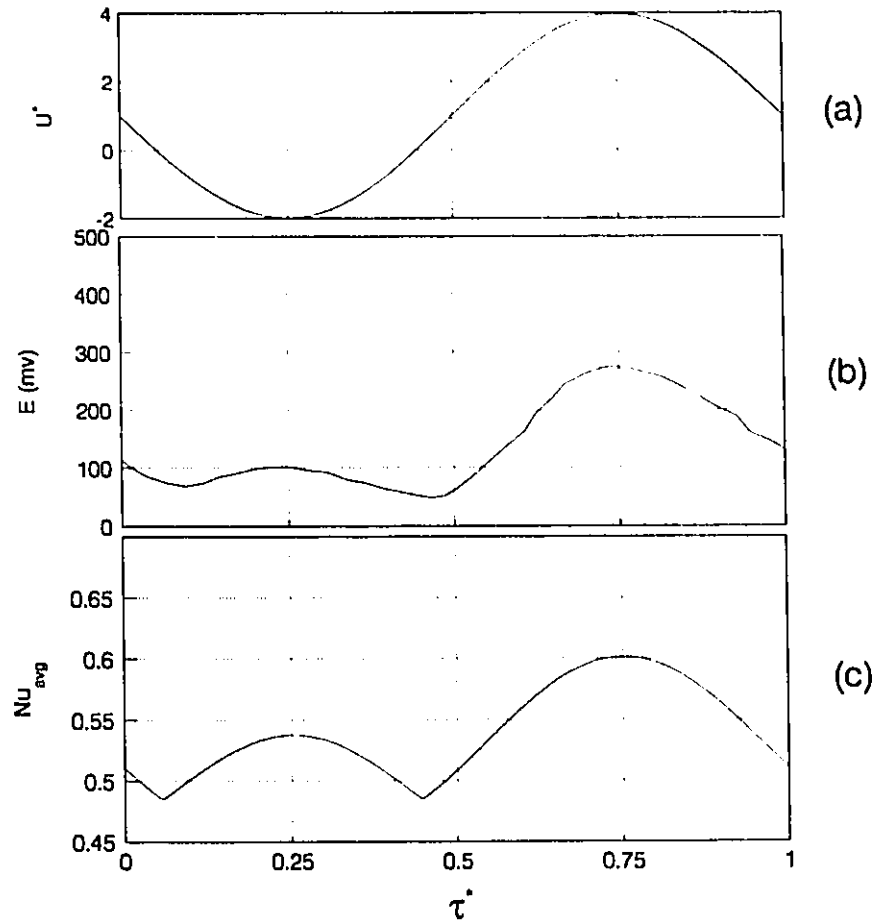


Figure 5.100 Oscillating hot-wire response ($Re = 0.06$, $Gr = 3.988 \times 10^{-6}$, $A_x = 2.986$, $F_x = 1.87 \times 10^{-3}$) (a) magnitude of the relative free stream velocity (b) experimental hot-wire response (H3) (c) computed Nu_{avg} in a cycle of oscillation

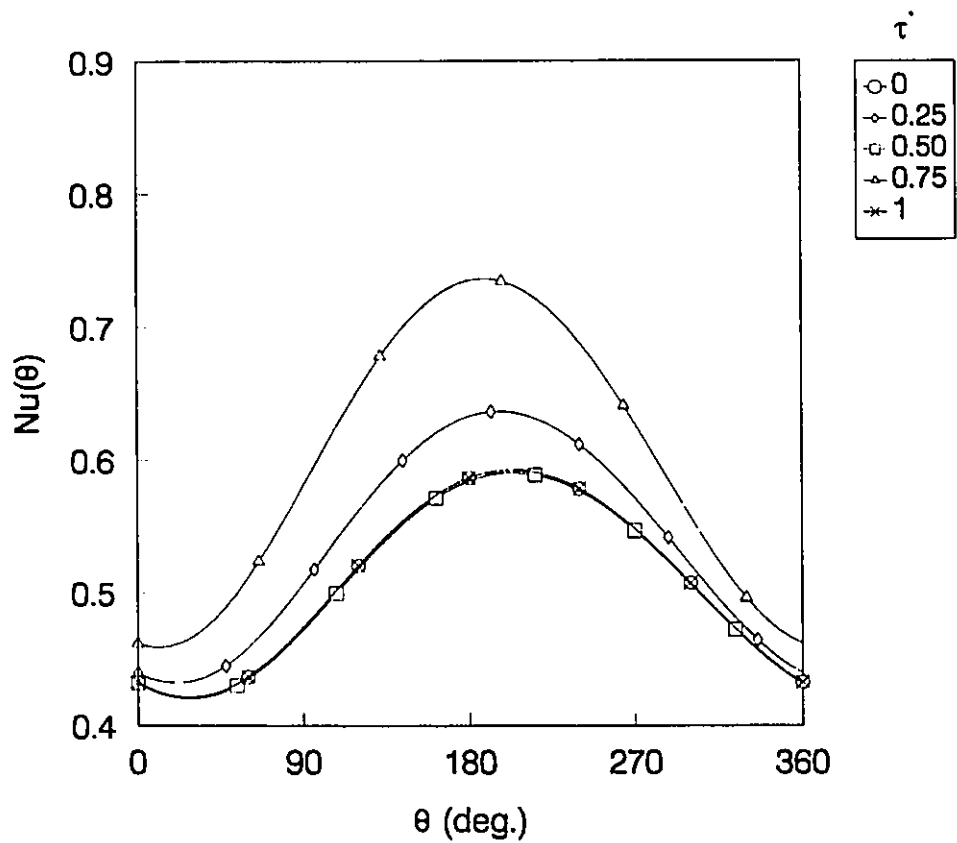


Figure 5.101 Local Nusselt number distribution in a full cycle of oscillation (oscillating hot-wire, $Re = 0.06$, $Gr = 3.988 \times 10^{-6}$, $A_x = 2.986$, $F_x = 1.87 \times 10^{-3}$)

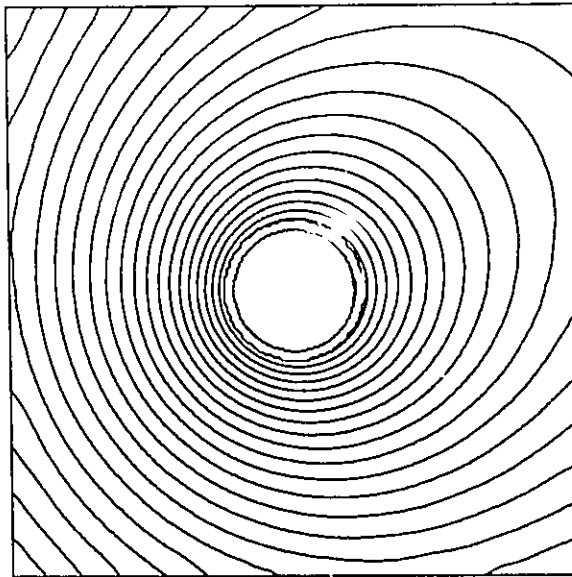


Figure 5.102 Isothermal contours surrounding the oscillating hot-wire
($\tau = 0$, $A_x = 2.986$, minimum and maximum contour levels: 0.4 and 1, contour interval: 0.025)

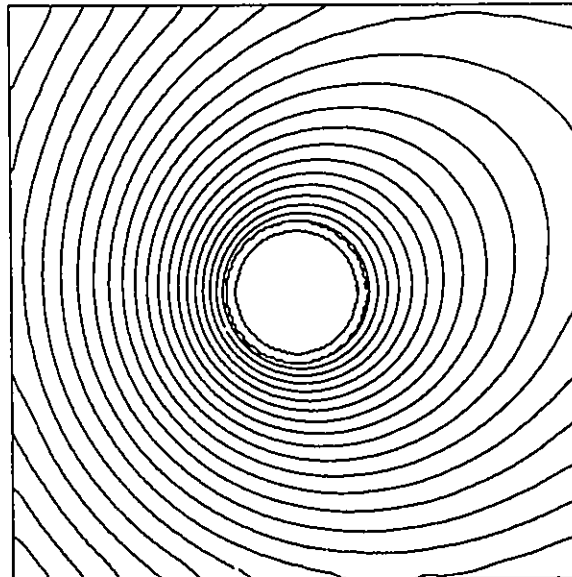


Figure 5.103 Isothermal contours surrounding the oscillating hot-wire
($\tau = 0.25$, $A_x = 2.986$, minimum and maximum contour levels: 0.4 and 1, contour interval: 0.025)

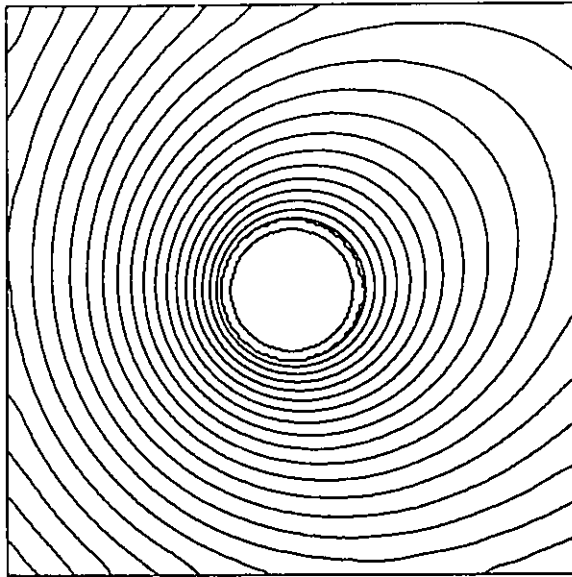


Figure 5.104 Isothermal contours surrounding the oscillating hot-wire ($\tau = 0.50$, $A_x = 2.986$, minimum and maximum contour levels: 0.4 and 1, contour interval: 0.025)

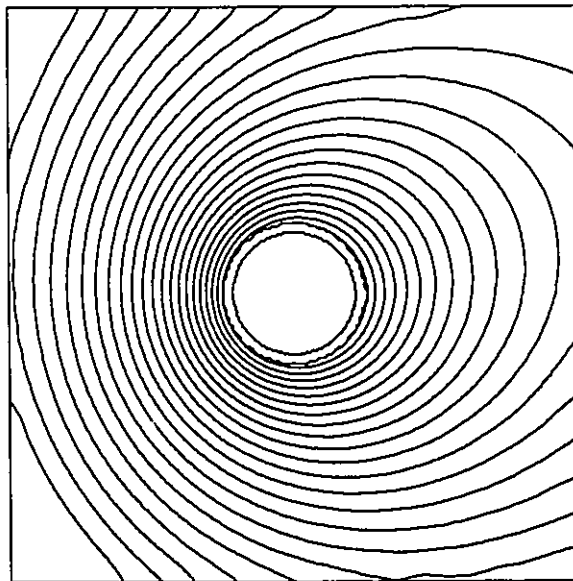


Figure 5.105 Isothermal contours surrounding the oscillating hot-wire ($\tau = 0.75$, $A_x = 2.986$, minimum and maximum contour levels: 0.4 and 1, contour interval: 0.025)

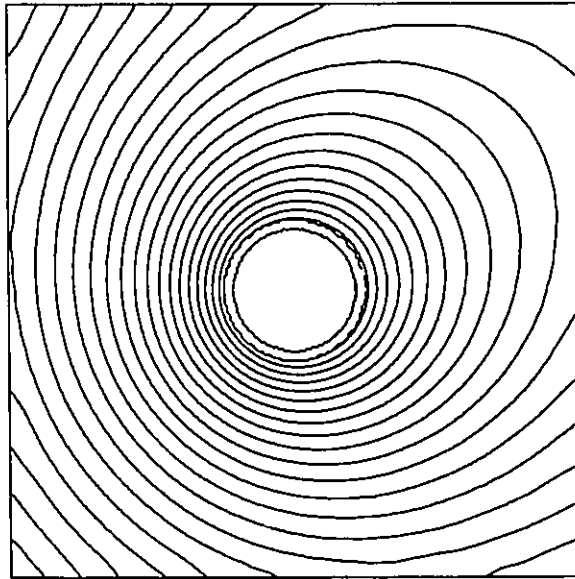


Figure 5.106 Isothermal contours surrounding the oscillating hot-wire ($\tau = 1$, $A_x = 2.986$, minimum and maximum contour levels: 0.4 and 1, contour interval: 0.025)

Chapter VI

CONCLUSIONS AND RECOMMENDATIONS

A general formulation for convective heat transfer from an oscillating cylinder in an incompressible fluid using vorticity and stream function as dependent variables, is presented. The problem of convective heat transfer from an oscillating cylinder has been analyzed numerically using a finite difference method. Based on the computational investigation using the validated numerical model, some conclusions are drawn for the oscillating cylinder and the oscillating hot-wire anemometer. They are listed below.

6.1 Conclusions

1. In the case of the stationary cylinder with forced convection, the average Nusselt number was found to vary with a small amplitude at twice the natural shedding frequency. With mixed convection, Nu_{avg} varied with the natural shedding frequency as the dominant frequency.
2. In comparison with the forced and mixed convective heat transfer from a stationary cylinder, an increased mean Nusselt number and amplitude of the Nu_{avg} was predicted with the in-line, transverse and combined oscillation. The position amplitude of oscillation has a strong influence on both the Nu_m

and the amplitude of Nu_{avg} .

3. In the range of the variables considered, this computational study predicts maximum increases of 18.46% and 15.30% in the mean Nusselt number with forced convection and mixed convection, respectively, with the cylinder oscillating at the mid-point lock-in frequencies in the in-line and transverse directions.
4. With in-line, transverse and combined oscillation, the dominant frequency in the Nu_{avg} variation was $2F_n$. With mixed convection, however, other harmonics of the forcing frequency of the cylinder do exist in the power spectra of Nu_{avg} .
5. The location of maximum local Nusselt number on the cylinder surface depends on the direction and velocity amplitude of the oscillation of the cylinder. The oscillation frequency of the location of the maximum local Nusselt number is the same as that of the incident angle of the relative free stream velocity.
6. The output voltage response of an oscillating constant temperature hot-wire qualitatively agrees with the computed average Nusselt number variation.
7. At very low Reynolds numbers, the influence of free convection is clearly evident in the local Nusselt number distribution on the hot-wire and in the isothermal contour maps in a cycle of oscillation.

6.2 Recommendations

The following suggestions are provided as possible ways of improving as well as extending the scope of the present study:

1. In order to gain a better understanding of the heat transfer from an oscillating cylinder, the influence of the frequency of oscillation should be studied in detail.
2. With a combined oscillation, the effects of phase difference between the in-line and transverse oscillation on the heat transfer should be investigated.
3. In addition to the in-line oscillation, the hot-wire anemometer with transverse oscillation should be investigated for obtaining the direction of the flow.
4. Accurate and faster solvers should be employed to solve the Poisson equation for the stream function. This will reduce the computer time requirements for solving time dependent problems.
5. An enormous amount of computer memory and time is required for simulating time dependent flow problems like the cylinder in a cross flow at different conditions of oscillation. In order to obtain an optimum number of simulation runs, it may be desirable to vary the influencing parameters such as a_x , a_y , F_x and F_y using the design of experiments (DOE) technique.

REFERENCES

- A1. Anagnostopoulos P., Numerical solution for laminar two-dimensional flow about a fixed and transversely oscillating cylinder in a uniform stream, J. of Computational Physics, 85, 1989, 434-456.
- A2. Anantanarayanan R. and Ramachandran A., Effect of vibration on heat transfer from a wire to air in parallel flow, ASME J. Heat Transfer, 80, 1958, 1426-1432.
- A3. Armaly B.F. and Madsen D.H., Heat transfer from an oscillating horizontal wire, ASME J. Heat Transfer, 93, 1971, 239-240.
- A4. Armaly B.F., Chen, T.S. and Ramachandran N., Correlations for mixed convection flows across horizontal cylinders and spheres, ASME J. Heat Transfer, 110, 1988, 511-512.
- B1. Badr H.M., Theoretical study of laminar mixed convection from a horizontal cylinder in a cross stream, Int. J. Heat Mass Transfer, 26, 1983, 639-653.
- B2. Badr H.M., Laminar combined convection from a horizontal cylinder-parallel and contra flow regimes, Int. J. Heat Mass Transfer, 27, 1984, 15-27.
- B3. Bearman P.W., Vortex shedding from oscillating bluff bodies, Ann. Rev. Fluid Mech., 16, 1984, 195-222.
- B4. Bearman P.W. and Obasaju, Transverse forces on a circular cylinder oscillating in-line with a steady current, Proc. Eighth Int. Conf. on Offshore Mechanics and Arctic Engg., Hague, 1989, 253-258

- B5 Berger S. B. and Rokni M., The motion of a circular cylinder in a cross flow, Proc. of 31st Heat Transfer and Fluid Mechanics Institute, Sacramento, 1989, 293-308.
- B6. Borthwick A., Comparison between two finite difference schemes for computing the flow around a cylinder, Int. J. Numerical Methods in Fluids, 6, 1986, 275-290.
- B7. Braza M., Chassaing P. and Minh H. H. , Numerical study and physical analysis of the pressure and velocity fields in the near wake of a circular cylinder, J. Fluid Mech., 165, 1986, 79-130.
- B8. Braza M. and Minh. H.H., Direct numerical simulation of certain 2-D transition features of the flow past a circular cylinder, Proc. 8th Int. Conf. on Offshore Mechanics and Arctic Engg., Hague, 1989, 401-410.
- B9 Bublitz P., Unsteady pressures and forces acting on an oscillating circular cylinder in transverse flow. Flow Induced Structural Vibrations Symposium, Karlsruhe, Germany, 1972, 443-453
- C1. Chilukuri R., Incompressible laminar flow past a transversely vibrating cylinder, ASME Journal of Fluids Engineering, 109, 1987, 166-171.
- C2. Chun W. and Boehm R.F., Calculation of forced flow and heat transfer around a cylinder in cross flow, Numerical Heat Transfer, 15, 1988, 101-122.
- C3. Chun W. and Boehm R.F., Forced convection from a nonisothermal cylinder in crossflow, ASME J. Heat Transfer, 112, 1990, 781-784.

- C4. Cole J. and Roshko A., Heat transfer from wires at Reynolds numbers in the Oseen range, Publication no. 354, Guggenheim Aeronautics Laboratory, Pasadena, CA, 1954.
- D1. Dawood A.S., Manocha B.L. and Ali S.M.J., The effect of vertical vibrations on natural convection heat transfer from a horizontal cylinder, Int. J. Heat Mass Transfer, 24, 1981, 491-496.
- D2. Dent J.C., The effect of acoustic and mechanical oscillation on free convection from heated cylinders in air, Chemical Engineering Science, 24, 1969, 1599-1605.
- F1. Fernandez V.M., An oscillating hot-wire for velocity measurements in recirculating flows, M.A.Sc. Thesis, Dept. of Mechanical Engg., Univ. of Windsor, 1985.
- G1. Green R.B. and Gerrard J.H., Vorticity measurements in the near wake of a circular cylinder at low Reynolds numbers, J. Fluid Mech., 246, 1993, 675-691.
- G2. Griffin O.M. and Hall M.S., Vortex shedding lock-on and flow control in bluff body wakes, ASME J. Fluids Engg., 113, 1991, 526-537.
- G3. Griffin O.M. and Ramberg S.E., The vortex-street wakes of vibrating cylinders. J. Fluid Mech., 66, 1974, 553-576.
- G4. Griffin, O.M. and Ramberg S.E., On vortex strength and drag in bluff-body wakes, J. Fluid Mech., 69, 1975, 721-728.
- G5. Griffin O.M. and Ramberg S.E., Vortex shedding from a cylinder vibrating

- in line with an incident uniform flow, J. Fluid Mech., 75, 1976, 257-271.
- G6. Griffin O.M. and Koopmann G.H., The vortex-excited lift and reaction forces on resonantly vibrating cylinders, J. Sound and Vibration, 54(3), 1977, 435-448.
- H1. Ha-Minh H., Boisson H. and Martinez G., Unsteady mixed convection heat transfer around a circular cylinder, Proc. of Winter Annual Meeting of ASME, Chicago, 1980, 35-44.
- H2. Hamielec A.E. and Raal J.D., Numerical studies of viscous flow around circular cylinders, Phys. Fluids, 12(1), 1969, 11-17.
- H3. Heckadon D. and Wong S., An experimental study of vibrating hot-wire characteristics, ME 420 Project Report, Dept. of Mechanical Engg., University of Windsor, 1986.
- H4. Hegge Zijnen B.G., Modified correlation formulae for the heat transfer by natural and by forced convection from horizontal cylinders, Appl. Sci. Res., A 6, 1957, 129-140.
- H5. Hegge Zijnen B.G., Heat transfer from horizontal cylinders to a turbulent air flow, Appl. Sci. Res., A 7, 1958, 205-223.
- H6. Hurlbut S.E., Spaulding M.L. and White F.M., Numerical solution of the time dependent Navier-Stokes equations in the presence of an oscillating cylinder, Proc. of Winter Annual Meeting of ASME, San Francisco, 1978, 201-206.
- H7. Hurlbut S.E., Spaulding M.L. and White F.M., Numerical solution for laminar

- two-dimensional flow about a cylinder oscillating in a uniform stream, ASME J. of Fluids Engineering, 104, 1982, 214-222.
- J1. Jain P.C. and Goel B.S., A numerical study of unsteady laminar forced convection from a circular cylinder, ASME J. Heat Transfer, 1976, 303-307.
 - J2. Jain P.C. and Lohar B.L., Unsteady mixed convection heat transfer from a horizontal circular cylinder, ASME J. Heat Transfer, 101, 1979, 126-131.
 - J3. Jain P.C. and Rao K.S., Numerical solution of unsteady viscous incompressible fluid flow past a circular cylinder, Phys. Fluids, Suppl. II, 1969, 57-64.
 - J4. Janna W. S., Introduction to Fluid Mechanics, 3rd Ed., PWS Publishing Co., 1993.
 - J5. Jordan S.K. and Fromm J.E., Oscillatory drag, lift and torque on a circular cylinder in a uniform flow, The Physics of Fluids, 15(3), 1972, 371-376.
 - K1. Kezios S.P. and Prasanna K.V., Effect of vibration on heat transfer from a cylinder in normal flow, ASME Paper No. 66-WA/HT-43, 1966.
 - K2. Kimoto H., Kadotsuji A. and Hirose T., Effect of vibration on the natural convection heat transfer of horizontal cylinder, Bulletin of the JSME, 26, 1983, 1154-1161.
 - K3. Koopmann G.H., The vortex wakes of vibrating cylinders at low Reynolds numbers, J. Fluid Mech., 28, 1967, 501-512.
 - K4. Kramers H., Heat transfer from spheres to flowing media, Physica, 12,

1946, 61-80.

- L1. Lecointe Y. and Piquet J., Flow structure in the wake of an oscillating cylinder, ASME J. of Fluids Engg., 111, 1989, 139-148.
- L2. Leung C.T., Ko N.W.M. and Ma K.H., Heat transfer from a vibrating cylinder, J. Sound and Vibration, 75(4), 1981, 581-582.
- L3. Li J., Sun J. and Roux B., Numerical study of an oscillating cylinder in uniform flow and in the wake of an upstream cylinder, J. Fluid Mech., 237, 1992, 457-478.
- L4. Loc T.P., Numerical analysis of unsteady secondary vortices generated by an impulsively started circular cylinder, J. Fluid Mech., 100, 1980, 111-128.
- L5. Loc T.P. and Bouard R., Numerical solution of the early stage of the unsteady viscous flow around a circular cylinder: a comparison with experimental visualization and measurements, J. Fluid Mech., 160, 1985, 93-117.
- M1. Mittal S. and Tezduyar T.E., A finite element study of incompressible flows past oscillating cylinders and aerofoils, Int. J. Num. Methods in Fluids, 15, 1992, 1073-1118.
- M2. Moe G. and Wu Z. J., The lift force on a vibrating cylinder in a current. Proc. 8th Int. Conf. on Offshore Mechanics and Arctic Engineering, Hague, 1989, 159-268.
- M3. Moon S.H., Shih T.M. and Johnson A.T., Pressure distributions for upward combined free and forced convection around cylinders and spheres, Num.

Heat Transfer, 13, 1988, 65-89.

- M4. Mori Y. and Tokuda S., The effect of oscillation on instantaneous local heat transfer in forced convection from a cylinder, Proc. 3rd Int. Heat Transfer Conf., Chicago, 1966, 49-56.
- O1. Ongoren A. and Rockwell D., Flow structure from an oscillating cylinder Part 1. Mechanisms of phase shift and recovery in the near wake, J. Fluid Mech., 191, 1988, 197-223.
- O2. Ongoren A. and Rockwell D., Flow structure from an oscillating cylinder Part 2. Mode competition in the near wake, J. Fluid Mech., 191, 1988, 225-245.
- O3. Oosthuizen P.H. and Madan S., Combined convective heat transfer from horizontal cylinders in air, ASME J. Heat Transfer, 92, 1970, 194-196.
- O4. Oosthuizen P.H. and Madan S., The effect of flow direction on combined convective heat transfer from cylinders to air, ASME J. Heat Transfer, 93, 1971, 240-242.
- P1. Payne R.B., Calculations of unsteady viscous flow past a circular cylinder, J. Fluid Mech., 4, 1958, 81-86.
- R1. Rao P.M., Kuwahara K. and Tsuboi K., Computational study of unsteady viscous flow around a transversely and longitudinally oscillating circular cylinder in a uniform flow at high Reynolds numbers, Computational Mechanics, 10, 1992, 414-428.
- R2. Roshko A., On the development of turbulent wakes from vortex streets, NACA Tech. Rep. 1191, 1953.

- R3. Roshko A., On the wake and drag of bluff bodies, J. Aero. Science, 22, 1955, 124-135.
- R4. Rumsey C.L. , Details of the computed flowfield over a circular cylinder at Reynolds number 1200, ASME J. of Fluids Engg., 110, 1988, 446-452.
- S1. Sa J. and Chang K., Shedding patterns of the near-wake vortices behind a circular cylinder, Int. J. for Num. Methods in Fluids, 12, 1991, 463-474.
- S2. Sarpkaya T., Vortex induced oscillations - A selective review, J. Applied Mechanics, 46, 1979, 241-257.
- S3. Saxena U.C. and Laird A.D.K., Heat transfer from a cylinder oscillating in a cross-flow, ASME J. Heat Transfer, 100, 1978, 684-689.
- S4. Sharma G.K. and Sukhatme S.P., Combined free and forced convection heat transfer from a heated tube to a transverse air stream, ASME J. Heat Transfer, 91, 1969, 457-459.
- S5. Son J.S. and Hanratty T.J., Numerical solution for the flow around a cylinder at Reynolds numbers of 40, 200 and 500, J. Fluid Mech., 35 (2), 1969, 369-386.
- S6. Sreenivasan K. and Ramachandran A., Effect of vibration on heat transfer from a horizontal cylinder to a normal air stream, Int. J. Heat Mass Transfer, 3, 1961, 60-67.
- S7. Stansby P.K., The locking-on of vortex shedding due to the cross-stream vibration of circular cylinders in uniform and shear flows, J. Fluid Mech., 74, 1976, 641-665.

- S8. Swanson J.C. and Spaulding M.L., Three dimensional numerical model of vortex shedding from a circular cylinder, Proc. of Winter Annual Meeting of ASME, San Francisco, 1978, 207-216.
- T1. Takahashi K. and Endoh K., A new correlation method for the effect of vibration on forced convection heat transfer, J. Chemical Engg. of Japan, 23(1), 1990, 45-50.
- T2. Takahashi K., Tsuruga H. and Endoh K., In-line forces on oscillating bodies in a fluid flow, J. Chemical Engg. of Japan, 21(4), 1988, 405-410.
- T3. Takami H. and Keller H.B., Steady two-dimensional viscous flow of an incompressible fluid past a circular cylinder, Phys. Fluids, Suppl. II, 1969, 51-56.
- T4. Tamura T., Tsuboi K. and Kuwahara K., Numerical simulation of unsteady flow patterns around a vibrating cylinder, AIAA Paper No. 88-0128, Reno, 1988.
- T5. Tamura T., Tsuboi K. and Kuwahara K., Numerical study for vortex induced vibration of a circular cylinder in high Reynolds number flow, AIAA Paper No. 89-0294, Reno, 1989.
- T6. Tanaka H. and Takahara S., Study on unsteady aerodynamic forces acting on an oscillating cylinder, Proc. Nineteenth Japan National Congress for Appl. Mech., Tokyo, 1969, 162-166.
- T7. Tanida Y., Okajima A. and Watanabe Y., Stability of a circular cylinder oscillating in uniform flow or in a wake, J. Fluid Mech., 61, 1973, 769-784.

- T8. Thom A., Numerical simulation of flow around a cylinder, Proc. Roy. Soc., A 141, 1933, 651-654.
- T9. Triantafyllou G.S. and Karniadakis G.E., Forces on a vibrating cylinder in steady cross flow, Proc. 8th Int. Conf. on Offshore Mechanics and Arctic Engineering, Hague, 1989, 247-251.
- V1. Vandiver K.J., Drag coefficients of long flexible cylinders, Proc. Offshore Technology Conf., Houston, 1983, 405-414.
- V2. Vandiver J.K. and Jong J.Y., The relationship between in-line and cross-flow vortex-induced vibration of cylinders, J. Fluids and Structures, 4, 1987, 381-399.
- W1. Wang X. and Dalton C., Numerical solutions for impulsively started and decelerated viscous flow past a circular cylinder, Int. J. for Num. Methods in Fluids, 12, 1991, 383-400.

Appendix A

DRAG AND LIFT INFORMATION

The nondimensional pressure distribution on the cylinder was obtained by integrating the following equation:

$$\begin{aligned} \frac{\partial P}{\partial \eta} = & \frac{2}{Re} \left(\frac{\partial \Omega}{\partial \xi} \right)_{\xi=0} - a^2 \{ -A_x F_x \cos(\pi(\tau - \tau_d)) F_x \sin(a\eta) \\ & + A_y F_y \cos(\pi(\tau - \tau_d)) F_y \cos(a\eta) \} + a^2 \frac{Gr}{2Re^2} \cos(a\eta). \end{aligned} \quad (A.1)$$

The vorticity gradient on the cylinder in the ξ direction was calculated using a fourth order accurate finite difference form. The time dependent drag and lift coefficients were calculated using the following expressions:

$$Cd = - \int_0^{2\pi} P \cos \theta d\theta - \frac{2}{Re} \int_0^{2\pi} \Omega \sin \theta d\theta, \quad (A.2)$$

$$Cl = - \int_0^{2\pi} P \sin \theta d\theta + \frac{2}{Re} \int_0^{2\pi} \Omega \cos \theta d\theta. \quad (A.3)$$

Table A.1 shows the mean drag coefficient and amplitude of the drag coefficient at various conditions of cylinder oscillation. Similarly, table A.2 shows the mean lift coefficient and amplitude of the lift coefficient at different conditions of cylinder oscillation.

Conditions of Oscillation			Cd_m		Cd_{amp}	
	a_x	a_y	$Gr/Re^2 = 0$	$Gr/Re^2 = 1$	$Gr/Re^2 = 0$	$Gr/Re^2 = 1$
Stationary Cylinder	0	0	1.2559	1.2594	0.0399	0.0375
In-line Oscillation $F_x = 2F_n$	0.1	0	1.5128	1.3974	1.1298	1.1385
	0.2	0	1.7758	1.3403	2.2040	2.1205
	0.4	0	1.5520	1.5835	3.9590	3.9717
Transverse Oscillation $F_y = F_n$	0	0.2	1.4069	1.3387	0.1565	0.1463
	0	0.4	1.5667	1.5425	0.3005	0.3814
	0	0.8	1.90326	1.8955	0.7722	0.8126
Combined Oscillation $F_x = 2F_n$ $F_y = F_n$	0.2	0.2	2.0296	1.4257	2.4260	2.2294
	0.2	0.4	2.1667	1.6924	2.4906	2.5406
	0.2	0.8	2.5716	2.2536	2.8529	2.8100

Table A.1 Mean drag coefficient and amplitude of the drag coefficient at various conditions of cylinder oscillation

Conditions of Oscillation			Cl_m		Cl_{amp}	
	a_x	a_y	$Gr/Re^2 = 0$	$Gr/Re^2 = 1$	$Gr/Re^2 = 0$	$Gr/Re^2 = 1$
Stationary Cylinder	0	0	0	-0.8505	0.6200	0.4901
In-line Oscillation $F_x = 2F_n$	0.1	0	0.0140	-0.7483	1.1030	1.0045
	0.2	0	0.0746	-0.5718	1.5873	0.7517
	0.4	0	0	-0.3455	0.0418	1.4089
Transverse Oscillation $F_y = F_n$	0	0.2	0.0028	-0.8551	0.4863	0.1564
	0	0.4	0.0024	-0.8153	0.1879	0.3983
	0	0.8	-0.0401	-0.3266	1.2209	1.6789
Combined Oscillation $F_x = 2F_n$ $F_y = F_n$	0.2	0.2	-0.0524	-0.6621	1.3073	0.6823
	0.2	0.4	-0.0966	-0.57878	1.1846	0.6754
	0.2	0.8	0.1296	-0.3979	2.9070	2.6021

Table A.2 Mean lift coefficient and amplitude of the lift coefficient at various conditions of cylinder oscillation

VITA AUCTORIS

- 1964 Born in Parampally, Udipi, India on April 16
- 1980 Completed high school at Chetana High School, Hangarcutta, Udipi, India
- 1982 Completed Pre-University Course at Viveka Junior College, Kota, Udipi, India
- 1986 Received the Degree of Bachelor of Engineering from the Mangalore University through Karnataka Regional Engineering College, Suratkal, India
- 1989 Received the Degree of Master of Technology in Mechanical Engineering from the Indian Institute of Technology, Madras, India
- 1995 Currently a candidate for the Degree of Doctor of Philosophy in Mechanical Engineering at the University of Windsor, Windsor, Canada